Electronic Theses and Dissertations

1996

Some thermodynamics of pore water in rock deterioration.

Martin. Ondrasik
University of Windsor

INFORMATION TO USERS

This manuscript has been reproduced from the microfilm master. UMI films the text directly from the original or copy submitted. Thus, some thesis and dissertation copies are in typewriter face, while others may be from any type of computer printer.

The quality of this reproduction is dependent upon the quality of the copy submitted. Broken or indistinct print, colored or poor quality illustrations and photographs, print bleedthrough, substandard margins, and improper alignment can adversely affect reproduction.

In the unlikely event that the author did not send UMI a complete manuscript and there are missing pages, these will be noted. Also, if unauthorized copyright material had to be removed, a note will indicate the deletion.

Oversize materials (e.g., maps, drawings, charts) are reproduced by sectioning the original, beginning at the upper left-hand corner and continuing from left to right in equal sections with small overlaps. Each original is also photographed in one exposure and is included in reduced form at the back of the book.

Photographs included in the original manuscript have been reproduced xerographically in this copy. Higher quality 6" x 9" black and white photographic prints are available for any photographs or illustrations appearing in this copy for an additional charge. Contact UMI directly to order.

UMI

SOME THERMODYNAMICS OF PORE WATER IN ROCK DETERIORATION

by

Martin Ondrášik

A Thesis
Submitted to the Faculty of Graduate Studies and Research
Through the Department of Earth Sciences in Partial Fulfilment of the Requirements
for the Degree of Master of Science
at the University of Windsor

Windsor, Ontario, Canada
1996

The author has granted a non-exclusive licence allowing the National Library of Canada to reproduce, loan, distribute or sell copies of this thesis in microform, paper or electronic formats.

The author retains ownership of the copyright in this thesis. Neither the thesis nor substantial extracts from it may be printed or otherwise reproduced without the author's permission.

L'auteur a accordé une licence non exclusive permettant à la Bibliothèque nationale du Canada de reproduire, prêter, distribuer ou vendre des copies de cette thèse sous la forme de microfiche/film, de reproduction sur papier ou sur format électronique.

L'auteur conserve la propriété du droit d'auteur qui protège cette thèse. Ni la thèse ni des extraits substantiels de celle-ci ne doivent être imprimés ou autrement reproduits sans son autorisation.

0-612-30923-1

Canada

Martin Ondrášik

© ——————————————————————— 1996

All Rights Reserved

Abstract

The purpose of this study was to investigate the thermodynamic properties of the pore water in rocks and the relationship between the thermodynamic properties and the rock durability determined by standard tests on rock durability and by performance record of the tested rock.

The rocks used in the study represent mostly strata of carbonate rocks and some argillitic and igneous and metamorphic rocks which are currently quarried in Southern and South East Ontario and widely used in the concrete industry. The tests were conducted on rock cores two centimetres in diameter and 4.5 centimetres high. In the first series of tests, physical properties such as water adsorption, 24 hour water saturation, vacuum saturation and rate of water absorption were determined. In the second series of tests dry cores, cores with adsorbed water and fully saturated cores were subjected to microwave energy in a standard microwave oven and the amount of absorbed heat was measured. In the third series of tests, the fully saturated samples were exposed to low temperature (-16 °C) and the amount of frozen pore water was determined by calorimetric means. Length change on freezing was also recorded. In the last, the fourth series of tests, changes in physical properties were determined by repeating the tests for vacuum saturation and water adsorption on specimens subjected earlier to wetting, freezing, and thawing.

All the results from tests on rock aggregate durability (including freeze-thaw and magnesium sulphate loss performed in previous study by J. Rigbey, 1980), were then subjected to statistical analysis. The statistical analysis included (1) correlation tests and line of best fit, (2) cluster analysis, (3) group mean tests and (4) factor analysis.

The results showed that adsorbed water has less free energy and absorbs less

microwave heat than bulk water. Further, the frozen pore water and length change determination on freezing revealed that highly durable and good performance rock had the highest amount of water frozen and highest expansion on freezing. On the other hand, samples with poor performance record as rock aggregates and poor durability resistance did not show any freezing, and minimal length change on freezing. They also had a high content of adsorbed water i.e. water with low free energy.

The presented research work revealed the thermodynamic properties of the pore water as the most important factor controlling rock durability.

Dedication

To My Patient Parents

Acknowledgements

.

I would like to express my sincere gratitude and appreciation to my supervisor Dr. Peter P. Hudec for his tireless guidance, advice, and encouragement in this research and for all the friendship and generosity which I have met in his heart and which made this research work a success.

I also wish to express my sincere thankfulness to Mrs. Susan Sherman for her support and help which she always gave me with a friendly smile. I thank Mr. Dieter K. Liebsch and Mr. James Hochreitsr for their technical assistance and advice during the assembling and tuning of the testing apparatus.

I further express my appreciation to all my new friends who made my stay in Canada worth the loneness from my home.

Table of Contents

List of Tables

List of Figures

List of Appendices

1 INTRODUCTION

A rock is one of the most common construction materials. It is used in its original form as decoration stone or it is crushed and used as aggregates in concrete. Whatever the purpose for utilising of the mined rock is, the physical properties of the rock dictate its actual use.

Rock is a natural matter composed of mineral aggregates and voids which are empty or filled with water. The voids may represent wide range of total rock space; from extremely low (0%) up to extremely high (60%) (Dullien, 1979). Many researches have proved that it is the porosity and liquid (water or solution) in the pores which control the performance of a rock as a construction material (Powers, 1949, Verbeck and Landgren, 1960, Bager and Sellevold, 1987a, Hudec, 1991). In a dry climate, most of the rocks, if not all, are weathering resistant; they disintegrate only by mechanical forces, such as wind erosion, thermal dilation or unloading, etc. which effect only an exposed surface and the results are visible only after a long period time. However, as soon as water is introduced into the porous system, the situation is dramatically changed. The water can cause severe weathering either as a medium which transports chemical weathering agents (chemical weathering), or as an agent of weathering of the rock itself by its chemical, physical or thermodynamic properties.

Porous rocks contain bulk water or adsorbed water. While the content of bulk water is controlled by a volume of macro and bulk pores, the amount of adsorbed water is controlled by total pore wall surface which increases with increasing amount of micro pores. The properties of adsorbed water are different from properties of bulk water. The main difference is in their chemical potentials (Dullien, 1979). Adsorbed water has, due to interaction in solid - liquid interface, lower chemical potential, which results in lower vapour pressures over adsorbed than over bulk water. The difference in vapour pressure causes migration of water

molecules from pores with a high vapour pressure (bulk pores) into pores with a low vapour pressure (micro capillary pores). The migration continues until the equilibrium of vapour pressures is established for given temperature and pressure (atmospheric). Since the equilibrium can be easily disturbed by changes of temperature or occurrence of a freezing in bulk pores, the migration of water molecules through pore system is very intensive. The migration is accompanied by building up of differential hydraulic pressure, which acts against the pore walls. If the pressure is greater then strength of the pore wall, than the wall can collapse and weaken the overall strength of a rock. These theoretical conclusions supported by experimental observations led researchers (Verbeck and Landgren, 1960, Litvan, 1972a and 1972b, Powers, 1975, Hudec, 1991) to revise the original hydraulic theory of rock disintegration on freezing proposed by Powers (1949). Each of them incorporated into his theory of rock deterioration on freezing the migration of water molecules due to thermodynamic imbalance. The combination of the hydraulic theory with thermodynamic phenomena has improved an agreement between theory and observation. However, all observations are not yet satisfactorily explained, for instance, large scaling of concrete in 3% salt solution for which Hudec (1991) has proposed a thermodynamic explanation.

As it was mentioned above, the understanding of thermodynamic properties of pore water is very important. Since most of the studies were carried out on artificial porous materials (ceramic, cement paste, concrete) there was need to conduct the studies on natural rocks. This was the goal of this study. Its main objective was the investigation of a relationship between thermodynamic properties of pore water and behaviour of the pore water and the whole rock on freezing.

2 LITERATURE REVIEW

2.1 Characteristics of Pores and Porosity

The porosity of a rock is defined as the ratio of the aggregate volume of interstices in a rock or soil to its total volume (Bates and Jackson, 1984). A distinction is usually made between total porosity and the effective porosity (North, 1985, Fetter, 1994). Total porosity includes all rock interstices; effective porosity includes only those, which are interconnected, i.e. permeable to water. As a results of research by numerous workers it has become apparent that many rock properties like adsorption, absorption rate, resistance to freezing, thawing, and drying, wetting, chemical stability and resistance to abrasion, are not controlled by total rock pore space, but by pore size. (Haynes, 1973b, Darr and Ludwig, 1973, Litvan, 1972a 1972b and 1975, Banthia et al., 1989, Bager and Sellevold, 1986a and 1987, Morioka et al., 1973, Hudec, 1989, 1991, 1993).

Hudec (1987) divided pores according their shortest distance into four general groups (Table 2.1). The smallest pores or *Force pores* are less than 1 μm and contain adsorbed water only. The *Micro capillary* pores have size between 1 μm - 5 μm and contain absorbed water and capillary water, and can saturate fully by capillary suction alone. The *Macro Capillary*

Table 2.1 Pore Size Classification (after Hudec, 1987)

Pore Class	"FORCE" PORES	MICRO - CAPILLARY	MACRO - CAPILLARY	BULK PORES
Pore Size	<1μm	1 - 5 μm	5μm - 1mm	>1mm
Dominant in:	shale, chert	fine-grained volcanics, argillaceous dolomite and limestone	medium grained dolomite - limestone, metamorphic rocks, igneous rocks	coarse grained dolomite - limestone, metamorphic rocks, igneous rocks

pores have diameter range 5μm - 1mm and can saturate only partly, because of entrapped capillary air. Prolonged vacuum saturation is required to fully saturate the pores. Large *Bulk Pores* are greater than 1 mm and contain mostly bulk water. They are readily saturated and drained provided they are interconnected. Since most water in micro pores and force pores is adsorbed water which is not free-drying, the pores fully saturate at high relative humidity, and are subjected to rapid deterioration due to freezing and thawing or drying and wetting (Dunn, 1972, Hudec and Sitar, 1975,).

2.2 The Thermodynamic Properties of Pore Water and Adsorption

The adsorption occurs because of a lack of thermodynamic equilibrium between gas or vapour and the solid surface in contact with it (Dullien, 1979). Equilibrium is achieved by accumulation of the molecules of the gas or vapour, the "adsorbate," at the solid surface, the "adsorbent.". As a result an adsorbed layer of the adsorbate is formed on the adsorbent. The process of adsorption continues until the adsorbed layer is in thermodynamic equilibrium with the gas or vapour in contact with it. In equilibrium the chemical potential of the adsorbed layer μ_a is equal to the chemical potential of the vapour μ_v'' (Dullien, 1979). Before reaching equilibrium, μ_a is less than μ_v'' and when dn moles of the adsorbate are transferred from the vapour to the adsorbed layer, at constant temperature (T) and pressure (P) of the vapour phase, the change in the Gibbs free energy ($dG_{T,P}$) is

$$dG_{T,P} = (\mu_a - \mu_v'')\, dn. \qquad\qquad 2.1$$

When the equilibrium is established, then $dG_{T,P} = 0$.

4
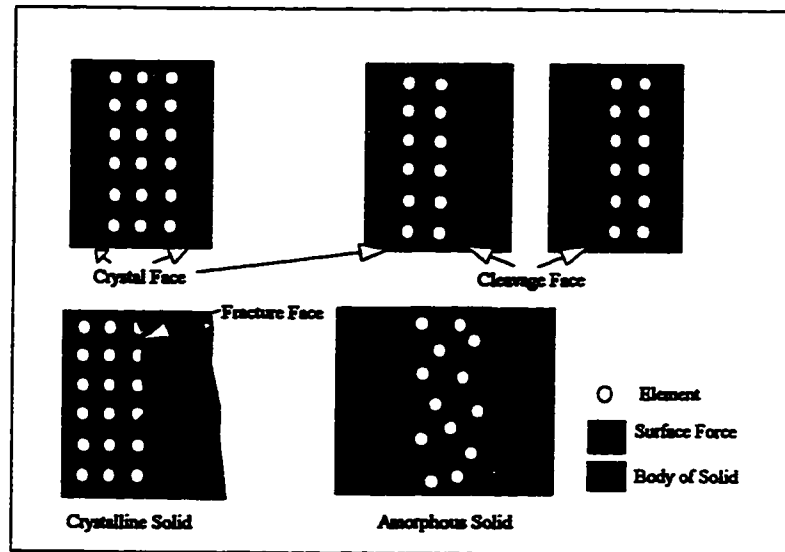
Figure 2.1 Illustration of surface forces active on crystal faces, cleavage faces, fracture faces of crystalline and on amorphous solids. Surface forces are indicatedby the width of band adjacen to the surface. (after Hudec, 1993)

The chemical potential of the adsorbed layer (μ_s) depends upon the cohesive forces between adsorbate (water) and adsorbent (rock mineral). The cohesive forces are in turn controlled by the charge of the adsorbent surface which attracts dipolar water molecules. Hudec (1987, 1993) proposed that the surface charge, usually negative, vary with the surface type. He distinguished four different surface types: (1) crystal surface, (2) cleavage surface, (3) surface of amorphous solid, (4) fracture surface. Crystalline surfaces are the least charged, because all chemical bounds (covalent and ionic) between atoms making up the absorbent are satisfied in a regular crystalline lattice, and only residual charges remain to adsorb the adsorbate. The fracture surface has the largest surface charges, because the break along a fracture surface takes place in a random direction across lattice of the solid leaves unsatisfied chemical bonds of the elements (atoms or ions) within the surface (Figure 2.1). Cleavage, has moderate surface charges. Surface on amorphous solids is active, since few of the elements in the solid are bonded to other surrounding elements, and the unsatisfied bonds are reflected

5

in high surface charges. Cleavage surfaces are planes along which the bonds between elements are relatively weak and can be cleaved. The more difficult it is to cleave the surface, the higher the surface charge. Hudec (1993) suggested that the thickness of adsorbed water layer is proportional to the surface activity of the solid . He also suggested, that the thickness of the layer can be enhanced by presence of cations adsorbed on the surface, because the cations have greater charges than surfaces.

The total surface area of pores may be very large, up to several ten thousands cm^2 per 1 cm^3 and is controlled by the pore size (Hudec 1993). The smaller the pores in the rock, the higher surface area. If the pore size is small enough (< 5 μm), then the pores can be completely filled with adsorbed water at given relative humidity (RH). The pore size, which can be completely filled with pore water at given RH can be calculated by Kelvin's equation:

$$\ln \frac{p}{p_o} = 2 \frac{\sigma}{r} \frac{M}{RTd} \qquad\qquad 2.2$$

Where:
p, p_o - vapour pressure over adsorbed water and bulk water respectively [Pa]
σ - surface tension of water, [N/m], at absolute temperature T [°K]
r   - capillary radius [m]
M   - molecular weight of liquid, [kg]
R   - the Gas constant
d   - density of liquid, [kg/m^3]

Calculations based on the equation shows, that pores with radius 5 μm can be completely filled with adsorbed water at 95% RH (Figure 2.2). However, if cations are present, the pore size fully saturated with adsorbed water can be even greater (Figure. 2.3) (Hudec, 1993). The difference between vapour pressure of bulk water and adsorbed water in pores with radius 0.1 μm and RH $\geq$ 0% is up to 610 Pa, as calculated by Kelvin's equation.
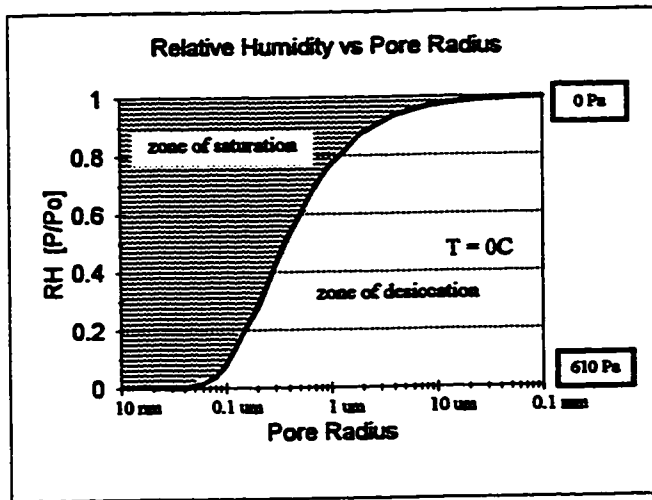
Figure 2.2 Relationship between relative humidity and pore radius and water vapor pressure at zero degree of Celsius as calculated from Kelvin's equation (Equation 2.2).
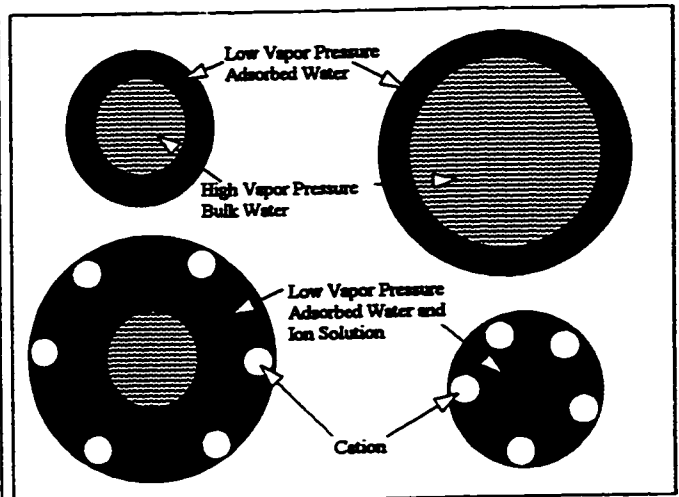
Figure 2.3 Illustration of the effect of cations on the size of pore fully saturated with adsorbed water. Presence of ions in the pores increase the number of pores saturated by adsorbed water by increasing the thickness of adsorbed layer. (after Hudec, 1993)

2.3 Ice Formation in Porous Media and Its Calorimetric Recording

Many researchers have reported that when the temperature of a porous system drops below the freezing point of water (0°C), freezing in capillary pores saturated with pure water does not occur immediately, but at temperatures lower than the normal freezing temperature of water (Morioka et al., 1973, Litvan, 1972b, 1973, Bager and Sellevold, 1986a and 1987, Banthia at al., 1989). Freezing first occurs in large capillaries and then the ice crystals grow by incorporating unfrozen water from the smaller capillaries (Everett, 1961). Freezing in smaller pores is depressed due to interactions between pore walls and pore water. The smaller the pore, the lower freezing temperature. Blachere and Young (1972) reported that the observed freezing point of water in pores of different size agreed with the freezing point lowering calculated from the thermodynamics of capillary theory based on Kelvin's equation (Figure 2.4). Similar results were reported by Fagerlund (1973a, 1973b), who calculated pore

7

size distribution based on freezing point depression. Litvan (1973) has found, in his research, that the presence of deicing salts (NaCl) in capillary pores does not have any influence on the first freezing point depression. Litvan observed the same freezing point in pores saturated with pure water and with
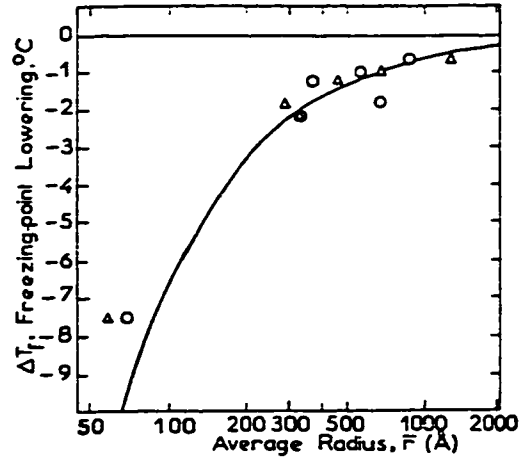
Figure 2.4 Relationship between pore water freezing point lowering and pore radius. (after Blachere and Youngh, 1972)

salt solutions of different NaCl concentrations. Bager and Sellevold (1986a, 1986b and 1987) used for his calorimetric tests on freezability of capillary water cement pastes with different water to cement ratio (the porosity of the paste increases with a higher ratio). Bager and Sellevold observed that the water in the paste freezes at three well-defined peaks on
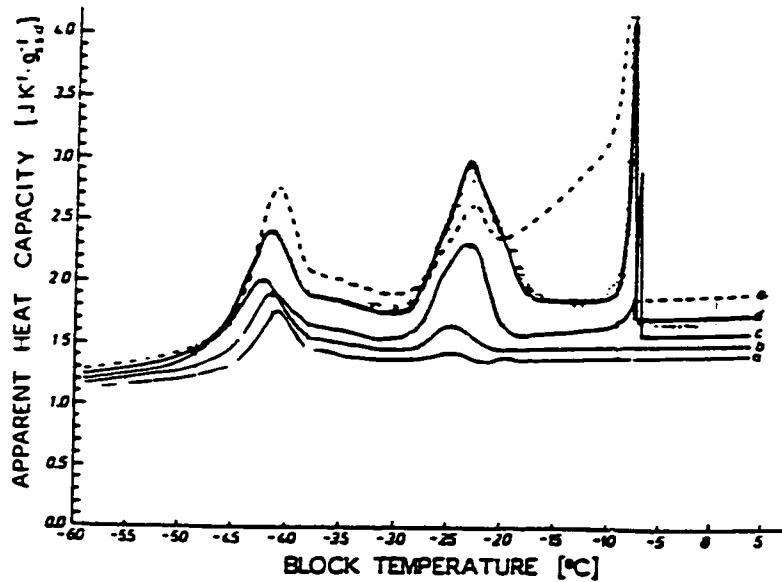
Figure 2.5 Apparent heat capacity curves of cooled samples; a, b, c, d, e, represents water saturated samples with different porosity : a<b<c<d<e. (after Bager and Sellevold, 1986a)

8

calorimetric output (Figure 2.5). The first freezing occurred at temperature about -8°C, the second freezing occurred at temperature about -23°C and the last freezing at about -43°C. The freezing peaks were equal for cement paste of any porosity. Bager and Sellevold have concluded, that the freezing peaks correspond to characteristic pore size ranges in the pore structures. Their results have showed, that the amount of non-frozen water at temperature -55°C increases with increasing porosity and with increasing water content. Furthermore, he observed existence of water content which is not freezable. He defined this content as equivalent of 3.1 BET monolayers what is about 1.3 nano meters thick water film (Grimshaw, , 1971). All researchers who conducted calorimetric tests with porous media, concluded that there is only one peak representing transition of ice to water. It occurs at temperature 0°C.

A detailed theoretical thermodynamic analysis of freezing water in porous media, as observed by a calorimetric output, has been published by Banthia at al. (1989). Banthia conducted his calorimetric studies on porous specimens (cement paste) exposed to temperature from +20° to -40°C. The energy ΔH evolved during a time step t_n he obtained by integrating the calorimetric output dH/dt (t_n):

$$(\Delta H)_n = \int_{(t)_n}^{(t)_{n-1}} (\frac{dH}{dt})dt \qquad\qquad 2.3$$

Further Banthia proposed that the heat output $(\Delta H)_n$ from the system may be equated to the change in the internal energy of the system:

$$(\Delta H)_n = \Delta H_s + \Delta H_w + \Delta H_i + Lw_i \qquad\qquad 2.4$$

Where

ΔH_s is the heat output from the solid part of the rock and is equal to

$$\Delta H_s = m_p * \Delta T * C_{pp} \qquad\qquad 2.5$$

9

ΔH_w is the heat output from liquid pore water and is equal to

$$\Delta H_w = [m_e - m_{i(t)}] * \Delta T * C_{pw(T)} \qquad 2.6$$

ΔH_i is the heat output from the ice and is equal to

$$\Delta H_i = m_{i(t)} * \Delta T * C_{pi(T)} \qquad 2.7$$

Lw_i is latent heat due to transition of water to ice or ice to water and is equal to

$$Lw_i = \Delta h_f (T) * \Delta m_i \qquad 2.8$$

$C_{pp}, C_{pw(T)}, C_{pi(T)}$ = specific heat of the paste, water and ice, respectively, at the temperature
      T, [J/g°C]
H   = energy evolved or absorbed [J]
t   = time [sec]
dH/dt = rate of energy evolved or absorbed [J/sec]
T   = temperature [°C]
$m_p, m_{w(t)}, m_{i(t)}$ = the masses of solid, water and ice, respectively at a time t [g]
ΔT = Temperature change during a time step [°C]
$(\Delta H)_n$ = heat output or input during the nth step [J]
m_e = mass of the total water in the system [g]
$\Delta h_{f(T)}$ = enthalpy of the fusion of water (ice) at temperature T°C [J/g]
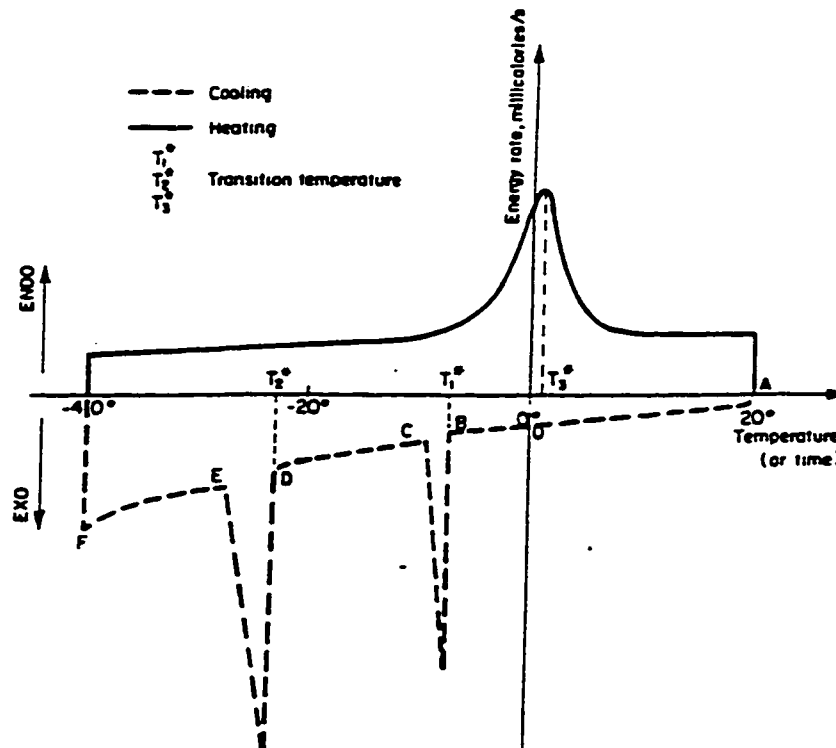
Figure 2.6. Schematic calorimetric output (after Banthia et al., 1989)

10

Banthia has divided the cooling curve of the calorimetric output (dashed line in Figure 2.6) into three parts. First is the part above 0°C (part AO). Second, the part below 0°C without transition from water to ice (parts OB, CD, EF); and the third is the part below 0°C with an ongoing transition (parts BC, DE). Part one represents output of heat proportional to heat capacity of solid and pore water. Part two represents heat output proportional to heat capacity of unfrozen water (supercooled water), ice already formed and solid. Part three represents heat output due to transition of water to ice. The amount of the heat is proportional to the amount of the frozen water. Heating curve (bold line in Figure 2.6) can be also divided into three parts, however, this time only one part with transition from ice to water takes place. First part is below 0°C without transition from ice to water. The curve represents heat input into the system, absorbed by unfrozen water, solid, and ice. The second part is the transition from ice to water. The line represents the heat input required for transition of ice to water. The amount of adsorbed heat should be equal to the amount of heat released on freezing (part BC and DE of the cooling curve in Figure 2.6). The third part of the heating curve is above 0°C. It represents heat input increasing temperature of solid and pore water.

2.4 Capillary Pressure and Absorption

When water is introduced into a porous medium, an interface of three phases (solid, liquid and gaseous) will occur in the pores. A border between the gaseous and liquid phase is made up by a curved meniscus which joins the solid phase (pore walls) at certain angle. Both, curvature of the meniscus (radius) and contact angle depend upon cohesive and adhesive forces between the molecules of the three phases and upon the pore radius. If the

11
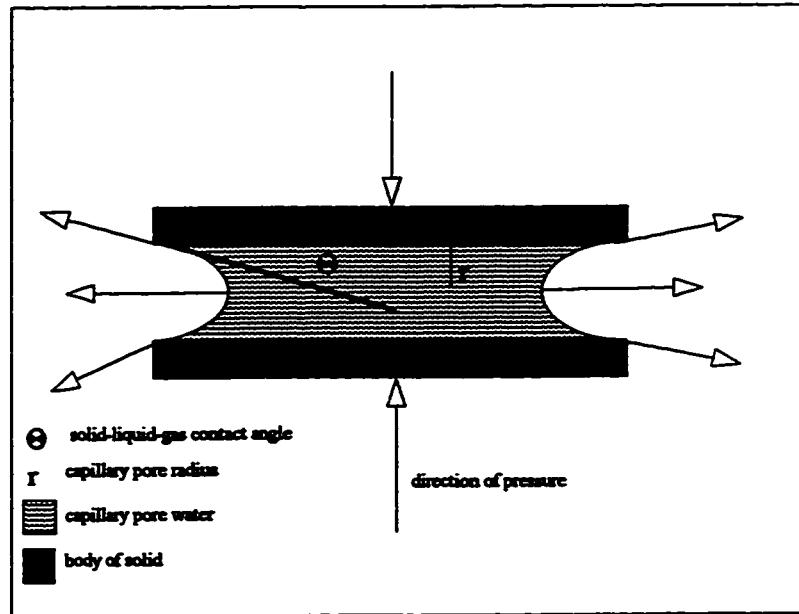
Figure 2.7 Illustration of tensile pressure on meniscus in capillar pores.

cohesive forces between solid and liquid phase are greater than adhesive forces, than the angle

is very sharp (Figure 2.7) and the meniscus, driven by the attractive forces, "pulls" the liquid

into the capillary pore. This creates tensile pressure on capillary pore walls already filled with

water (Figure 2.7). The pressure on the meniscus is expressed by equation:

$$P_c = h * d \, g = 2 * \cos \theta * \frac{\Upsilon}{r}$$ 2.9

Where:

h   - height of rise in the capillary [m]
d   - density [kg / m^3]
g   - gravitation constant [kg / m s^2]
Υ - surface tension [N/m]
r   - capillary (meniscus) radius [m]
θ - contact angle [degree]

Since only (r) in the above relationship is variable, the tension varies with change of the radius

in the capillaries.

12

Hudec and Sitar (1975) and Hudec (1989) have concluded from experimental evidence that the rate of contraction is very rapid, within seconds. As more water is available, larger capillaries are filled, the capillary tension decreases, and the rock relaxes. Under full saturation the meniscus at the solid - water - gas interface disappears and rock is fully relaxed. They observed larger contraction on rocks with higher amount of small capillary pores than on those with larger pores. The speed of the saturation, magnitude of the contraction and degree of the saturation are a function of pore size and their distribution. Rocks with uniform pore size distribution in small size ranges yields greater contraction and degree of saturation and faster rate of saturation (Hudec and Sitar 1975). Fagerlund (1973b) reported using this phenomena for determination of pore size distribution.

2.5 Pore Size and Degree of Saturation

The frost behaviour of aggregates is mainly related to the characteristics of their pore system. Not total porosity, but mainly, the pore size distribution controls the durability of the aggregate. Aggregates with small pore size tend to achieve a high degree of saturation under intermediate or high RH, as can be calculated from Kelvin's equation (Figure 2.2). Figure 2.8 shows the relationship between relative humidity and degree of saturation for four different aggregates. It shows that aggregates which have fine pores can achieve a high degree of saturation at a relatively low RH. The degree of saturation of aggregates which are known to have relatively coarse pore system decreases very rapidly with a decrease in RH. This means that aggregates with fine pore size can reach full saturation under field conditions much easier than the aggregates with larger pores. Hudec (1989) has demonstrated that a carbonate
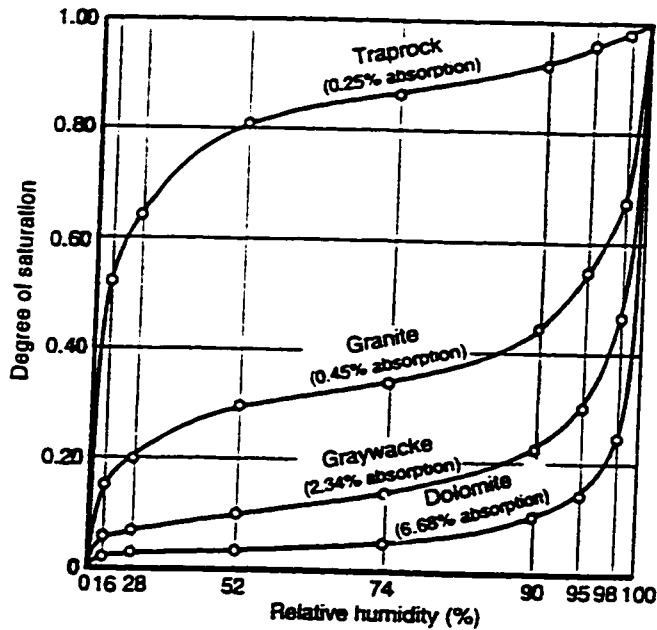
Figure 2.8 Relationship between the relative humidity and the degree of saturation for four different types of aggregates (after Verbeck and Landgren, 1960)

aggregate with a fine-grained pore system absorbs water approximately two times faster than a similar aggregates with a coarser pore size distribution. As will be discussed in the next chapter, degree of pore saturation is one of the main factors controlling aggregate frost resistivity.

2.6 Frost Action in Porous Media

Many researchers showed that freezing of pore water and events associated with the freezing are the most destructive factors deteriorating porous media. This deterioration can even lead to the complete disintegration of the particles composing the porous media.

The first mechanism of deterioration of porous media on freezing was described by Powers (1949). Powers has suggested the hydraulic pressure theory. According to this theory, high hydraulic pressure is generated by freezing water in closed pore space due to 9% volume

14

increase of water on freezing. Darcy's law of water flow through porous media was used to describe this pressure. Verbeck and Landgren (1960) defined this pressure as function of the total porosity, the degree of saturation, the permeability and the size of the aggregate particle. The generated hydraulic pressure is directly proportional to the particle size and rate of freezing and inversely proportional to the permeability of the particles. The particle dimension represents the maximum distance that water must travel to be expelled from the aggregate particle or in to air voids. At given permeability of the particles and rate of freezing of the water a critical size of fully saturated particle exists, which, if exceeded, results in the hydraulic pressure exceeding the tensile strength of the particle. The critical particle size is thus a function of the permeability, the tensile strength of the aggregate, the amount of freezable water and the rate of cooling (Verbeck and Landgren, 1960).

Since the hydraulic theory did not explain all the experimental observations, Powers continued improving his hydraulic theory. In 1975 he published his osmotic pressure theory. The water in capillary pores and in micro pores (gel pores) are in thermodynamic equilibrium at temperatures above 0°C. When the temperature is lowered, the water in capillary pores does not freeze immediately due to small size of the pores because surface tension prevents the immediate freezing of water. The lowering of the freezing can be also caused by presence of chemicals (for instance deicing salts). When the temperature is sufficiently low, for given pore size and concentration of chemicals, the ice begins to form and the thermodynamic equilibrium between water in micro pores and capillary pores is disrupted. The free energy of the ice is at any given temperature lower than that of water in micro pores. Thus the water in micro pores acquires potential energy to move toward capillary pores where ice has started to form. When this water reaches the capillary pores, it freezes and the ice crystals increase

in size. The growth of ice crystals creates pressure on unfrozen water film between ice and pore walls. If the pressure becomes too high permanent damage occurs because the porous system cannot expand. The presence of dissolved chemicals can enhance the mechanism. The formation of ice increases the concentration of chemical in capillary pores where the ice has started to form. Concentration of chemicals in smaller capillary pores and in micro pores where ice had not begun to formed has not been increased. Then the osmotic pressure drives the water molecules from small pores with low concentration into large pores with high concentration of chemicals and additional pressure is built up.

Litvan (1972b, 1975) concluded from his experiments that water in some capillary pores does not freeze, when the temperature decreases to below 0°C. The water is supercooled, which causes desorption of the porous material, because the vapour pressure over supercooled water is higher that over ice. The water is driven out the porous media, or into larger pores, where it freezes. When the freezing rate is too high or the distance which the water must travel is too long, the forced movement of water can caused very high stress and cracking.

Kaneuji et al. (1980) carried out tests on the influence of the pore size distribution on freezing-thawing performance of aggregates. The data indicated that for aggregates with similar total pore volume, those with the finer pore systems are generally less durable. Similar conclusions were reached by Hudec (1991). Based on his observations, Hudec doubts the ice formation as the main destructive mechanism of porous materials. Hudec argues that thermodynamically the water in small pores does not freeze at temperatures close to 0°C. However, aggregates with high content of small pores in which water does not freeze are

16
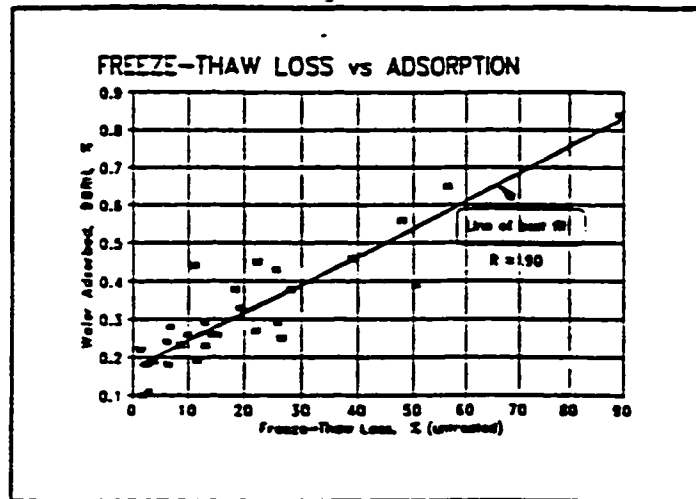
Figure 2.9 Relationship of adsorbed water on the freeze-thaw loss of aggregates. (after Hudec, 1991)

those which tend to have highest losses on freeze-thaw tests. Hudec documented this with very high correlation (R = 0.95) between freeze-thaw losses and adsorption (Figure 2.9). He concluded that the amount of adsorbed water in proportion to normal bulk water dictates whether the failure mechanism will be primarily due to osmotic forces, or due to freezing and subsequent hydraulic forces. The proportion of adsorbed and bulk water is in turn a function of the pore size. If the material contains mostly small pores, the osmotic process dominates; if the dominant pore size is large, then the hydraulic forces dominate, assuming that all the pores are critically saturated.

Prout and Hoff (1990) stressed the importance of entrapment of pore water by ice formed on the outer surface of freezing porous material. When unidirectional freezing occurs, the ice forms firstly on outer surface of a tested sample, which prevents expulsion of expanding freezing water and, the hydraulic pressure is built up.

Pigeon et al. (1995) concluded that, most of the time, the mechanism of frost action

17

in rock aggregate is in good agreement with that proposed in Powers' hydraulic pressure theory. Pigeon pointed out three basic aggregate properties controlling the mechanisms of aggregate deterioration: elastic accommodation, critical size, and critical degree of saturation.

Elastic accommodation Pigeon defined as the ability of the elastic deformation of the particles which increases the total pore volume available to the expanding freezing water. Disruption of the aggregate occurs when the pressure due to ice formation exceeds the tensile strength of the rock. This occurs particularly in the case of instantaneous freezing of a completely saturated aggregate. In such case, the total absorption of the aggregate is very important, since it determines the amount of freezable water and amount of water free voids, where the hydraulic pressure can be relaxed. Verbeck and Landgren (1960) have calculated the theoretical values of the ice pressure of three common aggregates with various absorptions. For quartzite aggregate with absorption 0.1% the ice pressure is 5.4 MPa, for chert with absorption 2.1% the pressure is 117 MPa. The ice pressure for dolomite with absorption 6.7 the pressure can be 241 MPa, which can be in some cases 10 times more than the tensile strength of the dolomitic aggregates.

When freezing is more gradual, the expulsion of water to the outside of the aggregate can contribute significantly to the relaxation of the pressures caused by the growth of ice crystals. The rate of the expulsion of the water to the outside of the sample generates hydraulic pressure in accordance with Darcy's law on the flow of liquid through a pores (Powers, 1949).

The magnitude of the hydraulic pressures, the required expulsion distance in the cement paste and the critical size of the aggregates are of course different when the aggregates are not fully saturated at the time of freezing. Theoretically, the aggregates should

18

be immune to frost when the degree of saturation is below 91% because; in this case, the pore

system contains enough empty spaces to accommodate the increase in volume of the water

due to the formation of ice.For a given aggregate, with a given maximum nominal size,
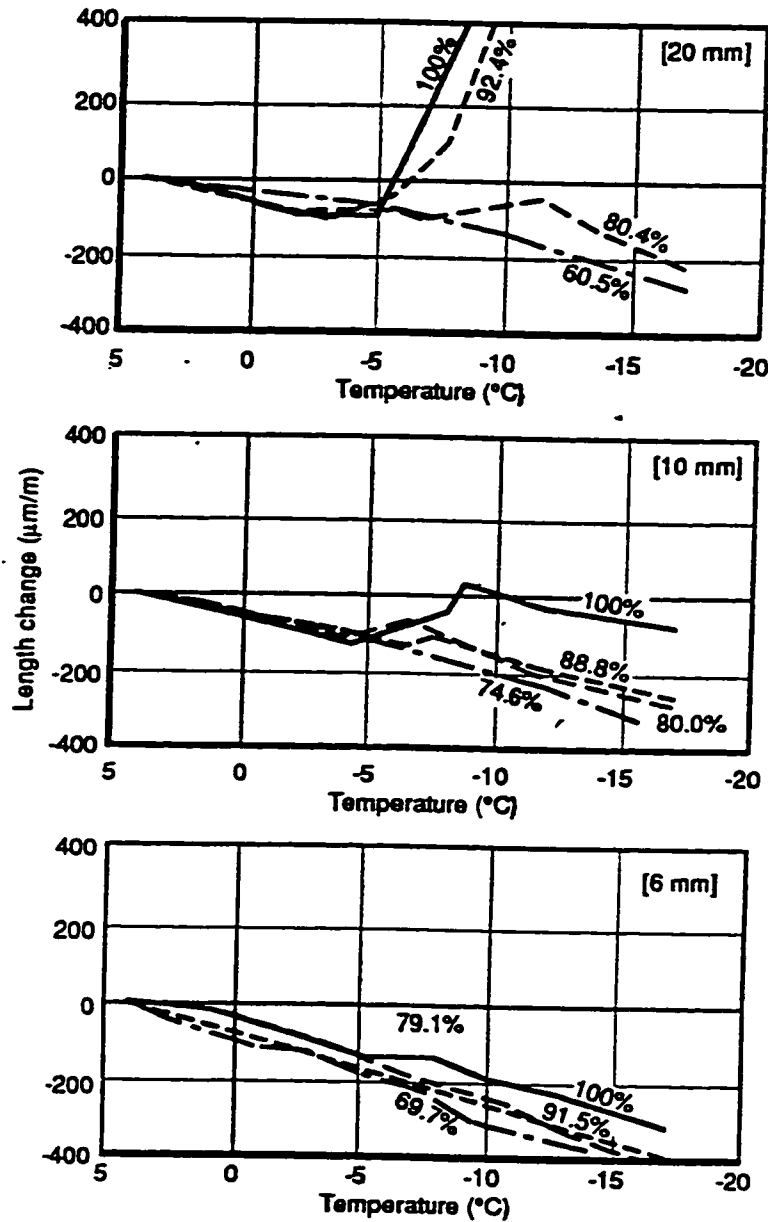
Figure 2.10 Influence of maximum size of aggregates
and of the degree of saturation (%) on the length change
of a 0.5 water/cement ratio concrete during freezing.
The size of the aggregate particles is indicated in
brackets on each graph. (after MacInnis and Lau, 1971)

19

embedded in a given cement paste and exposed to a given rate of cooling a critical degree of saturation can be defined below which this aggregate can be considered to be frost resistant. The influence of aggregate size and degree of saturation is well documented in Figure 2.10. The expansion of concrete on freezing increases with increasing aggregate size and the degree of saturation.

2.7 Length Change of Porous Media on Freezing

Many of the studies on frost damage in porous media studied length change of the porous media under different conditions and with different adsorbate (Beaudoin and MacInnis, 1974, Litvan, 1972a, 1971b, 1973 and 1974, Kenji, at al., 1990). Beaudoin and MacInnis conducted their studies on hardened cement paste, and as absorbate they used pure water and benzene. They observed 4 typical stages in the curve during freeze - thaw cycle. Figure 2.11 shows the curve, when the absorbate is saturated with pure water. Stage 0A Beaudoin and MacInnis attributed to the thermal contraction. Stage AB Beaudoin and MacInnis described as overlapping of three effects: contraction of small pores due to migration of unfrozen water toward interlayer regions (layers of unfrozen water between ice and pore walls), ice growth expansion, and hydraulic pressure. Stage BC Beaudoin and MacInnis described as overlapping of thermal expansion, release of pressure due to ice melting and expansion due to penetration of sorbate into small pores. Last observed stage CD Beaudoin and MacInnis explained as thermal expansion of the system. Their further observations conducted on the same adsorbate system (hardened cement past) saturated this time with benzene, suggested, that the expansion of freezing water does not itself account for

the expansion of the whole system. Although benzene contracts on freezing, it caused expansion of the whole system when benzene crystals formation has occurred (Figure 2.12). Stages 0A, AB, CD, DE are described as identical to the stages 0A, AB, BC and CD respectively observed on water saturated sample (Figure 2.4). The expansion on freezing he explained as effect of hydraulic pressure as a result of nucleation and crystal growth in capillaries due to migration of benzene from small pores toward the solid adsorbate. Stage BC recognized as accelerated shrinkage attributed to desorption because of a decrease in effective relative pressure on cooling.

Figure 2.11 Length change temperature relation for water saturated porous sample. (after Beaudoin and MacInnis, 1974)

Similar results were observed also by Litvan (1972b). He tested length change of cement paste with different porosity and cement paste saturated with pure water and with NaCl solution of different concentration of NaCl (Litvan, 1975). Litvan observed that expansion on freezing of fully
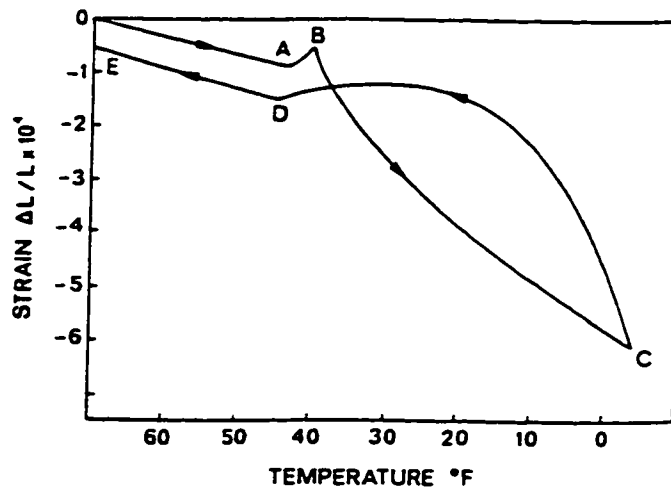
Figure 2.12 Length change temperature relation for benzene saturated porous sample. (after Beaudoin and MacInnis, 1974)

21

saturated cement paste increases with increasing porosity. The tests conducted with different

concentration of NaCl solution revealed concentration between 3% and 5% as the

concentration causing the highest expansion. The latter is in good agreement with observation

on freeze-thaw tests. Concentration 3% was found as the most aggressive on the rock

aggregate exposed to repeated freezing and thawing.

Kenji et al. (1990) tested thermal expansion of saturated rocks with different porosity:

mudstone, rhyolite, granite and schist. Mudstone had the highest porosity (n=47.47%) and

schist the lowest (n=0.95%). He found that only mudstone and rhyolite (m=2.54) expanded

on freezing. Granite (n=1.29%) and schist did not expand at all.

2.9 Microwave Oven and Principles of Dielectric Heating

Commercial microwave oven, which was used for the experiments, consists of 4 major

parts: megatron, cavities, transmission section, rotating disc. Megatron (Kleen, 1958) emits

nonionizing microwave energy (nonionizing electromagnetic waves do not cause changes in

atom or molecular structure, ionizing waves, like cosmic or gamma rays, do cause changes in the atom or molecular structure). The waves are transferred from megatron into heating a box-like cavities through the transmission section of the oven. In order to distribute the microwave waves
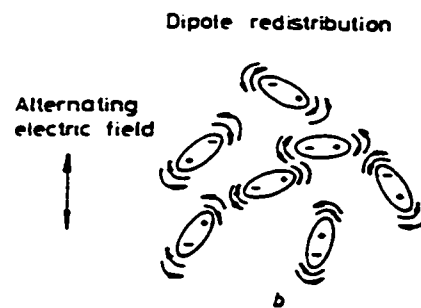
Figure 2.13 Dipole redistribution of polarization of bipolar molecules in alternating electric field. (after Metaxas and Meredith, 1983)

22

evenly throughout the oven, the waves are "stirred" by a rotating disc. Nonionizing electromagnetic waves cause a rise in temperature within the penetrated medium due to electromagnetic field changes at high frequency (usually 2450 MHz) (Metaxas and Meredith, 1983). The changes of electromagnetic field cause rotation of a dipolar particles into the direction of the electric field. Since this is happening at a high frequency, friction between particles (dipolar molecules) generates heat (Figure 2.13). It means, that microwave heating depends chiefly upon the presence of molecules with permanent electric dipole configuration and with freedom to rotate within a heated medium. Retarding forces preventing rotation of molecules are much weaker in the liquid state than in the solid state, and molecular polarization (rotation of molecules) can take place at a much higher frequency in a liquid than in a solid.

3 SAMPLING AND GEOLOGY

3.1 Sampling

Most of the tested samples were collected in the active quarries of East and South Ontario (Addington, Essex, Frontenac, Grenville, Haldimand, Halton, Hastings, Leeds, Lennox, Lincoln, Norfolk, Peel, Peterborough, Simcoe, Stormont, Welland, and Wentworth counties) by Rigbey (1980). The author has chosen the samples with sufficient size for sample preparation (drilling) from the Earth Science's rock deposit room. In addition to those samples, the author collected eleven samples in quarries in Eastern Ontario and Pelee Island (Essex, Niagara, Lincoln, Haldimand). The numbering of the samples has remained the same as numbering provided by Rigbey. Samples collected by author are marked with numbers greater than 120. Missing sample numbers are the numbers of those samples which were missing in the collection or were not suitable for drilling. Lithological description of the samples is given in Table A.3 (Appendix A). Location of all 38 quarries are given on Figure 3.1. Numbers of the quarries on the figure are identical with numbers of the quarries in the Appendix A.

3.2 Geology

3.2.1 Precambrian Rocks

All Precambrian rocks in the sampled region belong to the southern part of Canadian Shield, the Grenville Province. It is composed of highly metamorphosed Archean and Aphebian rocks (amphibolite, gneiss, quartzite, crystalline limestone etc.) intruded by younger igneous rocks (granite, syenite, diorite etc.) (Douglas, 1970). Eight tested samples are from

24

LAKE HURON

BRUCE PENINSULA

Georgian Bay

Collingwood

Goderich

LAKE ONTARIO

TORONTO

Hamilton

London

Kingston

Trenton

LAKE ERIE

Pelee Pt

St Clair

Windsor

LEGEND

PALEOZOIC

DEVONIAN

UPPER DEVONIAN

20 PORT LAMBTON GROUP
Grey shale and sandstone

19 KETTLE POINT FORMATION
Black shale

MIDDLE DEVONIAN

18 HAMILTON GROUP
Grey shale and limestone

17 DUNDEE FORMATION
Limestone

16 DETROIT RIVER GROUP
Limestone and dolomite

15 BOIS BLANC FORMATION [b]
Cherty limestone

LOWER DEVONIAN

14 ORISKANY FORMATION
Sandstone

SILURIAN

UPPER SILURIAN

13 BASS ISLANDS (BERTIE) FORMATION
Dolostone

12 SALINA FORMATION
Dolostone, shale, gypsum, salt.

MIDDLE AND LOWER SILURIAN

11 GUELPH FORMATION
Dolostone

10 LOCKPORT - AMABEL FORMATIONS
Dolostone

9 CLINTON AND CATARACT GROUPS
Sandstone, shale, dolostone [b]

ORDOVICIAN

UPPER ORDOVICIAN

8 QUEENSTON FORMATION
Red shale

7 GEORGIAN BAY
(CARLSBAD AND
RUSSELL [c]) FORMATION
Grey shale with limestone
interbeds, limestone
member on Manitoulin Island

6 BLUE MOUNTAIN FORMATION
Grey and black shale

MIDDLE ORDOVICIAN

5 SIMCOE GROUP (OTTAWA GROUP [c])
Limestone (5d, Lindsay Formation;
5c, Verulam Formation;
5b, Bobcaygeon Formation;
5a, Gull River Formation)

4 ROCKCLIFFE FORMATION
Limestone and shale

LOWER ORDOVICIAN

3 BEEKMANTOWN GROUP
Dolostone, sandstone

CAMBRO-ORDOVICIAN

2 POTSDAM GROUP
Sandstone

PRECAMBRIAN

1 Precambrian rocks

1 ● quarry number

NOTES

a Includes Onondaga Formation
in Niagara Peninsula
b Dolostone predominates on
Manitoulin Island
c Formations in Ottawa area

SOURCES OF INFORMATION

Compilation by B A. Liberty
and D F. Hewitt 1972, P G
Telford 1976, 1987

Geology from maps of the
Geological Survey of Canada and
the Ontario Geological Survey

MILES
0   25   50   75

KILOMETRES
0   40   80   120

**Figure 3.1 Map of Southern Ontario showing bedrock geology and sample location. (after Booth, et.all. 1989a)
The numbers refer to the quarries listed in Appendix A.**

Table 3.1 Stratigraphic columns of Paleozoic strata in Southern Ontario (after Booth, et.all. 1989a).

		SOUTHWESTERN ONTARIO	NIAGARA PENINSULA (SIMCOE – NIAGARA FALLS)	NIAGARA ESCARPMENT (NORTH OF HAMILTON TO MANITOULIN ISLAND)	CENTRAL ONTARIO	EASTERN ONTARIO
DEVONIAN	U	Port Lambton Gp.				
		Kettle Point Fm.				
		Hamilton Gp.				
	M	Marcellus Fm.	Dundee Fm.			
		Dundee Fm.				
		Detroit River Gp.	Lucas Fm.			
			Onondaga Fm.			
	L	Bois Blanc Fm.	Bois Blanc Fm. / Oriskany Fm.			
SILURIAN	U	Bass Islands Fm.	Bertie Fm.			
		Salina Fm.	Salina Fm.			
	M		Guelph Fm.	Guelph Fm.		
			Lockport Fm.	Lockport/Amabel Fm.		
			Clinton Gp.	Clinton Gp.		
	L		Cataract Gp.	Cataract Gp.		
ORDOVICIAN	U		Queenston Fm.	Queenston Fm.	Queenston Fm.	Queenston Fm.
				Georgian Bay Fm.	Georgian Bay Fm.	Georgian Bay Fm.
				Blue Mountain Fm.	Blue Mountain Fm.	Billings Fm.
				Collingwood Mbr.	Collingwood Mbr.	Eastview Mbr.
	M				Lindsay Fm.	Lindsay Fm.
					Verulam Fm.	Verulam Fm.
					Bobcaygeon Fm.	Bobcaygeon Fm.
					Gull River Fm.	Gull River Fm.
					Shadow Lake Fm.	Shadow Lake Fm.
						Rockcliffe Fm.
	L					Oxford Fm.
						March Fm.
						Nepean Fm.
CAMBRIAN						Covey Hill Fm.

Units not present because of erosion or non-deposition

Units in subsurface only

Gp. = Group, Fm. = Formation, Mbr. = Member

Position of the tested samples in the Stratigraphic Columns

26

Precambrian rocks. They represented four lithological rock types (crystalline limestone, granite, nepheline syenite and hornblende diorite), (Table A.1, Appendix A).

3.2.2 Palaeozoic Sedimentary Rocks

The Palaeozoic rocks in Ontario occur in a broad arc which stretches from Ottawa and the Quebec border, southwest to Windsor (Figure 3.1). Most of the sedimentary rocks in Ontario are of shallow marine origin, the local conditions at the time of deposition, such as water depth, salinity, current direction, proximity to shorelines, etc, strongly influenced the type of sediment (Booth, 1989a). The sedimentary rock types are dolostone, limestone, shally dolostone and limestone, shale, sandstone and evaporite. The Palaeozoic rock in southern Ontario possess a shallow southwesterly regional dip and, coupled with erosion, this has resulted in an exposure of successively younger rocks at the surface to the southwest (Figure 3.1). The stratigraphic formations and groups of present strata are given in ascending order in Table 3.1.

Eighty samples were collected from the Palaeozoic formations. Formations, represented in the collection are marked in Table 3.1 by black field in the narrow collum next to name of a formation. Sample numbers, rock type and formation name are given in Table A.2 (Appendix A). Brief sample descriptions are given in Table A.3 (Appendix A).

NOTE TO USERS

Page(s) not included in the original manuscript and are unavailable from the author or university. The manuscript was microfilmed as received.

This reproduction is the best copy available.

UMI

drilling. The diameter of the cores was 19 mm and the length varied from 40 mm to 55 mm. The length depended on character and dimensions of the drilled rock. If the rock was compact and large enough, the core was full size. If the rock was fractured or small, the core was not full size. The drilling was performed perpendicular to the bedding or foliation. Three cores were prepared from each rock. Numbering of the rock samples is identical with the numbering in Rigbey's work (1980). Missing sequence number means that the rock sample was not available or was too small to be drilled.

Each designed test required specific sample preparation. These sample preparations are described in section describing the tests.

4.3 Water Adsorption Test

Prior to the adsorption test, the samples were dried in the air circulating oven at 105°C and weighed on laboratory scale with accuracy 0.01g. Dry samples (drill cores) were put into air-tight chamber with 98% RH and room temperature (about 22°C). The 98% RH was maintained by using super saturated solution of hydrated copper sulphate ($CuSO_4.5H_2O$), (Weast, 1973). The previous studies (Hudec, 1983) proved that 72 hours was sufficient time to achieve equilibrium between the water vapour pressure in the chamber and the adsorbed water in the samples. After 72 hours the samples were individually removed from the chamber and weighed.

Variables which describe water adsorption test and their calculations are given in Table D.1 (Appendix D).

4.4 Water Absorption Test

All samples were dried at room temperature (22°C) and relative humidity of about 50% and weighed. Then they were submerged in tap water for 24 hours. After 24 hours in the water bath, the samples were towelled surface dry and weighed to an accuracy 0.01g. Water absorption test was done two times. It was done before and after the microwave and freezing tests.

Variables which describe water absorption test and their calculations are given in Table D.2 (Appendix D).

4.5 Vacuum Saturation

The dry samples were put into water in a cooking pot. The water was brought to boiling and remained boiling for 4 hours. After boiling, the samples remained in the water to cool down. Afterwards, they were towelled surface dry and weighed.

Variables which describe vacuum saturation test and their calculations are given in Table D.3 (Appendix D).

4.6 Rate of Water Absorption Test

In this test only one sample from each rock core was tested. Dry sample was put into flat container with water depth of 0.5 cm. As the samples started to absorb the water by capillary suction, the weight of the samples increased. Increase of the weight was recorded in exponentially increasing time intervals. The reading intervals were: 15, 30 seconds, 1, 2, 4, 8, 16 and 32 minutes.

Since in 32 minutes some of the samples were fully saturated while other were not, regression lines were calculated for each sample to determine the absorption rate. The regression was calculated between observed absorbed water weight increase and time.

Variables which describe rate of water absorption test and their calculations are given in Table D.4 (Appendix D).

4.7 Microwave Heat Absorption Test

4.7.1 Test Apparatus

The design of the apparatus for the microwave heat absorption test facilitates the recording of a sample temperature and its change after microwave heating of the samples.

Figure 4.2 shows the setup of testing apparatus for microwave tests. Source of microwave energy was *Solid State* microwave oven (model 420) with input power 1500 W made by Litton Systems Inc. Temperature of the samples was measured with T type thermocouple (copper versus a copper-nickel alloy). The thermocouple was housed in a hole drilled into a 3 millimetre thick circumferential wall of copper cylinder in which a tested sample was housed (Figure 4.3). The copper cylinder and the tested sample were insulated by the PVC cylinder. Since the microwave oven and housing cylinder with thermocouple were 6 m apart, a styrofoam case served as an insulator to transport the sample to the housing cylinder (Figure 4.3). The amplified signal from the thermocouple was converted to digital signal and collected by a PC computer. The data acquisition was controlled by program written by the author. The program was written in graphical programming language LabVIEW -student edition.
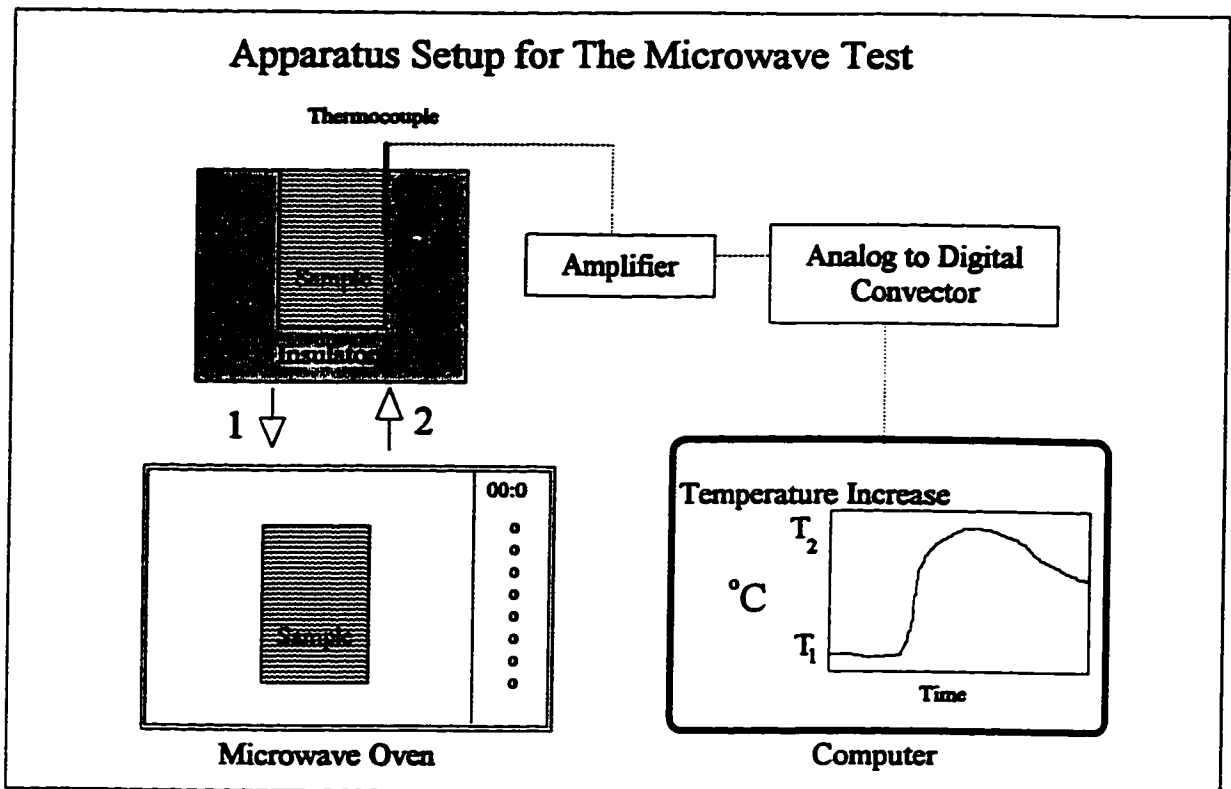
Figure 4.2 Illustration of the setup of the apparatus for the microwave heat absorption test.
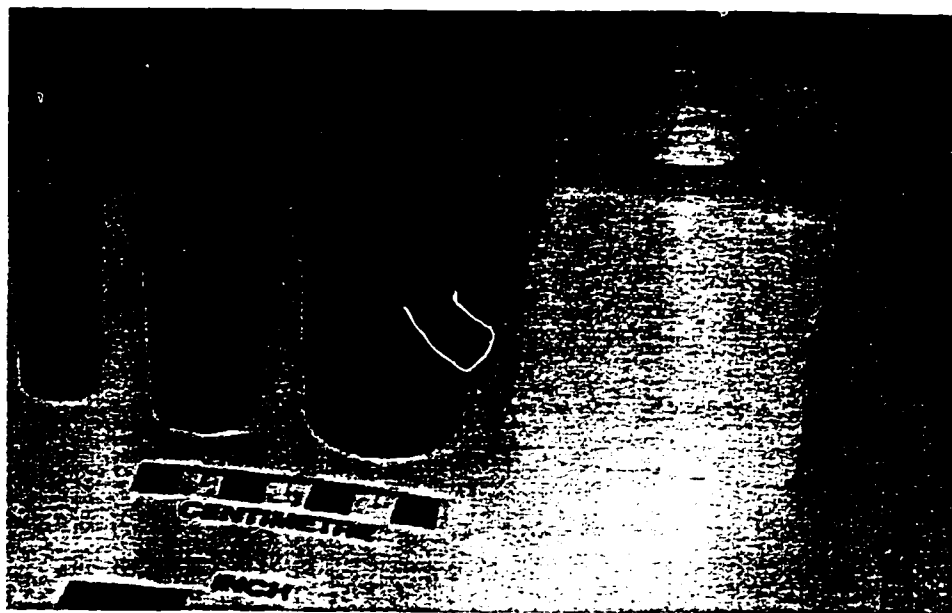
Figure 4.3 Photographic image of a tested sample, copper cylinder with thermocouple, PVC cylindrical insulator and styrofoam insulation case.

4.7.2 Sample Preparation

Each sample was tested three times. The first run of tests was done on dry samples. The second run was done on samples with adsorbed water. Third run was done on samples with absorbed water.

4.7.2.1 Sample Preparation for Microwaving of Dry Samples.

Samples were dried in a circulation oven at temperature 105°C for 24 hours. After drying they were sealed in a plastic bag with silica gel. The samples were then transferred into a desiccator with silica gel shortly before the test.

4.7.2.2 Sample Preparation for Microwaving of Samples with Adsorbed Water.

The dry samples were exposed to 98% humidity in an air-tight chamber with super saturated solution of copper sulphate ($CuSO_4.5H_2O$) at room temperature (22°C). They remained in the chamber for three days. Each day, only the samples which were to be tested were taken from the chamber and kept in the desiccator with humidity 98%. None of the samples were sitting in the chamber fore more than 4 days.

4.7.2.3 Sample Preparation for Microwaving of Samples with Absorbed Water.

The samples were saturated with water in water bath at room temperature for 24 hours. Each morning only samples which were tested during the next day were inserted into the water bath. A sample which was ready for testing was removed from the bath and surface dried before being inserted into the copper cylinder.

4.7.3 Test Procedure

At the beginning of each test a weight of tested sample was taken. The sample then was inserted into a copper cylinder where it sat until the temperature of the sample and copper cylinder equilibriated. The establishment of the temperature equilibrium was monitored by permanent recording of the temperature by the computer and displayed on the computer screen. It took about 1 minute to equal the temperatures. The reading intervals were set at 10 seconds. The sample then was removed from the copper cylinder and inserted into a styrofoam insulation case. The case with the sample was then inserted into a microwave oven at marked position and "zapped" for 9 seconds at full power. The zapped sample was inserted back into the copper cylinder and the temperature increase was recorded. The equilibrium between new sample temperature and copper cylinder was reached after about 1.5 minutes. Afterwards the recorded data were saved on the hard drive and next sample was weighed for testing.

4.7.4 Calculation of the Results

Calculation of the results is based on the observed temperature increases of the samples after microwave heating. The observed temperature increase of a dry sample (dT_1) is caused only by heat absorbed by dielectric molecules present in minerals (dTs_1), therefore:

$$dT_1 = dTs_1 \qquad (4.1)$$

The observed temperature increase of the sample with adsorbed water (dT_2) is equal to sum of temperature increase due to heat absorbed by minerals (dTs_2) and due to heat absorbed by adsorbed water (dTa_2):

$$dT_2 = dTs_2 + dTa_2 \qquad (4.2)$$

34

The observed temperature increase of the sample with absorbed water (dT_3) is the sum of temperature increases due to heat absorbed by rock minerals (dTs_3), adsorbed water (dTa_3), and bulk water (dTb_3):

$$dT_3 = dTs_3 + dTa_3 + dTb_3 \qquad (4.3)$$

Based on equations (4.1) and (4.2), the calculated temperature increase of the sample due to heat absorbed by adsorbed water (dTa_c) can be calculated:

$$dTa_c = dT_2 - dTs_1 \qquad (4.4)$$

Calculation of temperature increase of the sample due to heat absorbed by bulk water (dTb_c) are based on equation (4.2) and (4.3):

$$dTb_c = dT_3 - dT_2 \qquad (4.5)$$

Based on the equations (4.1), (4.4), (4.5), the total amount of heat absorbed by rock minerals (Hs), adsorbed water (Ha) and bulk water (Hb) can be calculated:

$$Hs = dTs * (Cs * Ms + Cc * Mc) \qquad (4.6)$$

$$Ha = dTa_c * (Cs * Ms + Ca * Maw + Cc * Mc) \qquad (4.7)$$

$$Hb = dTb_c * (Cs * Ms + Cb * Mbw + Cc * Mc) \qquad (4.8)$$

Where
dTs, dTa_c, dTb_c = temperature increase of the sample due to heat absorbed by rock minerals, adsorbed water and bulk water respectively,
Cs, Ca, Cb, Cc = heat capacity of dry rock, adsorbed water, absorbed water and copper cylinder respectively,
Ms, Ma, Mb, Mc = weight of dry rock, adsorbed water, absorbed water, and copper cylinder respectively.

Variables which describe results of the microwave test and their calculations are given in Table D.5 (Appendix D).

4.7.5 Source of errors

The potential sources of error are the precision and reliability of the thermocouple in measuring the absolute temperature and the steadiness of microwave energy flux. The thermocouple errors are discussed in Chapter 4.8.4, as source of errors in freezing test.

The error due to constancy of energy flux depends upon the steady power output of

Repeatability of The Microwave Heating

Std. Dev.	0.06 C	0.06 C	0.02 C	0.02 C
Range	0.18 C	0.18 C	0.07 C	0.05 C
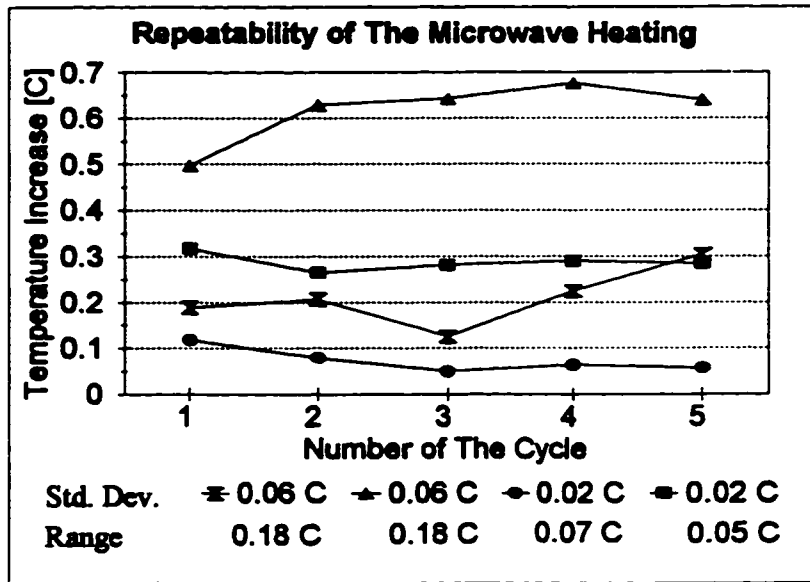
Figure 4.4 The repeatability test of the microwave heating test done in five cycles with four samples and under the same conditions.

the microwave oven and on a constant position of the tested samples in the oven. Repeatability test was used to determine the cumulative error of the microwave test. Four samples were heated in the microwave oven under the same conditions for five times. The result of the tests is shown in Figure 4.4. The graph suggests that the results of microwave heating are constant with ±0.2°C. None of the values of the standard deviations exceed 0.1 °C and none of the ranges axseed 0.2 °C. However, the graph also suggests that the standard deviations and ranges are large when smaller temperature increases are involved.

36

4.8 Freezing Test

4.8.1 Test Apparatus

The specially designed testing apparatus for the freezing test facilitated measuring of a sample temperature, freezing temperature, released latent heat of freezing pore water, and length change on freezing.

Figure 4.5 and Figure 4.6 show the testing apparatus and scheme of the setup for the freezing test respectively. The refrigerator (RTE 220 made by NESLAB Instrumentation Inc.) used for a freezing of the samples had two units. Cooling compressor, control panel and reservoir of antifreeze cooling fluid (glycol) were parts of one unit. Specially designed second unit (heat exchanger) was composed of massive aluminum block (cylindric shape) with three holes in it (Figure 4.7). The aluminum block served as heat capacitor which kept constant temperature in the system. Each hole was equipped with insulating PVC cylinder and copper cylinder for housing of tested samples. Two holes were used during the test, one was spare. PVC insulator slowed down the heat exchange between the sample and aluminum block. If the test was done without it, the loss of heat would be too fast and not measurable. Heat exchange between aluminum block and the cooling fluid was facilitated by copper pipe coiled around the aluminum block. The temperature of aluminum block was kept at about -17°C. The whole aluminum block was housed in an insulating box from PVC and styrofoam which insulated the aluminum block from the room environment. The two units were connected by two insulated plastic tubes through which the cooling fluid flowed. One tube served as an inlet of cooling fluid and the other as an outlet.

37
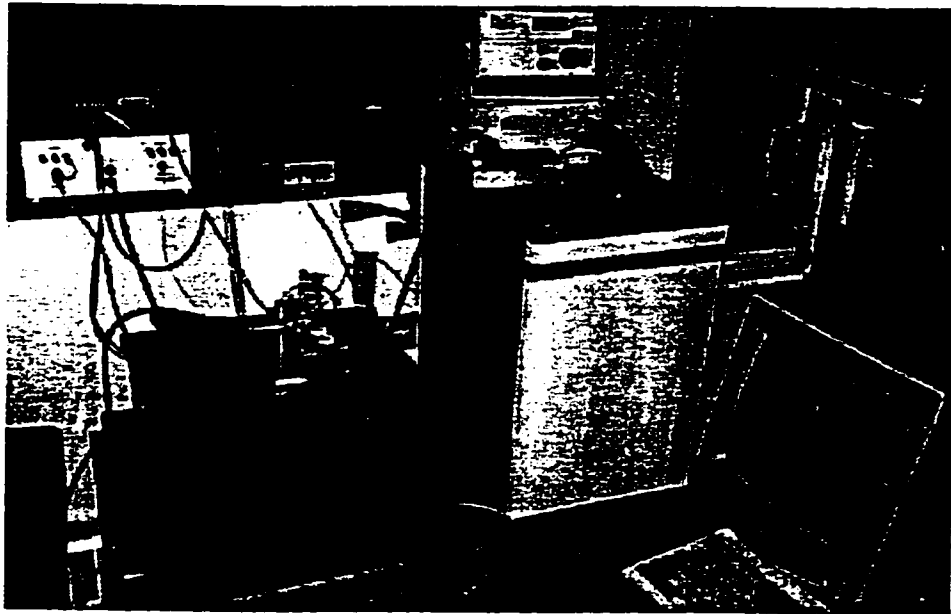
Figure 4.5 Photographic image of the testing apparatus for the freezing test.
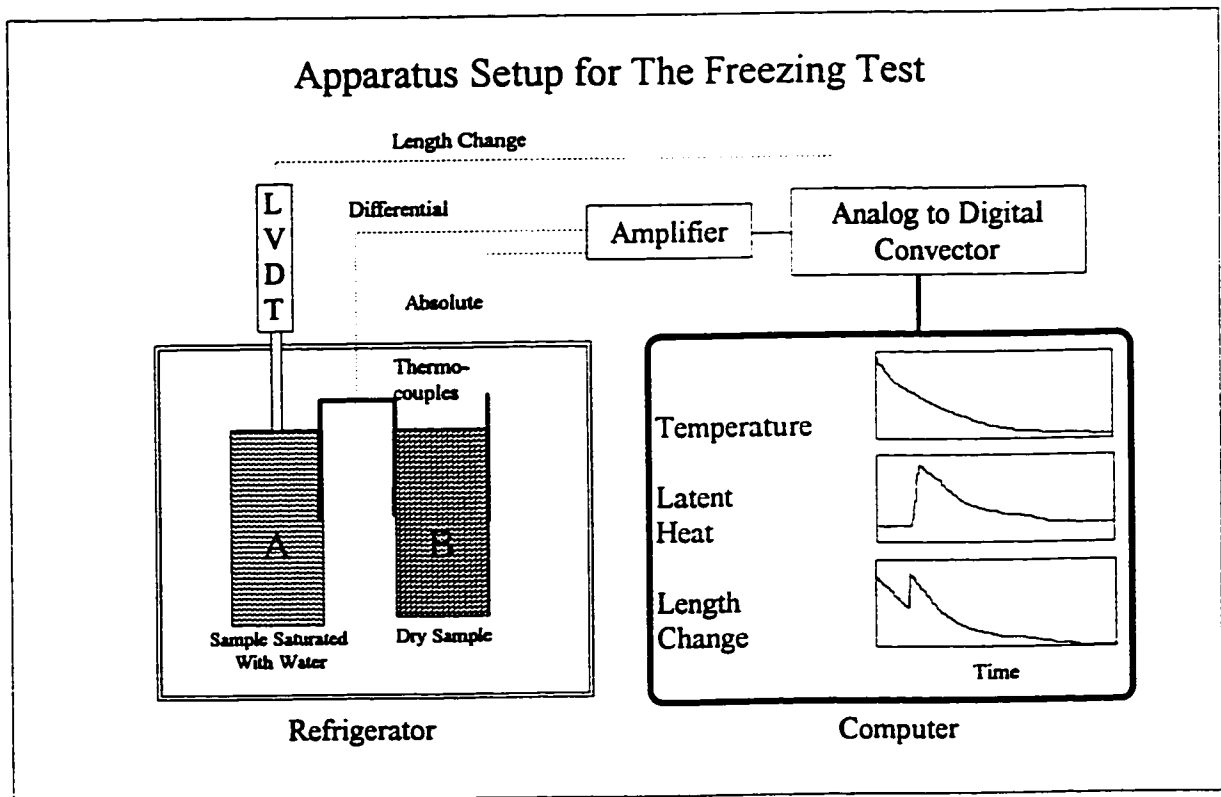
Figure 4.6 Illustration of the setup of the apparatus for the freezing test.

38
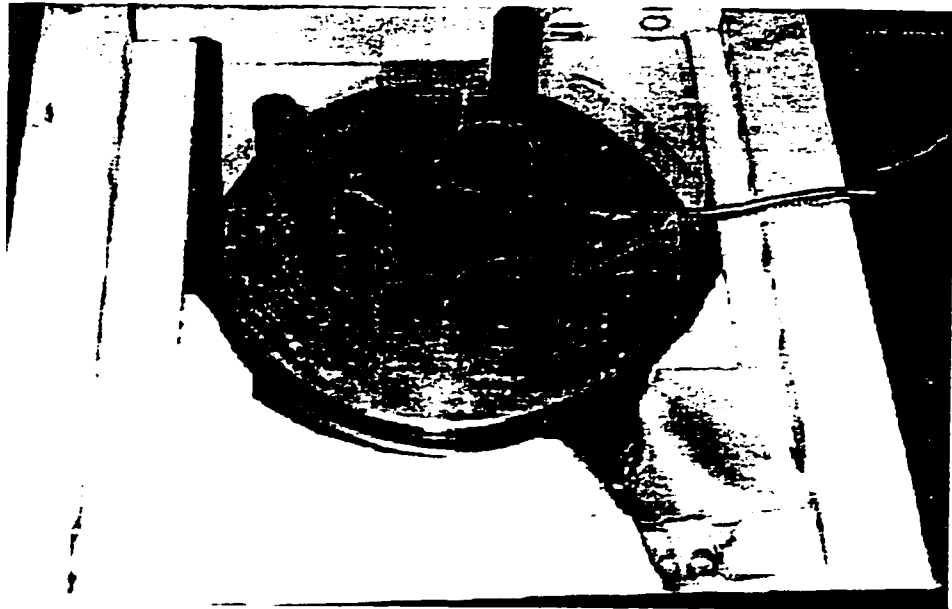
Figure 4.7 Photographic image of the aluminum block with three thermally insulated holes for housing the tested samples during the freezing test.

Thermocouple Configuration for Measuring of A Differential Temperature

Amplifier

copper wire
copper-nickel
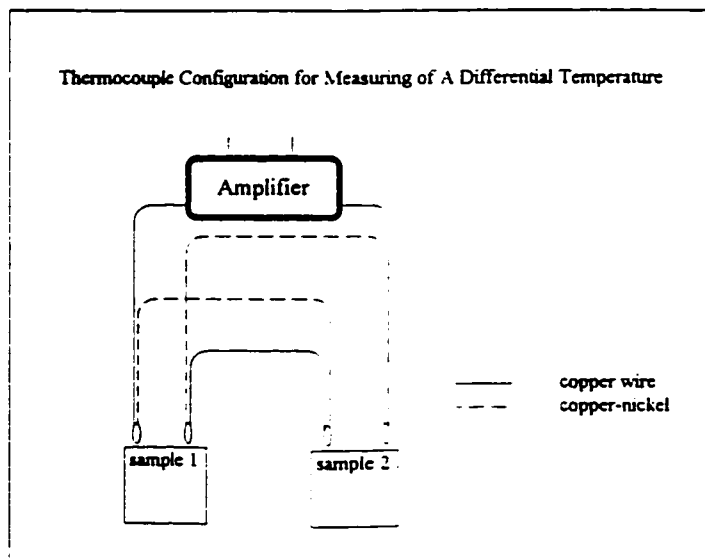
sample 1

sample 2

Figure 4.8 Illustration of the thermocouple configuration for measuring of a differential temperature.

The temperature of the test sample and the freezing temperature of the pore water were measured by single T type thermocouple (copper versus a copper-nickel alloy). The latent heat of freezing water was measured by T type thermocouple in differential mode (Figure 4.8). It was measured as differential temperature between tested sample and dry sample (see 4.8.3.1). The thermocouples were inserted into holes drilled into a 3 millimetres thick circumferential walls of the copper cylinders.

The length change on freezing was measured by electronic displacement transducer (LVDT 0242-0000 L6 made by TRANS-TEK Inc.). The LVDT was mounted on top of the lid of the insulating box. The LVDT rod was in direct touch with tested sample through a small hole in the lid.

Both the analog signal from LVDT, and amplified analog signal from thermocouple were converted into digital signals by analog to digital convertor and then recorded by the computer. The program controlling the data acquisition was written by the author in graphical programming language LabVIEW-student edition (Wells, 1995).

4.8.2 Sample Preparation and Test Procedure

Prior to freezing test the dry samples were put into water bath at room temperature, where they remained until the test. Sample, which was going to be tested, was towelled dry and weighed. Afterwards the sample was inserted into copper cylinder and sealed with plastic tape to prevent drying while cooling. The sample was then put into a refrigerator, together with dry sample, in order to lower and equilibrate the temperatures of both. It took about 10 minutes to cool the samples up to about 4°C (the cooling was done while another sample was being tested). Then the samples in the copper cylinder were put into PVC insulating cylinders

in the heat exchanger, and the thermocouple and LVDT were set up for recording of temperature and length change respectively. The controlling programme was turned on and the data recorded. One test took from 15 to 40 minutes.

4.8.3 Measurement and Calculation of the Latent Heat of Freezing Water.

4.8.3.1 Measurement of Latent Heat

A rate of temperature decrease of both the tested sample with saturated water and dry sample was a function of a heat conductivity of the PVC thermal insulator and the heat capacity of system inside of the insulator (copper cylinder, solid rock and pore water). The insulators of both samples had the same heat conductivity and also the rock mass and heat capacity of both samples was about the same. Since the thermal capacity of the pore water represented only about 4.3% of the total heat capacity of the system (Table 4.1), both samples had about the same rate of temperature decreases, i.e. the differential temperature between them was zero until the freezing of pore water occurred and the latent heat of freezing water was released. The latent heat of freezing pore water in the tested sample was proportional to the differential temperature between the tested sample with saturated water (sample A, Figure 4.6) and dry sample (sample B, Figure 4.6). Figure 4.9 shows a typical freezing curve (running average) of differential temperature from which the latent heat was calculated.

Differential Temperature vs Time

Area A is proportional to latent heat of freezen water.

Legend: — Observed Diff. Temp. — Running Average
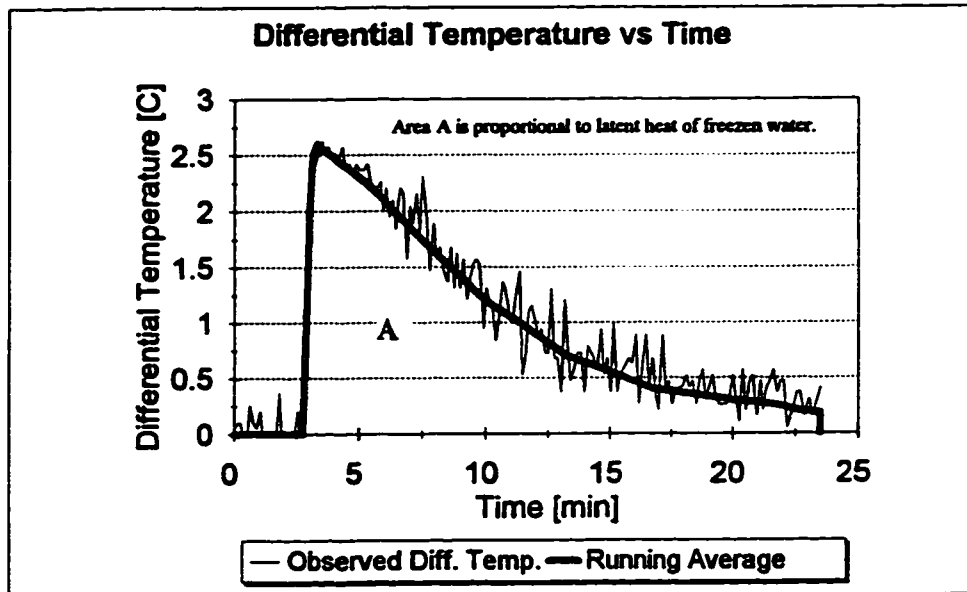
Figure 4.9 A typical calorimetric output from the apparatus for the Freezing Test.

TABLE 4.1, The total heat capacity of the dry rock, pore water and copper cylinder

	Average Weight	Heat Capacity		
		Per gram of mass	Total	% of total
	[g]	[J/(g*C)]	[J/C]	[%]
Dry rock	38.29	0.86	33.10	88.36
Pore water	0.38	4.22	1.60	4.28
Copper cylinder	125.36	0.02	2.76	7.36
Whole system	164.03		37.46	100

4.8.3.2 Calculation of the Latent Heat of Freezing Water.

Heat output H (in watts) from both samples is expressed by the equation:

$$H = K * S * \frac{Ta - Ts}{W} \qquad (4.9)$$

42

Where

K - heat conductivity (of the PVC insulator) [J/(C*m*sec)]

S - area of contact surface (area of the sample) in square meters [m^2]

W - width of heat conductor (insulator) in meters [m]

(Ta - Ts) - temperature difference between temperature of the sample Ts and the aluminum block Ta in degree of Celsius [°C]

As was discussed above, the heat capacity of the samples, copper cylinders and the heat conductivity of the thermal insulators were about the same. The only parameter which varied in the equation for both samples was the differential temperature between samples (Ts) and aluminum block. While the temperature of the aluminum block was the same for both samples, the temperature of the samples was equal only until the freezing of pore water in the tested sample occurred. The freezing of pore water generated latent heat which warmed up the test sample. The temperature increase of the tested sample was proportional to amount of frozen water. Since the latent heat of freezing pore water was the only heat input into the system, and it occurred only in the tested sample, the temperature increase could be recorded as differential temperature between tested sample and dry sample.

From the Equation (4.9) it is clear, that the heat transfer through the insulator increases with increasing differential temperature (Ta - Ts). It means, that more heat is conducted through insulator from the tested sample after it is warmed up by the latent heat of freezing water. It also means that the temperature of tested sample and dry sample equalize after a certain time. Figure 4.9 shows a graph with a plot of the differential temperature between the two samples. The zig-zag line represents observed the differential temperature and the bold line represents the statistically smoothed differential temperature. The spikes on the line are caused by unstable signal from amplifier. The curve of the differential temperature is proportional to the heat output in watts (Joules per second) and the area enclosed between

43

curve and X axis represents the total heat output in Joules (area A). The area A can be converted into total energy or amount of frozen water by the system constant.

The calculation of the system constant was based on freezing test in which both, the amount of frozen water and the area A were known. The only unknown was the system constant. Calculations of system constant are given in Table 4.2 . The area A is known from the calorimetric (freezing) test. The amount of frozen water is based on the assumption that 100% of pore water freezes in a sample with large pores (sand with the coarse grains of the same size). The system constant is an average of three calorimetric tests for the constant. Since the length of the samples was not constant, the system constant was related to one millimetre of the sample by dividing the constant by length of the tested sample. Then, when

TABLE 4.2   Calculation of calorimetric system constant

	Area A	Weight of frozen water	Length of the sample	System Constant
	A	FW	L	FW / (A * L)
	[C*s]	[g]	[mm]	[g / (C *s * mm)]
Test 1	7872.21	1.67	49.89	4.252E-06
Test 2	6454.61	1.71	50.19	5.279E-06
Test 3	5816.82	1.69	50.26	5.781E-06
Mean	6714.55	1.69	50.11	5.02257E-06
Std. Dev.	859.00	0.02	0.16	6.362E-07

NOTE
Sdt. Dev.   = Standard deviation   g   = gram
C   = Degree of Celsius   mm   = millimeter
s   = second

the amount of frozen water is calculated, the calorimetric output is multiplied by system constant and by the length of tested sample (see Table D.6 (Appendix D). Variables which describe freezing test and their calculations are given in Table D.6 (Appendix C).

44

4.8.4 Source of Errors

The result of calorimetric calculations depends on the precision of the thermocouple measuring the differential temperature. The summary of measurements of absolute and

TABLE 4.3 Results of the test of the calorimetric system and the LVDT at a constant temperature, zero differential temperature and zero length change.

	Unit	Mean	Std. Dev.	Range		Count
				Min	Max	
Differential temperature	[C]	0.0	0.2	-0.3	0.4	50
Absolute temperature	[C]	-14.4	0.0	-14.5	-14.4	50
LVDT	[mm]	0.000	0.001	-0.002	0.002	50

differential temperature, and length changes of samples with constant temperature and with zero differential temperature and zero length change is given in Table 4.3. The table shows that the standard deviation from readings of zero differential temperature is 0.2°C. It means that the average offset from the mean differential temperature is ±0.2°C. The range for 50 readings is within the interval <-0.3, 0.4> i.e. 1.1 °C. The mean of absolute temperature is -14.4 °C. The standard deviation is less than 0.0°C. The range is 0.1°C.

The absolute temperature was measured on dry sample (sample B, Figure 4.6). Since the differential temperature was not always zero prior the occurrence of freezing of pore water, the freezing temperature was calculated by subtracting of differential temperature between sample A and B (Figure 4.6) from the absolute temperature. Of course, it combines the errors of both thermocouple for measuring of differential temperature and thermocouple for measuring of absolute temperature.

Table 4.3 shows that the standard deviation for 50 readings of zero length change measured by LVDT is 0.001mm and the range is 0.004 mm.

4.8.5 Threshold Limit of the Calorimetric System.

The threshold limit of the calorimetric system measuring latent heat of the freezing water was controlled by the precision of the measurement of the differential temperature and by the heat capacity of the tested sample and copper cell. The latent heat of freezing water, in order to be detected, had to be greater than heat capacity of the sample and copper cell combined. Also, the signal picked up by the thermocouple had to be strong enough to be greater than the standard error (standard deviation) of the thermocouple measuring differential temperature. Table 4.4 shows input data for calculation of the threshold limit of the minimal detectable latent heat of freezing water and the minimal mass of the detectable frozen water. The calculation showed that the threshold limit for the calorimetric system was 0.06% content of water (by weight). Weights used in the calculation were the average weight of the tested samples and the average weight of four copper cylinders. Heat capacity of copper and latent

TABLE 4.4 Input data and the calculations of the threshold limit of the calorimetric system

	Weight (average) (m)	Heat capacity		Lateral Heat of fusion	Minimal amount of detectable frozen water
		per gram of mass (H)	total (H *m)		
	[g]	[J/(C*g)]	[J/C]	[J/g]	[%]
Dry Rock	38.29	0.86	33.10		
Copper Cell	125.36	0.02	2.76		
Frozen Water				333.77	0.06
Sum			35.86		

heat of fusion (latent heat of freezing water) were taken from the published tables (Weast, 1973). Heat capacity of dry rock is an average value of heat capacity of dry rocks (Smith and Van Ness 1975). The minimal detectable amount of frozen water (MFw) is calculated according to equation:

$$MF_w = \frac{C_r * m_r + C_c * m_{Cu}}{LH_w * m_s} * StD * 100 \%$$ 4.10

Where

C_r, C_c - heat capacity of dry rock and copper cell respectively [J/(°C*g)]

LH_w - latent heat of freezing water [J/g]

m_r, m_c - weight of dry rock and copper cell respectively [g]

StD - standard deviation on measuring of differential temperature [°C]

4.9 Tests on Aggregate Durability Adopted from Rigbey 1980.

The results adopted from Rigbey (1980) were the freeze-thaw loss and the magnesium

sulphate ($MgSO_4*5H_2O$) loss. Rigbey (1980) contains two sets of freeze-thaw test data. The

results used here are the average of the two sets results.. The complete description of

experimental procedure for the adopted tests is in Rigbey (1980).

47

5 STATISTICAL ANALYSIS AND DISCUSSION OF THE RESULTS

5.1 Statistical Analysis

5.1.1 Introduction

The statistical analysis was employed to study the relationship among variables describing the samples, and to distinguish sample groups with a distinct characteristics.

The list of variables included into statistics is given in Table 5.1. Variable's names describing results of microwave tests starts with capital letter "M". Variable's names describing results of freezing tests start with capital letter "C". Variable's names describing other properties of tested samples (porosity, adsorbed water etc.) start with capital "R". Detail descriptions of the variables and their calculations is given in Appendix D.

5.1.2 Sample Grouping

For statistical purposes, the tested samples were grouped into three groups:

(1) entire sample population (**Group ALL**)
(2) sample population which showed freezing during the freezing test (**Group F**)
(3) sample population which did not show freezing during the freezing test. (**Group N**)

Rock types of samples in each group are given in the Table 5.2. Sample distribution of each group is given in Appendix B, Table B2.

5.1.3 Description and Significance of Employed Statistics

Figure 5.1 shows the flow chart of the statistical methods employed. The statistical analyses included:

48

TABLE 5.1 List of the variables included into the statistical analysis.

	ACRONYM	NAME	UNIT
N	CRDL	Freezing expansion	[mm/10m]
N	CTF	Freezing temperature	[C]
N	RDEN	Density	[g/cm3]
L	RFRTH	Freeze-thaw loss	[% of dry r]
L	RMGSO4	MgSO4 loss	[% of dry r]
	RADS	Adsorbed water	[% of dry r]
	RBUS	Bulk water	[% of dry r]
	RCAP32S	Rate of water absorption (after 32 min.)	[% of dry r]
	RDRYLOSS	Loss of dry weight (after one drying cycle and freeze-thaw loss after one freezing cycle)	[% of dry r]
	RPORO	Porosity (vacuum absorbed water)	[% of dry r]
	RVABGNS	Gain of vacuum absorbed water	[% of dry r]
	CFWS	Observed frozen water	[% of dry r]
	CUFBUS	Observed unfrozen bulk water	[% of dry r]
	CUFWS	Observed total unfrozen water	[% of dry r]
	MQABS	Heat absorbed by absorbed water	[J/g of dry r]
	MQBUS	Heat absorbed by bulk water	[J/g of dry r]
	MQADS	Heat absorbed by adsorbed water	[J/g of dry r]
N	RVABGNV	Gain of vacuum absorbed water pore fraction	[% of Vac w]
N	RADSB	Adsorbed water fraction	[% of ABS w]
N	RBUB	Bulk water fraction	[% of ABS w]
N	RBUGNB	Gain of bulk water water fraction	[% of ABS w]
N	RBUV	Bulk water pore fraction	[% of Vac w]
N	RCAP32B	Rate of water fraction absorption (after 32 min.), (capillary ris	[% of ABS w]
N	CFWB	Observed frozen water fraction	[% of ABS w]
N	CFWV	Observed frozen water pore fraction	[% of Vac w]
N	CUFBUB	Observed unfrozen bulk water fraction	[% of Bulk w]
N	CUFBUV	Observed unfrozen bulk water pore fraction	[% of Vac w]
N	CUFWB	Observed total unfrozen water fraction	[% of ABS w]
N	CUFWV	Observed total unfrozen water pore fraction	[% of Vac w]
N	RSATAFT	Degree of saturation after testing	[% of Vac w]
N	RSATBIF	Degree of saturation before testing	[% of Vac w]
L	MQABAB	Heat absorbed by absorbed water fraction	[J/g of w
L	MQADAD	Heat absorbed by adsorbed water fraction	[J/g of w]
L	MQBUBU	Heat absorbed by bulk water fraction	[J/g of w]

L - log value was used in statistics
N - normal value was used in statistics
r rock
w water
g gram
J Joule
m meter
mm millimeter
ABS Absorbed water (24 h water bath)
ADS Adsorbed water
Bulk Bulk water
Vac Vacuum saturated water
% weight percent
■■■ variable related to weight of dry rock (either percent or gram of dry rock)
▒▒▒ variable related to weight of water (either percent or gram pore water)
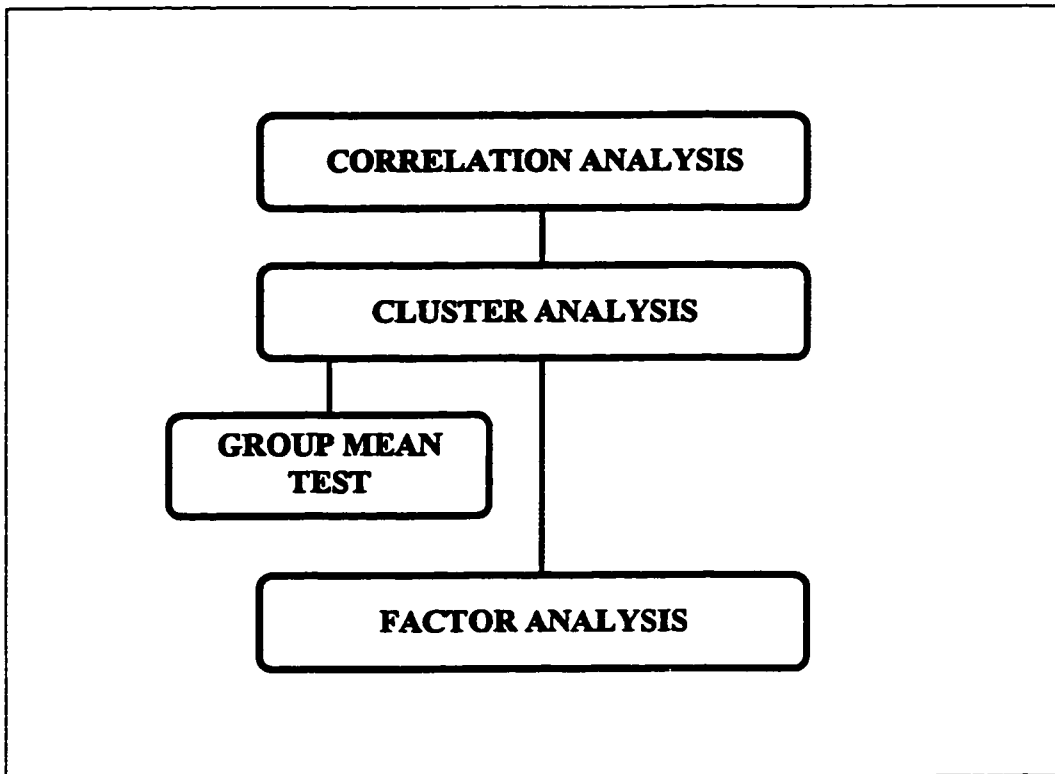
Figure 5.1 Flow chart of the statistical analysis.
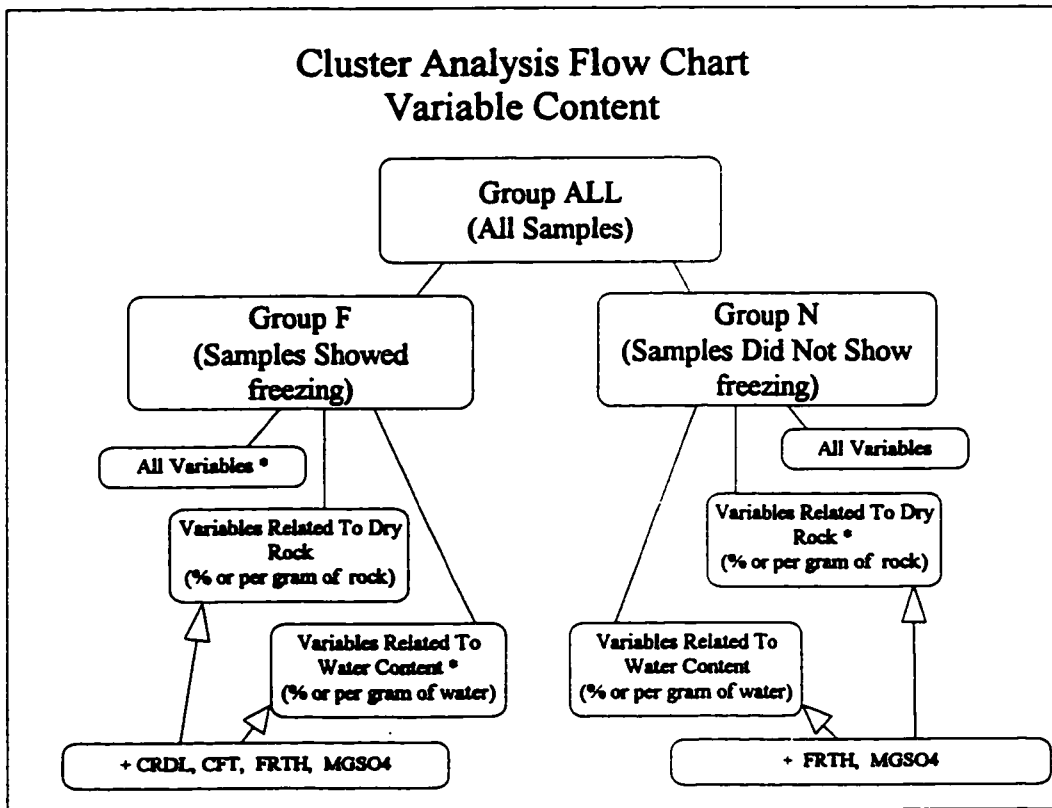
Figure 5.2 Flow chart of the cluster analysis and variables included into the analysis.
* - indicates variables which gave clusters with the most significant differences

TABLE 5.2 Rock type distribution in Group ALL, Group N and Group F

	Limestone		Dolomite		Sandstone		Igneous & Metamorpic		Shale	
	Count	% of tot. L	Count	% of tot. D	Count	% of tot. S	Count	% of tot. I&M	Count	% of tot.Sh
Gropu F	14	48	35	74	4	100	0	0	0	0
Group N	15	52	11	26	0	0	7	100	2	100
Group ALL	29	100	46	100	4	100	7	100	2	100

TABLE 5.3 Statistical summary of test results of the entire sample population

	MEAN	Range of Values		STD.DEV.	UNITS
		MIN	MAX		
CRDL	17.34	1.20	67.24	16.07	[mm/10m]
CTF	-3.50	-5.66	-1.16	1.17	[C]
RDEN	2.68	2.21	3.82	0.17	[g/cm3]
RFRTH	11.71	0.64	50.96	10.09	[% of dry r]
RMGSO4	12.45	0.55	97.10	21.75	[% of dry r]
RADS	0.18	0.01	1.40	0.24	[% of dry r]
RBUS	0.94	0.01	6.29	1.05	[% of dry r]
RCAP32S	0.30	0.00	4.69	0.67	[% of dry r]
RDRYLOSS	0.23	0.01	4.57	0.67	[% of dry r]
RPORO	1.64	0.02	8.96	1.49	[% of dry r]
RVABGNS	0.22	-0.55	1.07	0.23	[% of dry r]
CFWS	1.01	0.10	5.31	1.08	[% of dry r]
CUFBUS	0.75	0.25	2.13	0.39	[% of dry r]
CUFWS	0.88	0.29	2.16	0.39	[% of dry r]
MQABS	1.32	0.19	5.84	0.99	[J/g of dry r]
MQBUS	1.17	0.15	5.81	0.92	[J/g of dry r]
MQADS	0.21	0.00	1.05	0.23	[J/g of dry r]
RABGNV	19.11	0.00	186.96	25.87	[% of Vac w]
RADSB	23.63	1.12	85.71	20.99	[% of ABS w]
RBUB	76.56	13.21	99.53	22.27	[% of ABS w]
RBUGNB	21.53	0.00	228.26	82.30	[% of ABS w]
RBUV	51.81	12.79	86.20	16.58	[% of Vac w]
RCAP32B	20.96	0.26	100.00	22.38	[% of ABS w]
CFWB	45.90	16.72	100.00	18.35	[% of ABS w]
CFWV	36.05	11.49	81.77	16.68	[% of Vac w]
CUFBUB	44.88	0.00	81.05	17.84	[% of Bulk w]
CUFBUV	34.16	-2.10	69.66	13.62	[% of Vac w]
CUFWB	54.10	0.00	83.28	18.35	[% of ABS w]
CUFWV	41.64	0.00	74.31	15.19	[% of Vac w]
RSATAFT	77.69	45.14	96.47	13.06	[% of Vac w]
RSATBIF	78.89	12.66	100.00	18.35	[% of Vac w]
MQABAB	531.40	89.71	8666.70	955.75	[J/g of w
MQADAD	176.67	13.53	1199.60	182.61	[J/g of w]
MQBUBU	274.07	26.63	1864.52	346.00	[J/g of w]

51

(1) correlation tests,
(2) cluster analysis,
(3) cluster group mean test,
(4) factor analysis.

Table 5.3 shows summary of the tests results of the entire sample population. The analyses were done using the statistical program SPSS 6.1 for PC.

5.1.3.1 Correlation Test

A correlation test indicates the existence of a linear relationship between two variables (Williams, 1986, Norusis, 1990). The degree of this relationship is expressed by correlation coefficient (R). A correlation coefficient indexes two properties of a relationship. First is magnitude of the relationship, the second is the direction of the relationship. Value 1 indicates perfect direct relationship, value -1 indicates perfect inverse relationship, value 0 no relationship at all. Values between -1 and 0 indicate some degree of inverse relationship, values between 0 and 1 indicate some degree of direct relationship (Williams, 1986):

R from (-0.2, 0.2)   : slight relationship
R from (-0.4, -0.2) or (0.2, 0.4) : low relationship
R from (-0.7, -0.4) or (0.4, 0.7) : moderate relationship
R from (-0.9, -0.7) or (0.7, 0.9) : high relationship
R from (-1.0, -0.9) or (0.9, 1.0) : very high relationship

Each sample population has a critical correlation coefficient "C_k". It is a table value which depends upon number of cases in the sample population. Correlation coefficients which fall into an interval margined by $-C_k$ and $+C_k$ are not statistically reliable (Williams, 1986). The value of the critical correlation coefficient converges to 0 with increasing number of cases and with increasing significance level. Coefficients which are significant and are within the critical interval are indicated in the text and tables by " ' ".

52

Significance of the correlation is expressed by significance level. The two tailed significance level 0.01 means that the correlation coefficient is significant to 99%. The two tailed significant level 0.05 means that the correlation coefficient is significant to 95%. The significant level 0.01 and 0.05 are in the text and in the tables denoted by " * " and " ** " respectively.

Table 5.5 shows correlation coefficients for the entire sample population. Rows or columns in the table which do not contain any significant coefficients are excluded from the table.

The cases have been included into correlation pairwise. Since some results are missing or as erratic results were rejected from the statistics, the number of cases vary from correlation test to correlation test. Number of cases included into each correlation test are given in Appendix B, Table B.3.

5.1.3.2 Cluster Analysis

Cluster analysis is a statistical method facilitating the search for relatively homogeneous groups or clusters of cases in an analyzed sample population. Individual clusters are then tested and described according the cluster group mean t-test.

Cases of the tested sample population were clustered by the complete linkage method using the squared Euclidean distances between two cases as a measure of their similarity. Small squared Euclidean distances indicate that fairly homogeneous clusters are being merged. Large distances suggest the combination of quite dissimilar members into clusters. The results of clustering are shown on dendrogram plots (Appendix B, Figure B1, Figure B2)

53

Two sample t-test was used to compare the cluster means. The t-test is a statistical model that is used for testing of significance of difference between the means of two populations, based on the means and distributions of two sets of tested samples. The significance of difference is expressed by significance level. Two tailed significance level 0.01 means that the t-test result has significance 99%, i.e. the sample populations are different with 99% significance. Two tailed significance level 0.05 means that the compared sample population are different with 95% significance. The 99% and 95% significance are in the tables denoted by " * " and " ** " respectively.

Cluster analysis and cluster group mean tests were done in three steps which are illustrated on flow diagram given in Figure 5.2. In the first step the entire sample population (88 cases) was divided into two groups. First group named "Group F" includes samples which showed freezing (53 cases). Second group named "Group N" includes samples which did not show freezing (35 cases). Appendix B, Table B2 shows distribution of samples in Group F and Group N. The first step included group mean test between Group F and Group N. The results of the group mean tests are given in Appendix B, Table B1.

The second step of cluster analysis was performed on Group F. Several runs of the analysis with different combinations of variables were done. In the first run all the variables were included in the analysis. In the second run, variables values expressed in terms of percent or per gram of dry rock (PGR) were used (Table 5.1). In the third run variables expressing their values in terms of percent or per gram of water (PGW) were used (Table 5.1). In addition to those variables, freezing expansion, freeze-thaw and $MgSO_4$ loss, and freezing temperature (CRDL, RFRTH, RMGSO4, CFT) were included into the second and third runs.

The cluster analysis done with all variables and the PGW yielded similar sample distribution. In both cases the samples were distributed into three clusters. (Cluster 1, Cluster 2, Cluster 3; Appendix B, Figure B1). Cluster analysis based on PGR gave also tree clusters, but with different sample distribution. Comparison of the cluster group means (T-test) showed the clustering based on all variables and PGW as more distinctive i.e.. it has more distinctively different means.

The third step of cluster analysis was performed on Group N, i.e. on samples which did not show freezing (35 cases). Similar variable combinations were used as in the Group F (Table 5.1).

The cluster analysis in the first and second run yielded three clusters with comparable distribution of samples. The cluster analysis in the third run produced only two clusters (Cluster 4, Cluster 5, Appendix B, Figure B2). Since the latter cluster grouping showed more significantly different cluster means, the result of this clustering was used to describe the samples.

5.1.3.3 Factor analysis

Factor analysis is a statistical technique used to reduce a large number of variables into relatively small number of factors. Each factor is used to describe relationship among sets of many interrelated variables and to describe a defined property of a tested sample population (Norusis 1990, Williams 1985).

The principal component analysis method was used to extract the eigen values. The cut-off for significant factor was set at the number of eigen values greater than or equal to one. A rotated factor loading matrix was obtained by the varimax rotation method. How well

the variables correlate with extracted factors is described by a communality number. Communality number is a sum of squared correlation coefficients between variable and each factor. If the communality number is low, it means that the variable does not correlate with any of extracted factors, and should be rejected from factor analysis. The importance of each variable is described by a loading. The higher the loading the higher influence of variable on the factor. A high positive loading means direct relationship and a negative loading means inverse direction of relationship.

The factor analysis was performed in three stages, each with different sample population and different combination of variables. Factor analysis in the first stage is performed on the entire sample population. In the second stage, it is performed on the sample population which showed freezing (Group F) and the analysis in the third stage is performed on the samples population which did not show freezing (Group N).

Only those variables which showed significantly different cluster group means were included into factor analysis (Appendix B, Table B1). In addition to those variables, variables describing rock durability (RFRTH, RMGSO4) and freezing expansion (CRDL) were added. Factor analysis in the first stage included 14 variables (Table 5.4). Factor analysis in the second stage included 12 variables (Table 5.4). Factor analysis in the third stage included 10 variables (Table 5.4). In the first try of factor analysis the gain of vacuum saturated water (RVABGNS), and the bulk water content (RBUS) were included into analysis in the first and third stage respectively. However, they had communality number less than 0.5, and were rejected from the factor analysis in the second try. In both cases the rejection improved the cumulative percentage, with all the factors account for the total variance, by about 8%. The factor statistics is given in Tables 5.9, 5.10, 5.11.

Table 5.4 List of the variables included in the factor analysis.

Group ALL	Group F	Gtoup N
1 MQBUBU	CFWS	MQBUS
2 RBUB	CUFWB	MQABS
3 RADSB	CFWB	RDRYLOSS
4 RBUS	CUFWV	RPORO
5 MQABAB	RBUS	RADS
6 RBUV	MQADS	RBUGNB
7 RCAP32S	RADS	RSATBIF
8 RVABGNS	CRDL	MQADS
9 RDEN	RFRTH	RMGSO4
10 MQABS	RMGSO4	RFRTH
11 MQBUS	RVABGNS	
12 RDRYLOSS	RSATAFT	
13 RFRTH		
14 RMGSO4		

5.1.4 Correlation Test

Correlation coefficients are given in the correlation matrix (Table 5.5). Variables which describe the amount of frozen water (CFWB, CFWS, CFWV) have a very high direct correlation between themselves and moderate and very high correlation with absorbed water, bulk water and bulk water as pore fraction (RABS, RBUS, RBUV), absorption rate (RCAP32S), porosity (RPORO), and heat absorbed by absorbed water per gram of dry rock (MQABS). They have moderate to very high inverse correlation with total unfrozen water and bulk unfrozen water (CUFWB, CUFWV, CUFBUB, CUFBUV), heat absorbed by bulk water per gram of bulk water (MQBUBU) and with bulk density (RDEN).

Table 5.5 CORRELATION COEFICIENT MATRIX (part 1)

Two Tailed Significance, * - 0.01, ** - 0.05, ' - below critical coeficient value

	CFWB	LOG CFWS	CFWV	CRDL	CUFBUB	CTF	CUFBUV	LOG CUFBUS	CUFWB	LOG CUFWS	CUFWV	LOG DRYLOSS
LOG CUFBUS				0.52								
LOG CFWS	0.87*	1.00										
CFWV	0.92*	0.86*	1.00									
CRDL	0.42	0.62*	0.47	1.00								
CUFBUB	-0.84*	-0.76*	-0.84*	-0.30	1.00	-0.17						
CUFBUV	-0.6*	-0.62*	-0.66*	-0.20	0.66*	-0.09	1.00	0.10				
CUFWB	-1*	-0.9*	-0.93*	-0.42	0.84*	-0.08	0.79*	-0.31	1.00			
LOG CUFWS	0.28	0.68*	0.39*	0.57	-0.22	0.29	-0.06	0.99*	-0.28	1.00		
CUFWV	-0.85*	-0.7*	-0.67*	-0.25	0.65*	0.03	0.84*	-0.20	-0.05	-0.07	1.00	
LOG RFRTH	0.00	0.11	0.13	0.59*	-0.16	0.08	-0.04	0.04		0.18	0.09	0.12
LOG RABS	0.68	0.93*	0.75*	0.67*	-0.66*	0.22	-0.43*	0.74*	-0.74*	0.64*	-0.46*	0.46*
RBUB	0.37*	0.39**	0.26	0.27	0.15	-0.16	0.08	0.55*	-0.40*	0.17	-0.45*	0.08
LOG RBUS	0.7*	0.94*	0.75*	0.69*	-0.59*	0.18	-0.36*	0.60*	-0.76*	0.81*	-0.50*	0.42*
RBUV	0.40*	0.53*	0.65*	0.51***	-0.32***	0.18	0.08	0.47*	-0.40*	0.50*	0.01	0.18
MQABAB	-0.19	-0.51*	-0.28	-0.55***	0.18	-0.07	-0.01	-0.63*	0.24	-0.66*	0.04	-0.23***
LOG MQABS	0.42*	0.53*	0.45*	0.37	-0.57**	0.12	-0.44*	0.25	-0.41**	0.45*	-0.24	0.45
LOG MQADAD	0.01	-0.21	-0.07	-0.33	0.11	0.16	-0.03	-0.27	0.01	-0.41**	-0.11	-0.21
LOG MQADS	-0.10	-0.17	0.04	-0.17	-0.26	0.44**	-0.16	-0.43*	0.13	-0.13	0.24	0.25***
LOG MQBUBU	-0.44*	-0.64*	-0.46*	-0.47	0.24	-0.21	0.07	-0.63	0.51*	-0.54*	0.32***	-0.10
LOG MQBUS	0.35**	0.41**	0.33	0.15	-0.41**	-0.09	-0.36	0.22	-0.34**	0.34**	-0.27	0.46*
RABGNV	-0.41**	-0.44**	-0.34**	0.08	0.27	0.17	0.27	-0.30**	0.42**	-0.24	0.37*	0.12
LOG RADS	0.08	0.17	0.24	0.10	-0.46*	0.45*	-0.26***	-0.14	-0.07	0.26	0.16	0.39*
RADSB	-0.35**	-0.36**	-0.24	-0.32	-0.15	0.23	-0.06	-0.53*	0.36**	-0.13	0.45*	-0.09
RBUGNB	-0.44*	-0.53*	-0.40*	-0.16	0.27	0.07	0.23	-0.45*	0.45*	-0.38**	0.33*	0.21
RCAP32B	0.35**	0.37*	0.27	0.33	-0.15	-0.15	-0.22	0.39*	-0.37*	0.25	-0.42*	0.00
LOG RCAP32S	0.52*	0.69*	0.50*	0.71**	-0.33	0.07	-0.30***	0.70*	-0.56*	0.63*	-0.46*	0.34*
RDEN	-0.56*	-0.71*	-0.50*	-0.55***	0.40*	-0.04	0.43*	-0.68*	0.60*	-0.63*	0.59*	-0.01
RSATAFT	0.16	0.29***	0.50	0.31	-0.31***	0.31***	0.14	0.19	-0.18	0.37	0.31***	0.17
RSATBIF	-0.14	-0.04	0.15	0.34	-0.15	0.36**	0.16	-0.07	0.17	0.22	0.46*	0.24***
LOG RPORO	0.69*	0.92*	0.63*	0.66*	-0.56*	0.15	-0.46*	0.78*	-0.76*	0.79*	-0.63*	0.44*

58

Table 5.5 CORRELATION COEFICIENT MATRIX (part 2)
Two Tailed Significance, ' - 0.01, '' - 0.05, ' - below critical coeficient value

	LOG FRTH	LOG RABS	RBUB	LOG RBUS	MBUV	LOG MGSO4	LOG MQABAB	LOG MQABS	LOG MQADAD	LOG MQADS	LOG MQBUBU	LOG MQBUS
RBUB	-0.30*	0.39*	1.00									
LOG RBUS	0.14	0.95*	0.64*	1.00								
RBUV	-0.02	0.48	0.67*	0.63*	1.00							
LOG MQABAB	-0.07	-0.65*	-0.53*	-0.73	-0.58*	-0.41*	1.00					
LOG MQABS	0.22	0.67*	-0.03	0.53*	0.18	0.30*	-0.21	1.00				
LOG MQADAD	-0.15	-0.19	0.15	-0.12	0.01	-0.23	0.52*	-0.37*	1.00			
LOG MQADS	0.44	0.21	-0.46*	0.04	-0.11	0.18	0.36*	0.22	0.35	1.00		
LOG MQBUBU	0.01	-0.64*	-0.73*	-0.78	-0.66*	-0.31**	0.81*	0.01	-0.04	0.25**	1.00	
LOG MQBUS	0.12	0.70*	0.21	0.62*	0.22	0.27**	-0.18	0.96*	-0.30*	0.05	0.01	1.00
LOG RADS	0.51	0.46*	-0.46*	0.25*	-0.07	0.32*	-0.02	0.53*	-0.19	0.62*	0.15	0.32*
RADSB	0.31**	-0.43*	-0.95*	-0.86*	-0.62*	-0.09	0.54*	0.02	-0.06	0.47*	0.70*	-0.22
RCAP32B	-0.21	-0.00	0.36*	0.10	0.14	0.19	-0.23**	0.17	0.07	-0.39*	-0.38*	0.31**
LOG RCAP32S	-0.02	0.70*	0.62*	0.78*	0.47*	0.39*	-0.53*	0.42*	-0.03	-0.11	-0.63*	0.54*
RDEN	-0.15	-0.38*	-0.25**	-0.38*	-0.11	-0.42*	0.18	-0.24**	0.03	0.07	0.25**	-0.29*
RSATAFT	0.28	0.43*	-0.19	0.37*	0.85*	0.29	-0.30**	0.30**	-0.22	0.32**	-0.24	0.11
RSATBIF	0.30*	0.08	-0.44*	-0.05	0.09	0.15	0.09	0.28*	-0.14	0.56*	0.22	0.08
LOG RVABGNS	0.22	0.62*	0.39*	0.66*	0.35*	0.23	-0.43*	0.34*	-0.08	0.10	-0.46*	0.41*
LOG RPORO	0.20	0.97*	0.46*	0.96*	0.39*	0.38*	-0.64*	0.59*	-0.15	0.10	-0.67*	0.67*

	RABGNV	LOG RADS	RADSB	RBUGNB	RCAP32B	LOG RCAP32S	RDEN	RSATAFT	RSATBIF	LOG RVABGN	LOG RPORO
LOG RADS	-0.03	1.00									
RADSB	-0.07	0.46*	1.00								
RBUGNB	0.87*	-0.14	-0.14	1.00							
RCAP32B	-0.05	-0.39*	-0.26**	-0.10	1.00						
LOG RCAP32S	0.06	0.04	-0.56*	-0.12	0.53*	1.00					
RDEN	-0.02	0.02	0.33*	-0.05	-0.30*	-0.40*	1.00				
RSATAFT	0.00	0.50*	0.22	-0.11	0.06	0.06	0.06	1.00			
RSATBIF	0.33*	0.59*	0.37*	0.16	-0.35*	-0.12	-0.14	0.75*	1.00		
LOG RVABGNS	0.34**	0.20	-0.37*	0.37*	0.54*	0.03	-0.21	0.42*	0.11	1.00	
LOG RPORO	0.06	0.34**	-0.51*	-0.10	0.76*	0.06	-0.41*	0.06	-0.06	0.66*	1.00

59

Variables describing total unfrozen water and bulk unfrozen water as fractions of absorbed water and as fractions of total pore space (CUFWB, CUFBUB, CUFWV, CUFBUV) have very high direct correlation between themselves and very high inverse correlation with frozen water fraction and frozen water as pore fraction (CFWB, CFWV). They have moderate direct correlation with bulk density (RDEN). Further, they have moderate to high inverse correlation with absorbed water and bulk water (RABS, RBUS) with porosity (RPORO), and with heat absorbed by absorbed water (MQABS). In addition total unfrozen water as pore fraction (CUFWV) has moderate inverse correlation with absorption rate (RCAP32S) and adsorbed water fraction (RADSB).

Total unfrozen water per gram of dry rock (CUFWS) has a high direct correlation with bulk unfrozen water (CUFBUS) absorbed water (RABS), bulk water (RBUS), and porosity (RPORO). It has a direct moderate correlation with unfrozen water (CFWS), bulk water as pore fraction (RBUV), absorption rate (RAP32S) and with heat absorbed by absorbed water per gram of dry rock (MQABS). It has a moderate inverse correlation with bulk density (RDEN), heat absorbed by bulk water per gram of bulk water (MQBUBU), and with heat absorbed by absorbed water per gram of absorbed water (MQABAB).

Bulk unfrozen water (CUFBUS) has a high direct correlation with total unfrozen water (CUFWS), bulk and absorbed water (RBUS, RABS), porosity (RPORO), absorption rate (RCAP32S), bulk water fraction (RBUB), and with bulk water as pore fraction (RBUV). It has a moderate inverse correlation with heat absorbed by absorbed water per gram of absorbed water (MQABAB), heat absorbed by bulk water per gram of bulk water (MQBUBU), bulk density (RDEN), adsorbed water fraction (RADSB), and with gain of bulk water fraction (RBUGNB).

60

Freezing temperature (CFT) has a moderate direct correlation only with adsorbed water (RADS) and with heat absorbed by adsorbed water (MQADS). Freezing expansion (CRDL) has a moderate direct correlations with absorbed water, bulk water, and bulk water as pore fraction (RABS, RBUS, RBUV), porosity (RPORO) and with freeze-thaw loss (RFRTH). It has a high inverse correlation with bulk density (RDEN). It must be noted, that only cases with greater expansion than 15 mm/(m*10) were included into this correlation (17 cases).

Heat absorbed by absorbed water per gram of water (MQABAB) and heat absorbed by bulk water per gram of water (MQBUBU) have very high direct correlation between themselves and moderate to high inverse correlation with most of the variables describing content of pore water and amount of frozen and unfrozen water (RABS, RBUB, RBUS, RBUV, RPORO, CFWS, CUFBUS). Heat absorbed by adsorbed water per gram of adsorbed water (MQADAD) has a moderate correlation with heat absorbed by absorbed water (MQABAB)

Heat absorbed by absorbed water and heat absorbed by bulk water both per gram of dry rock (MQABS, MQBUS) have a very high positive correlation between themselves and a moderate to high positive correlation with most of the variables describing pore water content related to weight percent of dry rock (RABS, RBUS, RADS, RPORO).

Figures 5.3, 5.4, 5.5 show bivariate plots of the correlations between the data from the calorimetric tests. Figure 5.3 shows plot of the observed unfrozen bulk water fraction (CUFBUB) versus bulk water (RBUS). The inverse correlation of the variables has correlation coefficient R = -0.55 with 99% significance level. The plot revealed that the amount of observed unfrozen bulk water fraction decreases

61
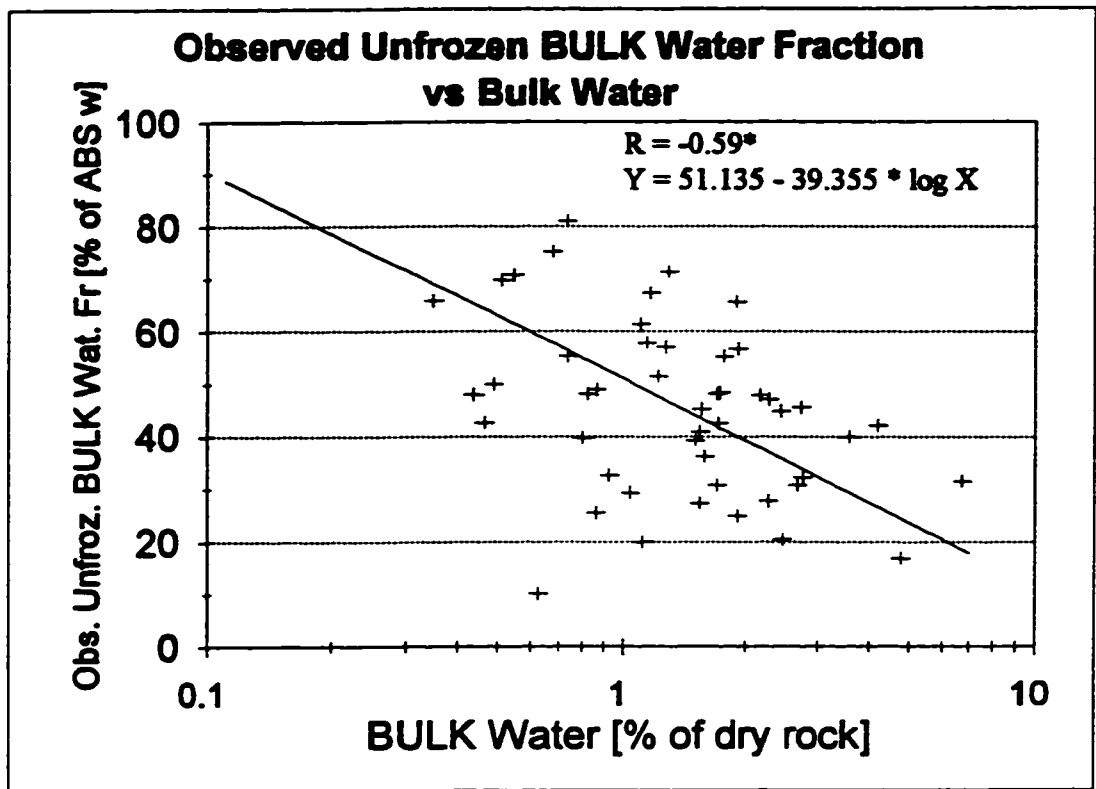
Figure 5.3 Graph of observed unfrozen bulk water fraction versus bulk water.
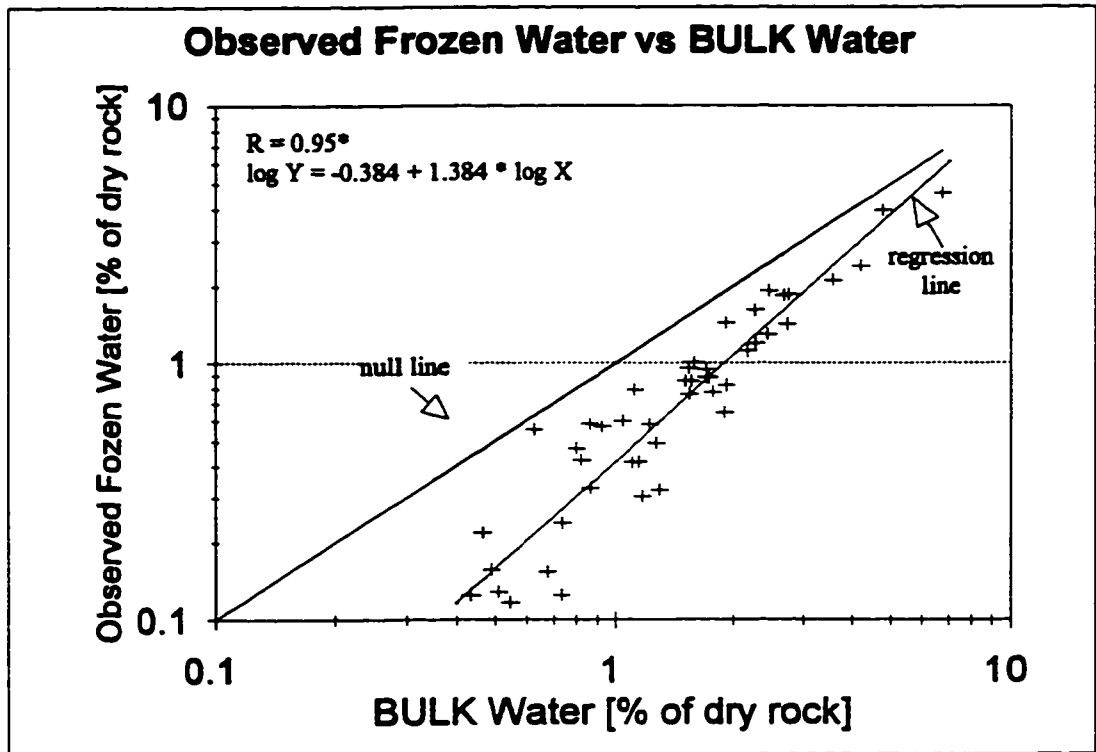
Figure 5.4 Graph of observed frozen water versus bulk water.
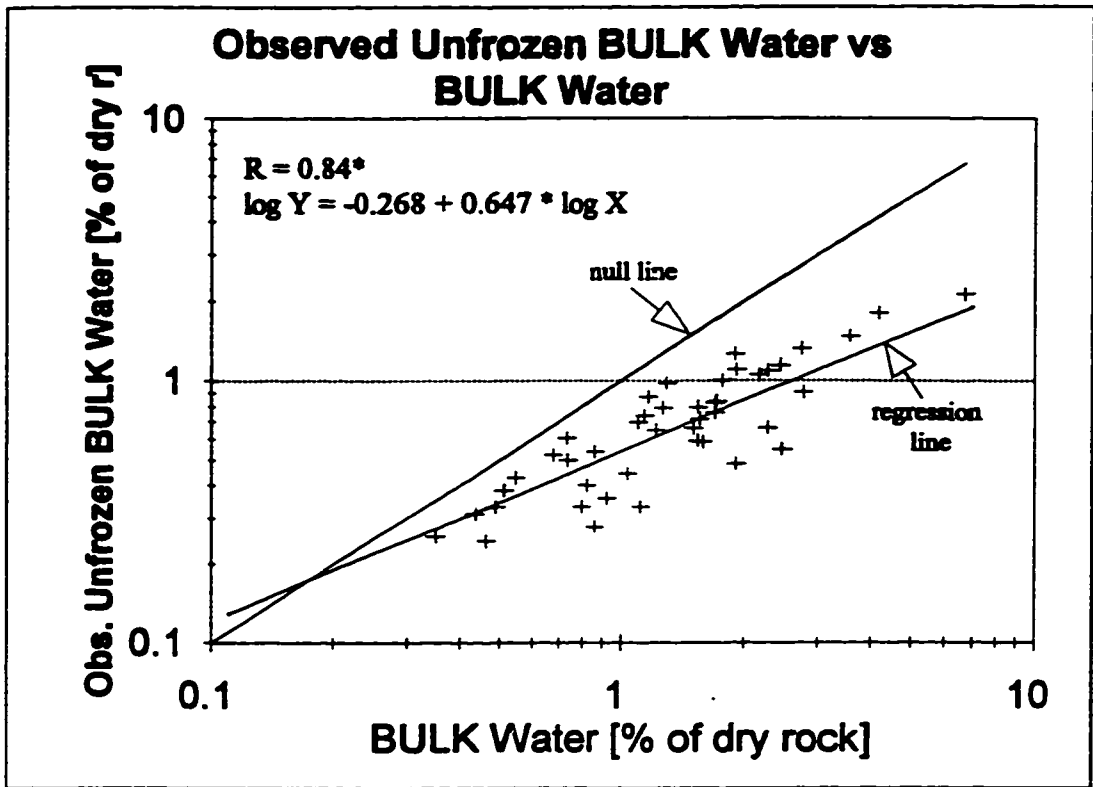
Figure 5.5 Graph of observed unfrozen bulk water versus bulk water.
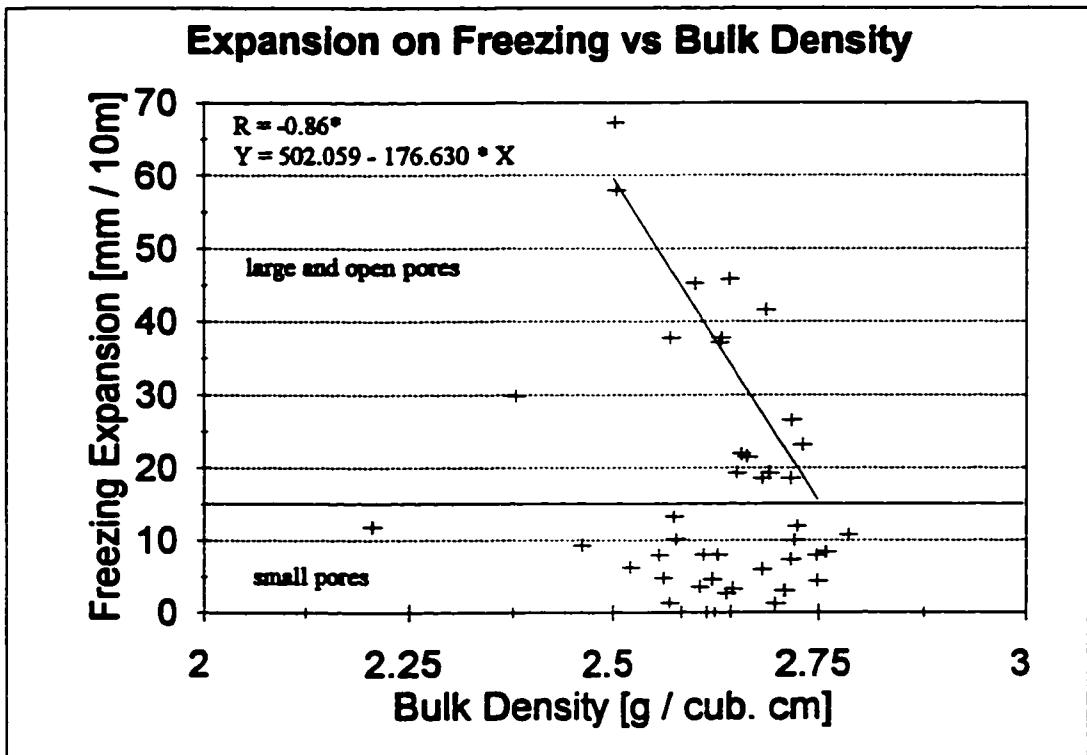
Figure 5.6 Graph of expansion on freezing versus bulk density.

63

with increasing amount of bulk water in the sample. Figure 5.4 shows plot of observed frozen water (CFWS) versus bulk water (RBUS) i.e. the portion of pore water which can freeze. The correlation between the variables has correlation coefficient $R = 0.95$ with 99% significance level. The plot suggests that the amount of observed frozen water increases with increasing amount of bulk water. The graph has two regression lines. One is regression line representing regression between the variables, and the other one is null line which represents theoretical regression between bulk water (X axis) and theoretically 100% frozen bulk water (Y axis). The regression line converge to the null line, which means that with increasing amount of bulk water higher fraction of the bulk water freezes.

Figure 5.5 is a plot of observed unfrozen bulk water (CUFBUS) versus bulk water (RBUS). The direct correlation has a correlation coefficient $R = 0.84$ with 99% significance. The plot shows that with increasing amount of bulk water the amount of unfrozen bulk water increase as well. Intersect of the null line with the regression line represents the point, where the amount of bulk water and unfrozen bulk water are equal. This suggests that the samples in which the content of bulk water is less than 0.18% (intersect of the lines) no water will freeze.

Figures 5.6, 5.7, 5.8, 5.9 show plots which have expansion on freezing (CRDL) on the Y axis, and bulk density, absorbtion rate, observed frozen water and bulk water respectively (RDEN, RCAO32S, CFWS, RBUS) on the X axis. All graphs are divided with a horizontal line at expansion on freezing 15 mm/(m*10) into two fields. Upper field contains cases with expansion on freezing greater than 15 mm/(m*10). All of the samples in this field have large and open pores. Lower field contains cases with expansion on freezing less than 15 mm/(m*10) with mostly small pores. However, the lower field contains also three cases

(out from 27 cases) with large pores. Correlation tests were performed only on samples with large and open pores which have expansion on freezing greater than 15 mm/(m*10). No correlation between expansion on freezing and any other variables was observed for the entire sample population.

Figure 5.6 shows plot between expansion on freezing (CRLD) and bulk density (RDEN). The correlation test revealed that only samples with open and large pores have high inverse correlation. Correlation coefficient is R = -0.86 with 99% significance level. The outlier case with expansion on freezing 30 mm/(m*10) (left half of the graph) was not included in the correlation. The graph suggests that in case of samples with large and open pores expansion on freezing increases with decreasing bulk density. Figure 5.7 is a plot of expansion on freezing (CRDL) and an absorption rate (RCAP32S). The high direct correlation has coefficient R = 0.71 with 99% significance level. Only samples with large and open pores have this high correlation. Samples with small pores which showed expansion on freezing did not show any correlation with absorption rate. The graph suggests that with increasing absorption rate, the expansion on freezing of samples with large and open pores increases as well.

Figure 5.8 shows plot between expansion on freezing (CRDL) and observed frozen water (CFWS). The direct correlation of cases with large and open pores has coefficient R = 0.69 with 99% significance level. The graph suggests direct relationship between amount of frozen water and expansion on freezing in case of samples with large and open pores. Figure 5.9 shows a plot of expansion on freezing (CRDL) and bulk water (RBUS). The correlation has coefficient R = 0.73 with 99% significance level. The graph reveals direct relationship between expansion on freezing of samples with large and open pores and bulk water, i.e.. with

increasing amount of bulk water the expansion on freezing is increasing as well (see Chapter 5.2.3).

Figures 5.10 and 5.11 show bivariate plots of the correlations between data acquired from the microwave tests. Figure 5.10 shows plot of total heat absorbed by bulk water per gram of bulk water MQBUBU versus bulk water (RBUS). The inverse correlation has correlation coefficient R = -0.64 with 99% significance. The inverse correlation suggests that with increasing amount of bulk water per gram of dry rock the amount of absorbed heat decreases. Figure 5.11 shows a plot of total heat absorbed by adsorbed water per gram of adsorbed water (MQADAD) versus adsorbed water per gram of dry rock (RADS). The inverse correlation is very low, the correlation coefficient (R) is only -0.27 with 95% significance level. The correlation suggests that with increasing amount of adsorbed water the amount of heat absorbed by adsorbed water decreases.

Figure 5.12 is a plot of porosity (RPORO) versus adsorbed water per gram of dry rock (RADS). Plot contains two sample populations, sample population which showed freezing during freezing test (Group F) and sample population which did not show freezing (Group N). Entire sample population has low direct correlation with coefficient R = 0.34, which is less than the critical correlation for given sample size. Group F does not have any correlation between porosity and adsorbed water. Group N showed high direct correlation with coefficient R = 0.81 and 99% significant level, which means that the porosity increase in the rock is due to the increase in the number of small pores with large surface area.
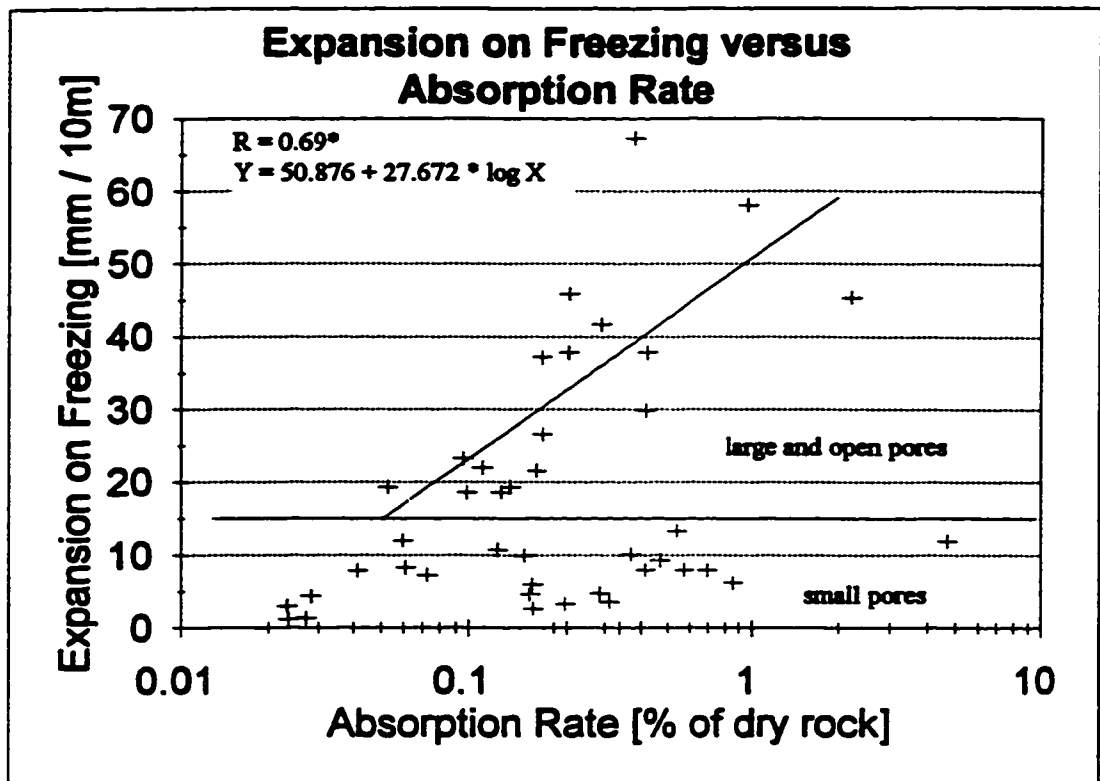
Figure 5.7 Graph of expansion of freezing versus absorption rate.
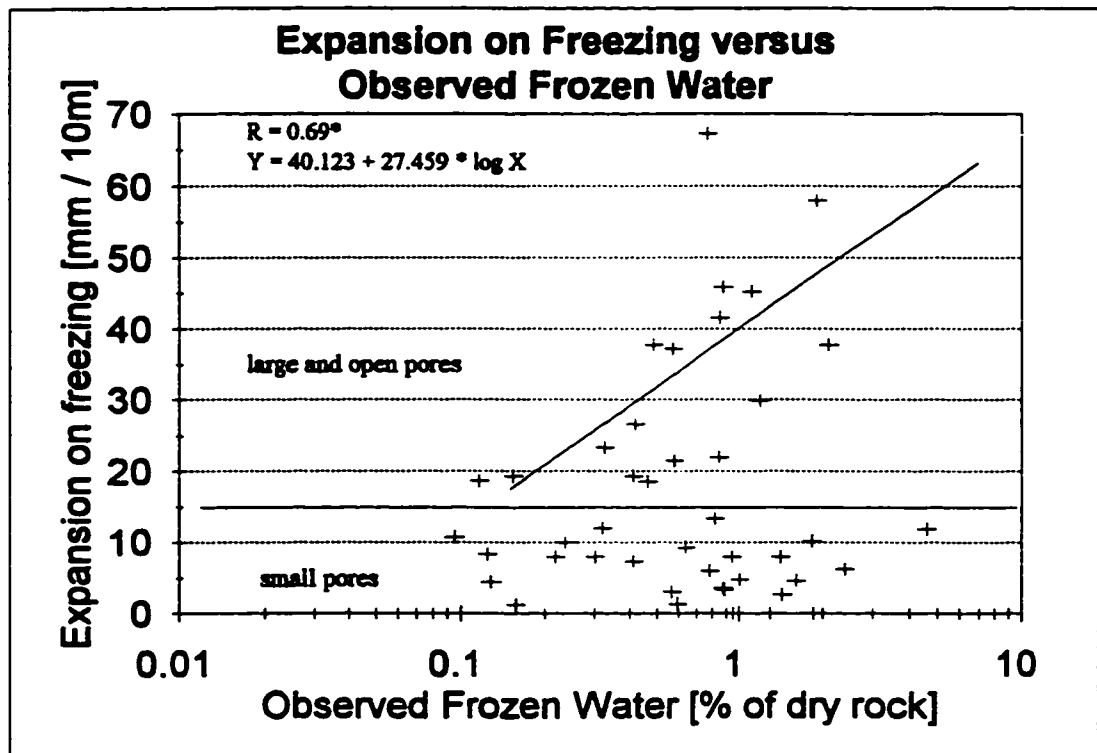
Figure 5.8 Graph of expansion on freezing versus observed frozen water.
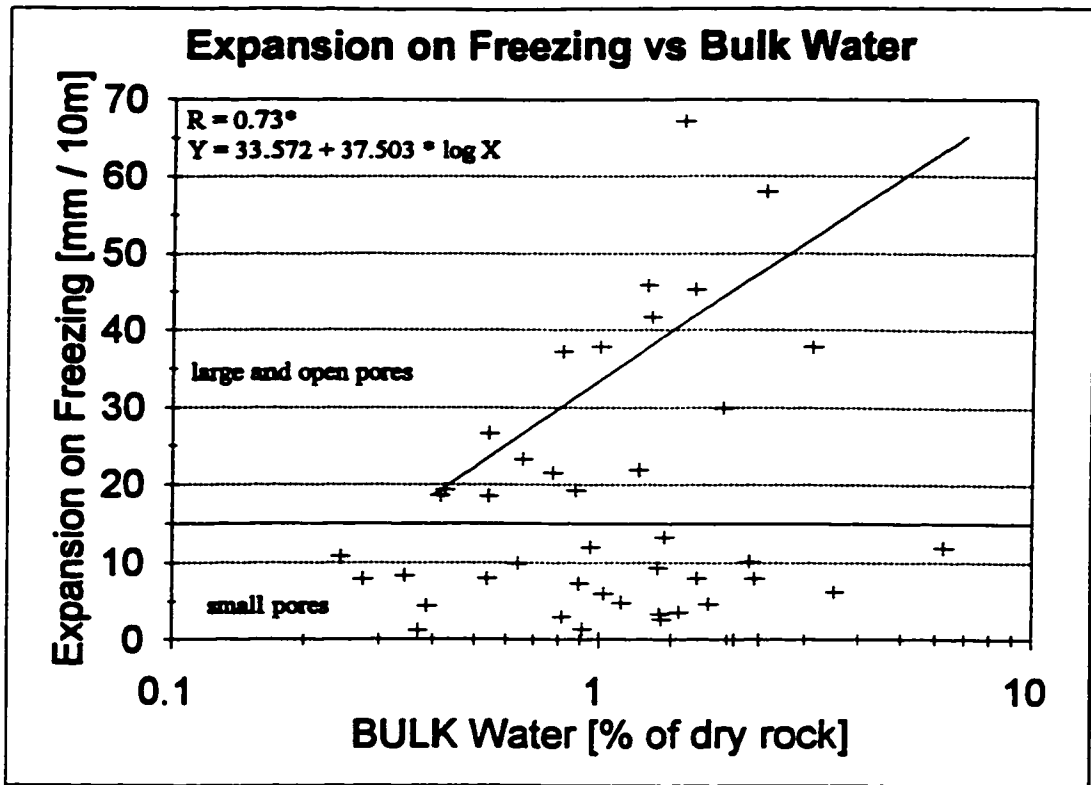
Figure 5.9 Graph of expansion on freezing versus bulk water.
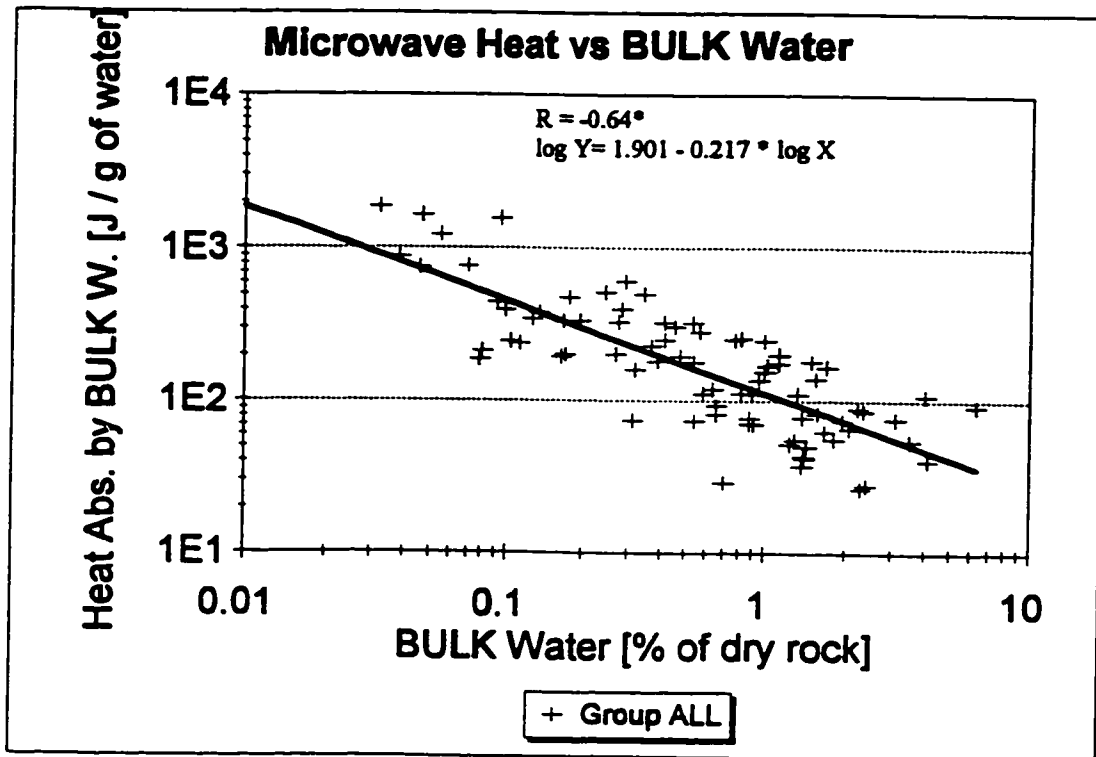
Figure 5.10 Graph of the total heat absorbed by bulk water versus bulk water.
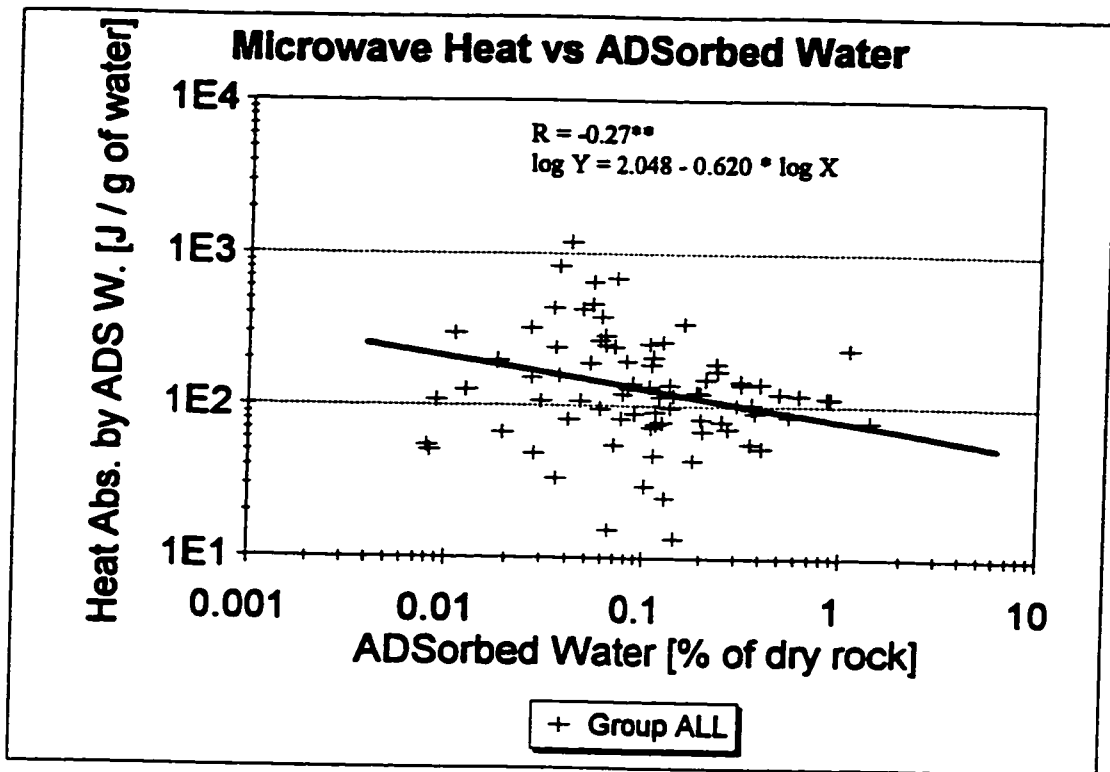
Figure 5.11 Graph of the total heat absorbed by adsorbed water versus adsorbed water.
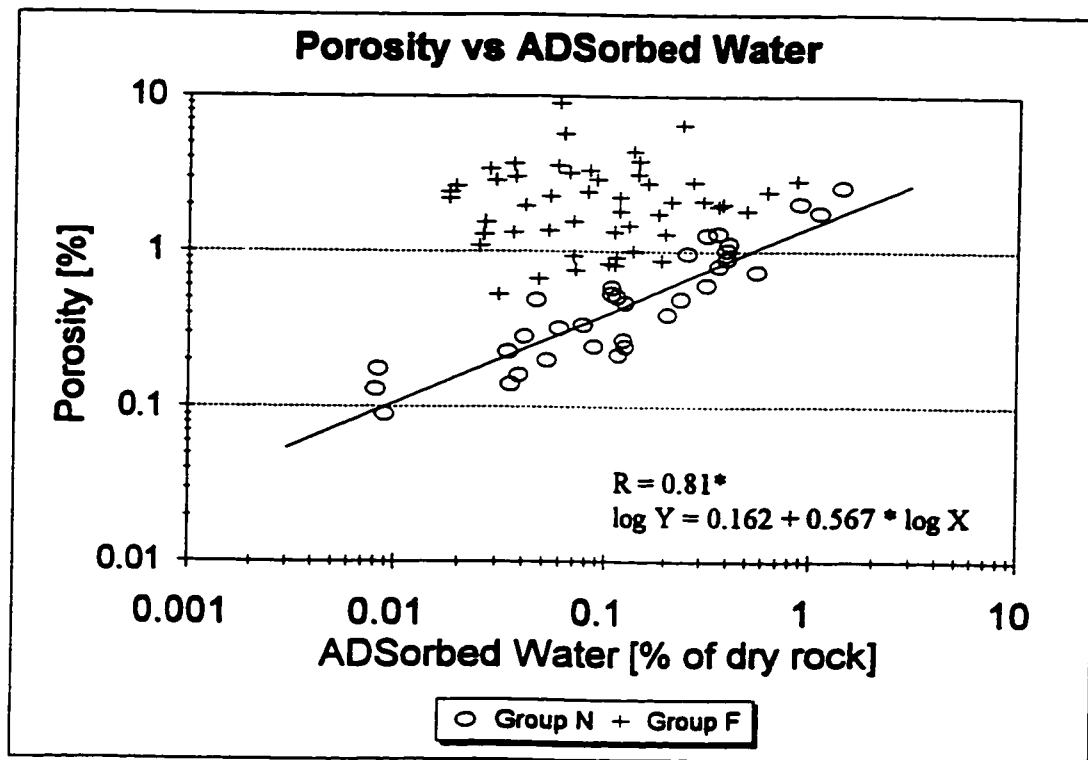
Figure 5.12 Graph of sample porosity versus adsorbed water.

5.1.5 Cluster Analysis And Cluster Group Mean Comparison

5.1.5.1 The Entire Sample Population (Group ALL)

Although the clustering yielded several sub-clusters, the grouping of the entire sample population can be determined by the performance of the samples in the freezing test. The freezing has divided samples into two groups. **Group F** which includes samples which showed freezing and **Group N** which includes samples which did not show freezing.

Group F.

Group F is sample population with freezable pore water. From 88 cases of the entire sample population 53 cases (60%) fall into this group (Appendix B, Table B2). The group is lithologically composed of 14 limestones (48% of total tested limestones), 35 dolostones (74% of total listed dolostones), and 4 sandstones (100% of total tested sandstones) (Table 5.2). The cluster statistics si given in Table 5.6. The variables are organized in the table in the same groups, as they are organized in factors. The factor, to which each variable belongs, is given on the left side of the table (the factors analysis will be discussed in the following section).

The most significant feature of this group is high porosity (RPORO), low bulk density (RDEN), and high bulk water fraction (RBUB). The group has high content of bulk water (RBUS). It has high proportion of bulk water in pores fraction (RBUV) and low adsorbed water fraction (RADSB), compared to Group N. The Group F has low value of heat absorbed and by bulk water per gram of water (MQABAB, MQBUBU) and high values of heat absorbed by absorbed and by bulk water per gram of dry rock (MQABS, MQBUS). It has high loss due to drying and one cycle freezing (RDRYLOSS), gain of vacuum saturated water

70

TABLE 5.6 Summary of group mean comparison and standard deviation and ranges of Group N and Group F

			Mean			Stand. Deviation		Range of Group N		Range of Group F	
			Group N	Group F		Group N	Group F	Min	Max	Min	Max
F	Heat absorbed by bulk water fraction	MQBUBU	302.00	112.20	*	450.23	108.75	29.18	1864.52	26.83	517.63
a	Bulk water fraction	RBUB	59.30	84.30	*	22.37	11.91	13.21	94.38	55.00	99.53
c	Adsorbed water fraction	RADSB	39.80	15.90	*	20.95	10.34	6.25	85.71	1.12	40.74
t	Bulk water	RBUS	0.14	1.02	*	0.28	1.14	0.01	1.12	0.24	6.29
o	Heat absorbed by absorbed water fraction	MQABAB	512.86	239.88	*	1394.45	172.40	153.58	8666.70	89.71	843.09
r	Bulk water pore fraction	RBUV	43.90	55.60	*	17.00	14.34	12.79	76.83	25.54	86.20
	Calculated rate of water absorption	RCAP32S	0.01	0.18	*	0.08	0.62	0.00	0.44	0.02	4.69
1	Porosity	RPORO	0.37	1.91	*	0.57	1.54	0.02	2.81	0.53	8.96
	Gain of vacuum absorbed water	RVABGNS	0.05	0.23	*	0.14	0.21	0.00	0.40	0.01	1.07
	Density	RDEN	2.81	2.64	*	0.20	0.12	2.60	3.82	2.21	2.79
F.	Heat absorbed by absorbed water	MQABS	0.72	1.32	*	0.77	1.05	0.23	3.40	0.19	5.84
2	Heat absorbed by bulk water	MQBUS	0.51	1.12	*	0.58	0.99	0.15	2.49	0.40	5.81
	Loss of dry weight	RDRYLOSS	0.05	0.12		0.24	0.84	0.01	1.32	0.02	4.57
F.	Freeze-thaw loss	RFRTH	0.07	0.07		11.57	8.63	0.64	50.96	1.05	36.97
3a	MGSO4 loss	RMGSO4	3.63	6.46	**	16.17	23.98	0.55	92.00	0.70	97.10

* = mean are different with two tailed signifacance 0.01
** = mean are different with two tailed signifacance 0.05

(RVABGNS) and absorption rate (RCAP32S).

Group N

Group N is sample population which did not show freezing. From 88 cases of the entire sample population, 35 cases (40%) falls into this group. The group is lithologically composed of 15 limestones (52% of total tested limestones), 11 dolostones (26% of total listed dolostones), 7 igneous and metamorphic rocks combined (100% of total tested igneous and metamorphic rocks), and 2 shales (100% of total tested shales) (Table 5.2). The cluster statistics is given in Table 5.6.

The most significant feature of this group is low porosity (RPORO) and bulk water fraction (RBUB) and high bulk density (RDEN) and adsorbed water fraction (relative to Group F). Further, the group has low content of bulk water (RBUS), and bulk water as pore fraction (RBUV). The Group N has high value of heat absorbed by absorbed and by bulk water per gram of water (MQABAB, MQBUBU) and low values of heat absorbed by absorbed and by bulk water per gram of dry rock (MQABS, MQBUS). It has low loss due to drying (RDRYLOSS), low gain of vacuum saturated water (RVABGNS) and low absorption rate (RCAP32S).

5.1.5.2 The Sample Population Which Showed Freezing (Group F)

The cluster analysis of Freezable Group reveals three clusters. The distribution of the samples in the clusters is shown on Figure B1 and in Table B2 (Appendix B) . Listwise rejection of missing values reduced the original number of cases (53) to 40 cases. Most from the 13 rejected cases are due to missing freeze-thaw loss and MgSO$_4$ loss data, which were

adopted from Rigbey (1980) The tests were not performed on the new samples collected by the author.

Cluster 1.

20 cases belong to this cluster. They represents mostly fine grained dolostones (13 cases) and fine grained limestones (7 cases). The cluster statistics is given in Table 5.7. As in the case of Table 5.6, variables in Table 5.7 are organized into groups as they are grouped in the factors.

Most significant feature of this cluster is the low content of bulk water (RBUS), low amount of frozen water (CFWS) and the low frozen water fraction (CFWB). On the other hand, it has high amount of adsorbed water (RADS) unfrozen water fraction (CUFWB) unfrozen water as pore fraction (CUFWV) and high amount of heat absorbed by adsorbed water per gram of dry rock (MQADS). The cluster has low expansion on freezing (CRDL) and moderate gain of vacuum saturated water (RVABGNS) and moderate degree of saturation (RSATAFT). Also it has moderate values for a aggregate durability, however, the values for freeze-thaw loss (RFRTH) and MgSO4 loss (RMGSO4) are not significantly different from those in the Cluster 2 and Cluster 3.

Cluster 1 represents samples with a high adsorption and low content of water freezable at temperatures ranges from 0°C to -18°C and with low expansion on freezing.

Cluster 2

Cluster 2 has 11 cases. They are dolostones with cavities (9 cases) and coarse grained sandstones (2 cases). The cluster statistics si given in Table 5.7.

TABLE 5.7 Summary of cluster group means comparison and standard deviation and ranges of Cluster 1, Cluster 2 and Cluster 3

Factor			Mean			a	b	c	Standard Deviation		
			Cluster 1	Cluster 2	Cluster 3				Cluster 1	Cluster 2	Cluster 3
Factor 4	CFWS	Observed frozen water	0.37	0.72	1.46	*	*	*	0.29	0.26	0.48
	CUFWB	Observed total unfrozen water fraction	65.70	53.30	41.20	*	*	*	10.89	8.56	8.61
	CFWB	Observed frozen water fraction	34.30	46.70	58.80	*	*	*	10.89	8.56	8.61
	CUFWV	Observed total unfrozen water pore fraction	53.00	34.30	37.20	*	*	*	12.90	8.24	8.44
	RBUS	Bulk water	0.72	1.15	2.09	*	*	*	0.41	0.38	0.60
Factor 5	MQADS	Heat absorbed by adsorbed water	0.22	0.03	0.08	*	**	*	0.23	0.03	0.10
	RADS	Adsorbed water	0.22	0.03	0.11	*	**	*	0.21	0.03	0.06
	CRDL	Freezing expansion	8.01	26.49	14.70	*			6.56	13.47	20.15
Factor 3b	RFRTH	Freeze-thaw loss	7.84	4.68	9.12				7.75	7.33	11.86
	RMGSO4	MGSO4 loss	6.61	4.37	10.96				8.56	27.47	28.79
Factor 6	RVABGNS	Gain of vacuum absorbed water	0.26	0.12	0.44	**	*	*	0.16	0.10	0.20
	RSATAFT	Degree of saturation after testing	81.10	63.80	90.10	*	*	*	10.35	9.00	4.22

TABLE 5.7 - continuing

	Range of Cl. 1		Range of Cl. 2		Range of Cl. 3	
	min	max	min	max	min	max
CFWS	0.12	0.96	0.41	1.19	0.85	2.40
CUFWB	46.73	80.90	37.78	66.58	28.55	50.93
CFWB	19.10	53.27	33.42	62.22	49.07	71.45
CUFWV	29.23	67.16	17.05	48.32	27.30	46.70
RBUS	0.28	1.70	0.54	1.98	1.32	3.53
MQADS	0.03	0.87	0.01	0.10	0.01	0.37
RADS	0.05	0.86	0.02	0.12	0.04	0.27
CRDL	1.20	23.27	4.80	45.87	3.58	58.05
RFRTH	1.46	28.78	1.05	22.67	1.31	36.97
RMGSO4	0.70	31.90	1.30	95	1.27	85.30
RVABGNS	0.11	0.77	0.01	0.36	0.14	0.77
RSATAFT	61.04	95.65	45.14	73.30	83.78	96.47

NOTE
a - Cluster 1 vs. cluster 2
b - Cluster 1 vs. cluster 3
c - Cluster 2 vs. cluster 3
* = mean are different with two tailed sign. 0.01
** = mean are different with two tailed sign 0.05

74

The most significant features of this cluster, beside cavities and coarse grain size, are low amount of adsorbed water (RADS), low degree of saturation (RSATAFT) and low gain of vacuum saturated water (RVABGNS). This cluster is further characterized by moderate amounts of frozen water (CFWS), frozen water fraction (CFWB), unfrozen water fraction (CUFWB) and by moderate content of bulk water (RBUS). The content of unfrozen water as pore fraction (CUFWV) is low. It has a very high value of expansion on freezing (CRDL), which is in contrast to the low freeze-thaw and MgSO4 losses (RFRTH, RMGSO4). However, the latter two are not significantly different from Cluster 1 and Cluster 3.

Cluster 2 are samples with large and open pores with low degree of saturation. Further, cluster samples have a moderate amount of water freezable at temperature range from 0 to -18°C, moderate amount of adsorbed water and a high expansion on freezing.

Cluster 3

Cluster 3 has 9 cases. They represent fine grained dolostones (7 cases) and fine grained limestones (2 cases). The cluster statistics are given in Table 5.7.

The most significant feature of this cluster is the very high content of bulk water (RBUS), frozen water (CFWS), frozen water fraction (CFWB) low content of unfrozen water fraction (CUFWB). Further, it has high degree of saturation (RSATAFT) and high gain of vacuum saturated water (RVABGNS). Adsorption (RADS) and expansion on freezing (CRDL) have moderate value, however, the expansion on freezing is not significantly different from that in Cluster 2.

Freeze-thaw loss (RFRTH) and MgSO4 loss (RMGSO4) have greater values than those in Cluster 1 and Cluster 2, however, they are not significantly different.

Cluster 3 are samples with low content of adsorbed water and high content of bulk water - water freezable at temperature range from 0°C to -18°C. Samples from the cluster have also very high degree of saturation.

5.1.5.3 The Sample Population Which Did Not Show Freezing (Group N)

The cluster analysis of Group N extracted two clusters. The distribution of the samples in the clusters is shown on Figure B2 and in Table B2 (Appendix B). Listwise rejection of missing values reduced the original number of cases (35) to 21 cases.

Cluster 4

Cluster 4 has 12 cases. They represent fine grained limestones (7 cases), fine grained dolostones (2 cases), fine to coarse crystalline marbles (2 cases), and one case of granite. The cluster statistics si given in Table 5.8.

The most significant feature of this cluster is very low porosity (RPORO), and low content of pore water, both adsorbed (RADS) and bulk (RBUS). Further, it has high gain of bulk water fraction (RBUGNB) and high degree of saturation (RSATBIF), however the latter is less than in Cluster 5. The heat absorbed by absorbed water, bulk water and by adsorbed water per gram of dry rock (MQABS, MQBUS, MQADS) is low. The cluster has good freeze-thaw resistivity (RFRTH), the loss is 5 times less than in the Cluster 5. MgSO4 loss (RMGSO4) is also less in this cluster, however, the difference is not significant.

Cluster represents samples with very low porosity and low content of adsorbed and bulk water and high freeze-thaw resistivity.

76

Cluster 5

Cluster 5 has 9 cases. They are fine grained dolostones (5 cases) and fine grained limestones (4 cases). The cluster statistics si given in Table 5.8.

The most significant features of this cluster is high porosity (RPORO) and high content of pore water, both bulk and adsorbed (RBUS, RADS). The heat absorbed by absorbed water, bulk water and by adsorbed water per gram of dry rock (MQABS, MQBUS, MQADS) is high. However, all the values except the adsorbed water are much less than those in clusters extracted from samples in Group F.

Cluster 5 has very large freeze-thaw loss (RFRTH), far greater than any of the extracted clusters from all populations. MgSO4 loss (RMGSO4) is also high but not significantly different from that in Cluster 4.

Cluster 5 are samples with low porosity, low content of bulk water and of and low freeze-thaw resistivity. Further, cluster samples are characteristic with high content of adsorbed water.

TABLE 5.8 Summary of cluster group mean comparison and standard deviation and ranges of Cluster 4, and Cluster 5

		Mean			Standard Deviation		Range of Cl. 4		Range of Cl. 5	
		Cluster 4	Cluster 5		Cluster 4	Cluster 5	Min.	Max.	Min.	Max.
Factor 7	Heat absorbed by bulk water	MQBUS	0.38	0.85	*	0.17	0.49	0.17	0.77	0.21	1.79
	Heat absorbed by absorbed water	MQABS	0.52	1.29	*	0.16	0.57	0.35	0.89	0.77	2.46
	Loss of dry weight	RDRYLOSS	0.04	0.08	*	0.07	0.04	0.02	0.27	0.03	0.17
	Porosity	RPORO	0.30	0.74	*	0.13	0.27	0.18	0.59	0.47	1.27
	Adsorbed water	RADS	0.05	0.26	**	0.04	0.13	0.01	0.13	0.11	0.56
	Bulk water	RBUS	0.11	0.30	*	0.07	0.19	0.04	0.31	0.09	0.71
Factor 8	Gain of bulk water fraction	RBUGNB	24.10	13.80	**	55.39	67.43	9.52	220.00	8.86	228.28
	Degree of saturation before testin	RSATBIF	84.80	93.40	*	8.39	3.91	70.59	100.00	86.67	98.36
	Heat absorbed by adsorbed water	MQADS	0.09	0.32	*	0.09	0.18	0.00	0.30	0.07	0.67
Factor 3c	MgSO4 loss	RMGSO4	3.39	7.41		3.84	30.10	0.55	12.90	0.65	92.00
	Freeze-thaw loss	RFRTH	0.05	0.25	*	7.12	10.80	1.25	27.05	15.65	50.96

NOTE

* = mean are different with two tailed significance 0.01

** = mean are different with two tailed significance 0.05

5.1.6 FACTOR ANALYSES

Factor analyses were performed in three stages and yield eight factors, one of which is identical for all three stages. For this reason this factor was assigned the same factor number for all three stages (Factor 3). The factor analysis in the first stage gave three factors which account for 79.1% of the variance in the measured data. Factor analysis in the second stage gave four factors which accounted for 84.3% and analysis in the third stage gave three factors which accounted for 80.4% of the variance. Factor statistics is given in Tables 5.9, 5.10, 5.11.

Factor 1 (ROCK FREEZABILITY FACTOR)

Factor 1 describes freezability of pore water in the entire sample population. It includes 9 variables and counts for 50.8% of the variance in the measured values (Table 5.9a). The factor is dominated by variables describing the nature of pore water in a rock (Table 5.9b). It has high positive loading of bulk water content (RBUB, RBUS, RBUV), absorption rate (RCAP32S), and porosity (RPORO). It has high negative loading of heat absorbed by bulk water (MQBUBU), heat absorbed by absorbed water (MQABAB), water adsorption (RADS), and bulk density (RDEN).

The freezability factor confirms that the content of a bulk water in a rock has a direct relationship to its freezable content of pore water. In other words, the greater the content of bulk water the more of the pore water freezes. On the other hand, adsorbed water fraction has high inverse relationship with a freezability of water in this sample population.

Factor 2 (MICROWAVE HEAT ABSORPTION FACTOR)

Factor 2 describes heat absorption by pore water in the entire sample population. It includes 3 variables and accounts for 18.1% of variance (Table 5.9a). The factor is dominated by variables describing heat absorbed by pore water (Table 5.9b). It has high positive loading of heat absorbed by absorbed water per one gram of dry rock (MQABS), heat absorbed by bulk water per one gram of dry rock (MQBUS) and positive loading of weight loss (RDRYLOSS).

The positive loading of the variables in this factor suggests that as the amount of pore water increases the amount of absorbed heat by pore water, and dry weight loss increases as well.

Factor 3 (AGGREGATE DURABILITY FACTOR)

Factor 3, factor describing rock durability, is identical for sample populations in all three stages of factor analyses (Tables 5.9b, 5.10b 5.11b). It consist of two variables, which both directly describe rock durability: freeze-thaw loss (RFRTH) and $MgSO_4$ loss (RMGSO4). Both variables are positively loaded, which means that the rock durability decreases with increasing freeze-thaw and $MgSO_4$ losses.

The aggregate durability factor accounts for 10.2% of the variance of the entire sample population (Table 5.9a), 12.7% of the variance in the values of the variables included into factor analysis of Group F (Table 5.10a), and 11.0% of the variance in the values of the variables of the factor analysis of Group N (Table 5.11a). The data for aggregate durability are adopted from Rigbey (1980), where they are discussed in more detail.

TABLE 5.9 Summary of factor analysis statistic - Group ALL

a) Final statistics (extraction, principal components)

	Eigenvalue	Pct of Var	Cum Pct
Factor 1	7.117	50.8	50.8
Factor 2	2.533	18.1	68.9
Factor 3a	1.425	10.2	79.1

b) Rotated factor matrix (avarimex rotation)

Pct of Var	Factor 1 50.8%	Factor 2 18.1%	Factor 3a 10.2%	Communality
MQBUBU	-0.942	0.038	-0.169	0.917
RBUB	0.915	0.074	-0.247	0.903
RADSB	-0.910	-0.084	0.263	0.903
LOG RBUS	0.831	0.502	0.162	0.970
LOG MQABAB	-0.800	-0.118	-0.248	0.716
RBUV	0.786	0.068	0.081	0.629
LOG RCAP32S	0.748	0.454	0.098	0.775
LOG VACABS	0.692	0.606	0.196	0.884
RDEN	-0.497	-0.414	-0.374	0.559
LOG MQABS	0.062	0.944	0.182	0.929
LOG MQBUS	0.155	0.940	0.050	0.910
LOG RDRYLOSS	0.059	0.732	0.015	0.540
LOG RFRTH	-0.178	0.035	0.851	0.757
LOG RMGSO4	0.286	0.193	0.750	0.682

Pct of Var   Percentage Variance
Cum Pct   Cumulative percentage of variance

Factor 4 (DEGREE OF FREEZABILITY OF PORE WATER FACTOR)

Factor 4 describes the content of freezable water in a sample population with freezable water. It consists of four variables and it accounts for 37.3% of the variance (Table 5.10a). The factor is dominated by variables expressing total amount of frozen and unfrozen water (Table 5.10b). It is positively loaded by variables expressing amount of frozen water (CFWS, CFWB) and amount of bulk water per gram of dry rock (RBUS). It is negatively loaded by variables describing total unfrozen water fraction and total unfrozen water as pore fraction (CUFWB, CUFWV).

The factor suggests, that the total amount of frozen pore water is an exclusive function of content of bulk water in pores. With increasing amount of bulk water the amount of frozen water increases as well.

Factor 5 (FREEZING EXPANSION FACTOR)

Factor 5 describes the expansion on freezing in the sample population which showed freezing (Group F). It consists of three variables (Table 5.10b) and it account for 24.9% of the variance in the measured values (Table 5.10a). The factor is positively loaded by log of adsorbed water (RADS), log of heat adsorbed by adsorbed water (MQADS). It is negatively loaded by expansion on freezing (CRDL).

The factor suggests that expansion on freezing and adsorption of water are in inverse relationship. The expansion on freezing increases with decreasing adsorption. This suggests that the freezing of water in larger pores with lower surface area and adsorption is responsible for rock expansion on freezing.

82

TABLES 5.10 Summary of factor analysis statiostic - Group F

a) Final statistics (extraction, principal components)

	Eigenvalue	Pct of Var	Cum Pct
Factor 4	4.584	38.2	38.2
Factor 5	3.048	25.4	63.6
Factor 3b	1.425	11.9	75.5
Factor 6	1.077	9.0	84.5

b) Rotated factor matrix (avarimex rotation)

Pct of Var	Factor 4 38.2%	Factor 5 25.4%	Factor 3b 11.9%	Factor 6 9%	Communality
CFWB	0.975	0.005	0.061	-0.044	0.957
CUFWB	-0.975	-0.005	-0.061	0.044	0.956
LOG CFWS	0.944	-0.006	0.146	0.210	0.956
CUFWV	-0.841	0.254	-0.012	0.371	0.910
LOG RBUS	0.825	-0.031	0.205	0.343	0.841
LOG MQADS	-0.183	0.858	0.174	0.083	0.806
LOG RADS	0.041	0.850	0.329	0.162	0.858
CRDL	0.029	-0.717	0.539	-0.020	0.806
LOG RFRTH	0.022	0.102	0.814	0.208	0.717
R LOG MGSO4	0.365	0.247	0.751	0.015	0.759
LOG RVABGNS	0.008	0.009	0.099	0.868	0.764
RSATAFT	0.089	0.505	0.157	0.719	0.805

Pct of Var   Percentage Variance
Cum Pct   Cumulative percentage of variance

Factor 6 (PORE WALL STRENGTH FACTOR)

Factor 6 describes the rock pore wall strength of the sample population with freezable water. It consists of two variables (Table 5.10b) and it account for 9.5% of the variance in the measured values (Table 5.10a). The factor is positively loaded by log of gain of vacuum saturated water (RVABGNS) and by degree of saturation after the tests (RSATAFT).

Factor suggests that the pore wall strength expressed by gain of vacuum saturation (destruction of ink bottle pores) is related to degree of saturation. High degree of saturation means greater number of small pores whose walls can collapse (due to capillary tension during drying or hydraulic pressure during freezing).

Factor 7 (ROCK POROSITY FACTOR)

Factor 7 describes the porosity of sample population which did not show freezing (Group N). It consists of 5 variables and it accounts for 52.8% of the variance in the measured values (Table 5.11). The factor has positive loading of heat absorbed by absorbed and by bulk water (MQBUS, MQABS), loss of weight after the tests (RDRYLOSS), vacuum saturated water (RPORO), and adsorbed water (RADS), (Table 5.11b).

Factor describes direct relationship between rock porosity and the amount of pore water, and the relationship between rock porosity and amount of water expressed as amount of heat absorbed by pore water (absorbed and bulk water).

Factor 8 (SATURABILITY FACTOR)

Factor 8 describes saturability of Group N. In consists of three variables and it accounts for 16.7% of the variance in the measured values (Table 5.11a). The factor has

positive loadings of degree of saturation (RSATBIF) and log of heat absorbed by adsorbed

water (MQADS). It has negative loading of gain of bulk water (RBUGNB), (Table 5.11b).

Factor suggests that with degree of rock saturation and increasing heat absorbtion by

adsorbed water the enlargement of rock pores on freezing decreases.

TABLE 5.11 Table of factor analysis statistic of Group N

a) Final statistics (extraction, principal components)

	Eigenvalue	Pct of Var	Cum Pct
Factor 7	5.275	52.8	52.8
Factor 8	1.674	16.7	69.5
Factor 3C	1.095	11.0	80.4

b) Rotated factor Matrix (avarimex rotation)

Pct of Var	Factor 7 52.8%	Factor 8 16.7%	Factor 3c 11.0%	Communality
LOG MQBUS	0.920	0.041	0.101	0.858
LOG MQABS	0.887	0.267	0.153	0.882
LOG RDRYLOSS	0.777	0.045	-0.379	0.750
LOG RPORO	0.703	0.473	0.293	0.804
LOG RADS	0.672	0.582	0.323	0.894
RBUGNB	0.169	-0.852	-0.184	0.789
RSATBIF	0.426	0.804	-0.113	0.840
LOG MQADS	0.419	0.725	0.206	0.743
LOG MGSO4	-0.059	0.073	0.826	0.690
LOG FRTH	0.501	0.278	0.682	0.793

Pct of Var -   Percentage Variance
Cum Pct -   Cumulative percentage of variance

5.2 DISCUSSION

5.2.1 Microwave Heat Absorption

Rocks heated in a microwave oven absorb heat proportional to the microwave flux, size of a sample and the number of dielectric molecules present in the sample. Dielectric molecules are present in both phases of rock, solid and liquid. Dielectric molecules of solid phase compose rock minerals. Liquid dielectric molecules in liquid phase are represented by bulk and adsorbed water which have different physical properties and degree of control by pore surface forces.

Solid body and bulk and absorbed water present in a rock absorbed different amount of heat. The fractions, by which a dry rock, absorbed water and bulk water contribute to the total absorbed microwave heat, are given on triangular plot (Figure C.1, Appendix C). The graph shows that most of the heat is absorbed by bulk water and by dry rock. Adsorbed water absorbed only 11% of total absorbed heat. Dry rock absorbed 21% and bulk water absorbed 68%. These proportions were expected. Dry rock containing dielectric molecules in minerals is the highest fraction of total mass. Bulk water is the second highest portion with water molecules without any restriction in movement in the pores i.e. with high thermodynamic or free energy, and with high dielectric constant. Adsorbed water is the lowest proportion of the total mass and the adsorbed water molecules are restricted in a free movement in the pores by surface forces of the pore walls i.e. the have low thermodynamic energy. The attractive forces between water molecules and pore walls could make water reluctant to line up with a polarity of microwave waves and absorb their energy, or in other words, the adsorbed water generates less heat by friction of water molecules against each other, than bulk water. It needs

more microwave energy to move the molecules off the surface and polarize into field direction of the microwave.

Figure C.2, (Appendix C) shows overlapping of Figures 5.10 and 5.11, which are the plots of total absorbed microwave heat per gram of water by adsorbed water and bulk water, respectively, versus adsorbed water and bulk water, respectively. The differences in the trends of the plots suggest that the amount of absorbed heat by adsorbed water and by bulk water are not equal. Single sample t-test mean comparison of the values of absorbed heat by adsorbed water and by bulk water showed that the amount of absorbed heat by bulk water (10.9 J/(g*g*s)) is 1.9 times less than heat absorbed by bulk water (21.0 J/(g*g*s). The t-values is -4.57, what with confidence 99% means that tested means are not equal (Table 5.12). This supports the idea that more microwave heat can be absorbed by bulk water then by adsorbed water. It is important to note that only those cases were included in the mean comparison which have content of adsorbed and bulk water within interval 0.1% -1% of dry rock. This selection of cases makes the two variable's mean comparable.

Another theoretical consideration supports the idea that more microwave heat can be absorbed by bulk water than by adsorbed water. Each sample was zapped three times. First

TABLE 5.12 Comparison of the total microwave heat absorbed by adsorb(water and by bulk water (Group ALL).

	Number of Cases	Mean [J/(g*g*9sec)]#	SD
MQADAD	44	98.7	1.8
MQBUBU	41	188.8	2.0
t-test value	- 4.57 - YES they are different		
2-Tail Sig	0.000		

Note #
Unit [J/(g*g*9sec)] is total heat in Joules absorbed per gram of dry rock and gram of water and per 9 seconds.

time as dry rock, afterwards with adsorbed water and afterwards with adsorbed water and bulk water (Figure C.3, Appendix C). In all three cases the constant heat flux increased the sample temperature in certain amount (dT_1, dT_2, dT_3), which was proportional to absorbed microwave heat. In all observed cases was true that:

$$dT_1 < dT_2 < dT_3 \qquad (5.1)$$

Since in the first time only dry rock was zapped, then the total observed temperature increase dT_1 is equal to a temperature increase due to heat absorbed by dry rock (Equation 4.1).

The second time, sample with absorbed water was zapped. The total observed temperature increase dT_2 is then equal to a temperature increase due to heat absorbed by dry rock and to temperature increase due to heat absorbed by adsorbed water (Equation 4.2).

The third time sample with adsorbed and bulk water was zapped. The total observed temperature increase dT_3 is then equal to temperature increase due to heat absorbed by dry rock and temperature increase due to heat absorbed by adsorbed water and temperature increase due to heat absorbed by bulk water (Equation 4.3)

It is obvious that each time more mass was exposed to the same energy flux. The increasing amount of new mass (water) could block some of the microwave rays (energy), which were originally absorbed by dry rock or adsorbed water. It should be true that:

$$dTs_1 \geq dTs_2 \geq dTs_3 \qquad (5.2)$$

and

$$dTa_2 \geq dTa_3 \qquad (5.3)$$

The temperature increases dTa_c and dTb_c which were used to calculate the microwave heat absorbed by adsorbed water and by bulk water respectively are based on Equations 4.4

88

and 4.5. Calculation of temperature increase of bulk water (dTb_c) is based on Equation 4.5. From the Equations 4.2, 4.3, 5.2 and 5.3 can be assumed, that the real sample temperature increase due to heat absorbed by bulk water can be even greater than the calculated temperature increase:

$$dTb_3 \geq dTb_c. \tag{5.4}$$

This suggests, that the difference between compared heat adsorbed by bulk water (MQBUBU) and heat absorbed by adsorbed water (MQADAD) should be even greater, than the mean comparison by t-test has revealed (Table 5.12).

Comparison of Figure 5.10 and 5.11 shows a great difference in sample distribution and correlation. While cases on the Figure 5.10 are more inline (R = -0.64), the cases on the Figure 5.11 are scattered (R = -0.27). This could mean that the molecules of bulk water in pores of any rock type can turn freely into direction of microwave rays and absorb their heat. However, this is not the case with adsorbed water. Adsorbed water is influenced by surface forces whose strength is controlled by the nature of the surface (Hudec 1993). For instance, surface of fracture face has greater attractive forces than surface of amorphous solids, which in turn has greater forces than surface of crystalline solids.

The two regression lines from Figure 5.10 and Figure 5.11 are also given in Figure C.2, (Appendix C). They converge and intersect above X axis at about 2.5% water content. The declining trend of regressions is caused by the absorption of heat from a constant microwave flux by increasing amount of pore water in the same rock volume. The slopes of regression lines represent the coefficients by which the heat absorbed by adsorbed water or by bulk water is "diluted" by a given amount of adsorbed or bulk water respectively. The steeper the slope, the more "diluted" is the absorbed heat. The intersect represents the

amount of water at which both, bulk and adsorbed water, absorbed equal amounts of heat per the same water content.

5.2.2 Freezability of Pore Water

The ability of a pore water to freeze is described by Rock Freezability Factor (Factor 1) and by Degree of Freezability of Pore Water Factor (Factor 4).

The most outstanding differences between the sample population which showed freezing during freezing test (Group F) and the sample population which did not show freezing (Group N) are in their porosity, and in the pore water content and its type (adsorbed and bulk water). The average porosity of Group N is 0.37%, which is 5.16 times less than porosity of Group F which has porosity 1.91%. This results is in an harmony with average bulk densities of the groups. Group N has high bulk density (2.81g/cm3) and Group F low (2.64g/cm3).

The lowest porosity of Group N is 0.5% and the highest porosity is 2.5%. The wide range of porosity containing unfrozen water means that the porosity is not the only factor controlling presence of freezable water in rocks. A triangular plot (Figure C.4, Appendix C) shows bulk water, adsorbed water, and void space as proportional fractions of total pore space. The plot suggest that if the pores are occupied with more than 35% adsorbed water, the pore water is prevented by surface forces from freezing at temperatures close to zero °C. If this is the case, then all samples with values above the limit (they have more than 65% of pore space occupied by bulk water) contain freezable water. However, several samples which did not show any freezing are above the limit. This suggests that either the system was not able to pick up the latent heat, or that pore characteristics prevented freezing at temperatures

90

at which the test was performed. They may freeze at much lower temperatures. The second assumption is in good agreement with published works (Bager and Sellevold 1986a, 1986b, 1987, Banthia et al., 1989, Sellevold and Radjy 1986). Example of freezing signals occurred at three different temperatures are shown on Figure 2.5. (after Bager and Sellevold 1986a).

The amount of unfrozen bulk water after the freezing at "high" temperatures can be calculated either from a regression between bulk unfrozen water fraction (CUFBUB) and bulk water (RBUS), (Figure 5.3) or from a regression between bulk unfrozen water (CUFBUS) and bulk water (RBUS), (Figure 5.5).

Figure C.5, (Appendix C) is a plot of bulk water fraction (RBUB) against bulk water (RBUS). The superimposing of the regression line from Figure 5.3 (line "a") divides the Figure C5 into two fields. Above the line "a" is a field "A" with a high relative and absolute content of bulk water which is freezable. Below the line "a" is a field "B" with a lower relative and absolute content of bulk water which is unfreezable in the temperatures of the freezing test. Line "b" represents 0.06% detection threshold limit of the system, i.e. the system does not pick up freezing signal from samples which contain less than 0.06% of freezable water (see Chapter 4.8.5).

Figure C.5 (Appendix C) shows that all but two samples which showed freezing (Group F) fall into field A. Samples which did not show freezing (Group N) and are in field A are along line "a". Field B with exception of two samples contains only the samples which did not show freezing (Group N). None of the samples from Group F are near line "b" which is a line of 0.06% detection threshold limit. The distribution of the samples in the fields A and B and along the line "a" suggests that the bulk water in the samples which are in the field B does not freeze in the temperature range from 0 °C to -18 °C. Further it suggests that samples

91

from Group N which are in field A contain freezable bulk water, but the system was not able to pick up the freezing signal. In such case, if the amount of bulk water which cannot freeze at temperatures range to -18 °C is subtracted from the values of bulk water on X axis of the Figure C.5, (Appendix C), then: (1) All cases from field B should have zero content of bulk water. (2) All cases from Group F should be shifted closer but above threshold line "b" (right-hand side of the line) . (3) All cases from Group N which are in the field A should have content of freezable bulk water less than 0.06% i.e. should be shifted below the threshold line "b".

The amount of bulk water which cannot freeze at temperature range 0 °C to -18 °C (BulNotFr) can be calculated for each sample from the equation:

$$BulNotFr = \frac{a + b * RBUS}{100} * RABS \qquad 5.4$$

Where
RBUS -Bulk Water as percent of dry rock
RABS -Absorbed water as percent of dry rock
a   - constant
b   - slope

"a" and "b" are constant and slope, respectively, calculated from the a regression correlation given on Figure 5.3.

The calculated amount of freezable water (CFBUSc) should be equal to the observed amount of frozen water (CFWS) . The two variable were compare with paired T-test. The result of the test is given in Table 5.13. The T value is equal 0.9 with significant level 0.361 which suggests that the two variables are not different i.e. they are the same.

92

Table 5.13 Comparison of the amount of the calculated freezable bulk water with observed frozen water by paired T-test.

Variable	Number of pairs	Corr (R)	2-tail Sig	Mean	SD	SE of Mean
LOG CBFRBUS			0.000	-0.1883	0.329	.047
	48	0.922				
LOG CFWS				-0.2114	0.42	.061

Paired Differences			SE of			
	Mean	SD	Mean	t-value	df	2-tail Sig
	0.0231	0.173	0.025	0.92	47	0.361

CBFRBUB - calculated freezable bulk water

Figure C.6 shows cases from Figure C.5 (Appendix C) after subtracting of the calculated unfreezable bulk water (BulNotFr) from the total bulk water in the samples (RBUS). The distribution of the cases in Figure C.6 has been changed in respect to Figure C.5, as was predicted above: (1) All cases from field B in Figure C.5 have zero content of bulk water in Figure C.6. (2) All but two cases from Group F which were in field A in Figure C.5 were in Figure C.6 shifted closer but above threshold line "b". (3) All but three cases from Group N, which were in the field A in Figure C.5, have content of freezable bulk water less than 0.06% i.e. were shifted below the threshold line "b" (Figure C.6).

Figure C.7, (Appendix C) is a plot of bulk water fraction (CRBUB) versus observed frozen water (CFWS). As a visual comparison of the calculated freezable water and the observed frozen water suggest, that their values are very similar. The distribution of cases in Figure C.7 is similar to the distribution of the cases in Figure C.6. In this figure, the presence of the two samples, which showed freezing (Group F) below the threshold line "b", and presence of the three samples which did not show freezing (Group N) above the line "b" is

93

most likely either due to error in the determination of pore water content or due to errors in calorimeter readings.

Comparison of Figures C.5, C.6, C.7 (Appendix C) reveals, that cases with either observed frozen water or calculated freezable bulk water fall above horizontal line which represents 55% bulk water fraction. The distribution of the cases suggest that only cases with pore water composed of more than 55% bulk water have freezable pore water. The 55% line could be equivalent of 35% line from Figure C.4 (Appendix C). The line 35% represents 65% percent of bulk water from total pore space.

5.2.3 Expansion on freezing

Expansion on freezing of samples is described by Factor 5. In this factor, the expansion on freezing (CRDL) is related to adsorbed water per gram of rock (RADS) and to heat adsorption by adsorbed rock (MQADS).

Cluster analysis split the samples which showed freezing into three clusters (Table 5.7). Their main significance is the amount of frozen water, degree of saturation, and expansion on freezing. Contrary to all theories describing mechanism of frost action in porous media, the highest expansion on freezing (expansion on freezing) was in samples with lowest saturation i.e. samples from Cluster 2 with degree of saturation only 63.8%. Furthermore, the amount of frozen water of the samples in this cluster is only moderate. However, visual study of samples of each cluster shows that while samples from Cluster 1 and Cluster 3 are fine-grained and with fine, not visible pores, the samples from Cluster 2 have coarse grain size or they have large or open pores. This together with hydraulic theory could explain the high expansion on freezing.

94

Figure C.8 (Appendix C) shows schematic sketch of the four theoretical cases. Cores or rocks A represents rocks from Cluster 1. They have low amount of frozen water 80% degree of saturation and low expansion on freezing. Core B represents rocks from Cluster 3, highest amount of frozen water, 90% degree of saturation and high expansion on freezing (however, the expansion is not significantly different from those in Cluster 2.). Core C and core D represent two rocks from Cluster 2 with moderate amount of frozen water, low degree of saturation (64%) and very high expansion on freezing. The hydraulic pressure theory (Powers, 1955) suggests that when pore water freezes and expands, the unfrozen water is expelled from the pores toward free space - outer boundary of the core or pores with air. When ice formation is instantaneous, the rock permeability must be sufficiently high for a given pore water discharge and distance through which the unfrozen water must flow to reach the free space. If not, the pressure is built up and the core expands proportionally to the ice pressure. In case of core A (Figure C.8, Appendix C) the amount of frozen water is the lowest and the degree of the saturation is less than critical 91%. This is in agreement with the lowest expansion on freezing. However, core B with highest amount of frozen water and degree of saturation close to critical value does not have greater expansion on freezing than core C with moderate amount of frozen water and only 64% degree of saturation. This could be explained by the fact that the core has an even pore distribution, or an even distribution of pore water throughout the core. Then each part of the core must expel the same amount of unfrozen water and the water discharge from any part of the core to the free space does not exceed the critical discharge for given permeability and flow path and none or only limited pressure is build up. The discharge of the water from the pores was well documented on the tested samples. After the freezing test, each sample which showed freezing was covered with

95

large amount of small frozen water drops. The frozen water drops were not observed on the samples which did not show freezing.

The core C does not have an even distribution of pores where the water can freeze and also the water is not evenly distributed throughout the core. Some large pores are empty, others are fully filled with absorbed freezable water. When instantaneous freezing occurs a large discharge of unfrozen water is accumulated into relatively small discharge area (cumulative cross section at area of pores through which the water is expelled). If the pore water which is going to freeze in one moment occupies more than 91% of the pore space, it must involve pressure on the pore walls and expand the core. From simple calculation it is clear, that the larger the pore is, the large fraction of the pore space can be occupied by freezable water. The idea of generating pressure due to insufficient permeability of the pore system for a given discharge is well documented on Figure 5.7. It is plot of expansion of the cores on freezing versus rate of capillary absorption. From the numerous literature about hydraulic of water flow through porous media (Freeze and Cherry, 1979, Fetter, 1994) is known that permeability decreases with decreasing pore diameter. Hudec (1989) proved that with decreasing pore diameter, the rate of water absorption increases. The Figure 5.7 shows that with increasing absorption rate, the expansion on freezing of cores with large pores and cavities increase as well.

Figures 5.8 and 5.9 suggests that if the conditions for trapping of unfrozen water into core are met, then the expansion on freezing is controlled by amount of freezable water (bulk water) or frozen water. Figure 5.9 is a plot of expansion on freezing versus bulk water. Figure 5.8 is a plot of expansion on freezing versus observed frozen water. Both graphs show that expansion on freezing increases with increasing amount of bulk water or with frozen water.

96

In both cases the correlation is high (R = 0.73, and 0.69 respectively) with 95% significance. The bulk water, or freezable water is present in large pores or cavities. The larger the fraction of the total rock volume that is occupied by cavities or large pores, the lower the bulk density the rock has. Similarly, the larger the amount of very small pores causing low permeability of the rock is present, the lower the bulk density of the rock. These can explain the high correlation (R=0.86) between expansion of rocks with large pores and cavities and bulk density (Figure 5.6).

Not in all observed cases do the cores with large pores of cavities have large expansion on freezing. Three cores had lower expansion than would be expected according to high correlation between expansion on freezing and amount of frozen water. This could be explained by example of core D (Figure C.8, Appendix C) Core D represents a case similar to core C i.e. similar to cases in Cluster 2. However, this time the large pores (cavities) are open to the outer surface of the core, or are not fully saturated with water. Thus, when the freezing occurs, the relatively large discharge of unfrozen water is not restricted and the pressure which causes expansion of the core is not built up. This could be the case of the three cases from Cluster 2 which did not show large expansion proportional to the amount of frozen water.

5.2.4 Thermodynamic Properties of Pore Water and Rock Deterioration on Freezing.

It is well known that aggregates from rocks with high adsorption have the worst performance record in concretes. The main reason of their poor record is their poor performance in drying-wetting and freezing-thawing cycles. As shown by Hudec (1991), the aggregate freeze-thaw loss has very a high correlation with adsorption (Figure 2.9). The

97

higher the adsorption the higher freeze-thaw loss. This is also in good agreement with observed results. Cluster 5, representing rocks with highest adsorption, have a distinctively higher freeze - thaw loss in comparison to other clusters (Appendix B, Table B1). However, the observed results of calorimetric measurement described in chapter "Freezability of pore water" (5.2.2.) suggested that pore water which is composed of more than 45 % of adsorbed water does not freeze at all. This contradicts the idea that the expansion of forming ice and accompanied hydraulic pressure is the main reason of rock deterioration on freeze - thaw cycling. Furthermore, comparison of the cluster means (Appendix B, Table B1) suggests, that the cluster with the lowest adsorption has the highest expansion on freezing (Cluster 2).

The observed results together with conclusions of other researchers described in the literature suggest that the main reason of frost deterioration of rocks can be explained by the thermodynamic properties of adsorbed and bulk water (Litvan, 1972a and 1972b, Hudec 1991, 1993). Adsorbed water, which is attracted and held by surface forces on the pore wall surfaces, has lower free energy. Since Bulk water is free of solid - liquid interaction, it has higher free energy. This difference of free energy generates differences in vapour pressure between bulk water and adsorbed water. This difference in vapour pressure can be calculated from Kelvin's equation, which suggests that the difference in vapour pressures is a function of pore radius, surface tension and temperature. Since at temperatures above 0°C the vapour pressures of bulk water is higher then vapour pressure of adsorbed water, the water flows toward small pores with adsorbed water and with lower vapour pressure. This generates pressure on pore walls, which can be damaging. A different situation occurs when the temperature is below the freezing point of bulk water (0°C). Vapour pressure over ice is lower than the vapour pressure over adsorbed water (ice has less free energy than adsorbed water).

This of course means, that unfrozen water starts to move from small pores (high relative vapour pressure) toward capillary pores containing ice with lower vapour pressure. This water increases the already high pressure due to expansion of ice. If a capillary pore is next to a small pore with no frozen water, then the cumulative pressure (pressure from ice formation and tensile pressure due to water leaving from small pores) can break up the pore wall. Such scenario supposes high overall saturation, or high local saturation with low permeability of the rock. The low permeability prevents the expelling of unfrozen water and facilitates the build up of high hydraulic pressure.

Natural or artificial rocks in nature are not fully saturated under normal conditions. The reason why can by illustrated on Figure C.9, (Appendix C). If large pores are completely surrounded by smaller pores (capillaries), the cohesive forces between water and pore walls does not allow the water to move into the large pores (ink bottle effect). This pore (void) remains as buffer zone for expelled unfrozen water during ice formation. This is a very important phenomenon which is widely used in the concrete industry and is called air entrainment (Pigeon et al., 1995, Powers, 1955). However, the local high saturation can be easily achieved. Hudec (1989) showed that with decreasing pore diameter, the ability of pores to achieve a high degree of saturation in a very short time increases. Furthermore, calculations based on Kelvin's equation (Figure 2.2) shows that pores with size less than $5\mu m$ can be fully saturated at RH 95%. These pore sizes are the domain of adsorbed water i.e. water with low thermodynamic energy. The higher the adsorption the rock has the higher the number of fully saturated pores are presented and the higher the amount of water can be moved to reestablish equilibrium when the temperature is changed. This may lead to disintegration of consistency of interior structure of the rock. Figure C.10 (Appendix C) shows the sequences of possible

disintegration of rock with small pores saturated mostly by adsorbed water. Case 1 shows sorption of the water into small pores. 100% saturation is soon achieved and due to low vapour pressure Vp1 in the pores (relative to vapour pressure Vp2 of bulk water), the sorption continues and compression pressure P_c in small pores is build up until the equilibrium between Vp1 and Vp2 for a given temperature is established. The pressure pushes the pore walls apart and the rock expands (Hudec and Sitar, 1975). The small ellipse in the middle of the rock cross section is used to illustrate what would happen if the pore walls are weak and collapse under the cyclical sorption and desorption (either due to dry - loss cycles of freeze - thaw cycles). When the temperature decreases below the freezing point of bulk water (Case 2, Figure C.10, Appendix C), the vapour pressure in the large pores is controlled by the vapour pressure over ice. Since this is lower than vapour pressure in small pores, the water starts to migrate out of the small pores into larger pores. This generates tensile stress P_t inside of the small pores. If the small pores are in a vicinity of large pores into which the water migrates, then the tensile stress P_t is exaggerated by compression pressure P_c in the large pores. Both tensile and compression pressure have the same vector i.e. act against the pore walls in the same direction, however, each from the opposite side of the pore walls. This situation can result in the collapse of pore wall, as illustrated on case 3 (Figure C.10, Appendix C).

The scenario from Case 1 is repeated after the temperature again rises above freezing point. However, this time the rock contains newly created fully saturated large pore, right in the middle of fully saturated small pores. When the temperature again drops below freezing point, this time the water in the new large pore freezes (case 4). Since it is surrounded with saturated small pores with very small permeability, the ice generates pressure proportional to

100

the volume increase. Furthermore, since the vapour pressure in the new large pore is lower than in the smaller pores, the water moves toward the new pore and the pressure P is increased. There can be many new pores in fully saturated part of the rock with small pores. When freezing takes place, they generates the pressure and literally squeeze and break the rock (Figure C.11, Appendix C))

5.2.5 Porosity of Group N.

The porosity of the not freezable group is described by Factor 7 (Rock Porosity Factor). All the variables belonging to the Factor 7 have a close relationship to the pore space and size, and to the content of pore water (MQBUS, MQABS, RDRYLOSS, RADS). Porosity of the group is directly expressed by the variable describing porosity (RPORO). The porosity of entire sample population (Group All) has moderate and low correlation with the rest of the variables from Factor 7 (Table 5.5).

Figure 5.12 shows plot of porosity (RPORO) versus adsorbed water (RADS). The cases from Group N are aligned along regression line, and the cases from Group F are scattered in the upper middle part of the graph. This distribution of the cases suggests that porosity of entire sample population (Group ALL) has low correlation with adsorbed water. The correlation coefficient (R) is 0.34 which is less than critical coefficient of given core size (the coefficient is not given on the graph). On the other hand, the graph suggests that porosity (RPORO) of Group N has high correlation with adsorbed water (RADS). The coefficient (R) is 0.81 with 99% significance. The large difference between the two correlations is caused by the different content of bulk water in pores of Group F and Group N. In the case of Group F, lower fraction of the total pore space is occupied by adsorbed water. In the case of Group

101

N, higher fraction of pore space is occupied by adsorbed water. Then logically, the correlation between porosity and adsorbed water is better in the case of Group N, where the adsorbed water occupies larger fraction of the pore space, then in the case of Group F where the adsorbed water occupies only small fraction. Due to low correlation of cases from Group F, the correlation of Group ALL is than also low.

The differences in correlations than suggests, that porosity of Group N is controlled mostly by small pores, which contains high fraction of adsorbed water.

6. CONCLUSIONS AND RECOMMENDATIONS

6.1 Conclusions

Based on the tests results and statistical analysis the research presented in this thesis has the following conclusions:

(1) Bulk water can absorb 1.9 times more microwave heat than adsorbed water.

(2) The total amount of microwave heat absorbed by adsorbed water is controlled in part by amount of adsorbed water present and in part by the activity of surface forces. Amount of the microwave heat absorbed by bulk water is controlled mostly by amount of bulk water present in the rock. Correlation between microwave heat absorbed by adsorbed water and amount of adsorbed water has a coefficient of correlation of -0.27 with 99% confidence. However, correlation between microwave heat absorbed by bulk water and amount of bulk water has a coefficient of correlation of -0.64 with 99% confidence.

(3) In most of the rock samples studied, the amount of frozen water and the amount of bulk unfrozen water increases with increasing amount of bulk water in the rock. The correlations between frozen water and bulk water and between unfrozen bulk water and bulk water have coefficients of correlation 0.95 and 0.84, respectively, with 99% confidence. However, with increasing amount of bulk water the ratio of unfrozen water to frozen water decreases.

(4) Freezability of water in rock pores is controlled by internal surface area. The amount of adsorbed water is proportional to the internal surface area. Rocks, in which more than 35% of the total pore space is occupied by adsorbed water do not contain water which

freezes at the temperature range of 0°C to -18°C, i.e. the surface forces are strong enough to prevent the rearrangement of water molecules into ice crystals.

(5) The main reason for length changes in rocks on freezing is the freezing of water in large pores. The degree of saturation is not important in the overall length change of a rock. Samples which have large and open pores have the highest expansion on freezing (2.6 mm/m), and have a degree of saturation of only 48.8%. Samples with fine pores had low expansion on freezing (8 mm/m) and high degree of saturation of 88.3%. Degree of saturation is important in the weakening and destruction of the interior structure of a rock on freezing, which can result in break down of a rock.

(6) The expansion of pore water due to freezing is not the primary cause for rock deterioration during freezing - thawing cycles. Tested samples, which contained freezable water (bulk water) and showed freezing, had low losses during freeze-thaw test (mean loss is 7.1%). On the other hand, samples which did not contain freezable water and did not show freezing had significantly higher losses on freeze - thaw test (24.5%).

(7) Change in length of rock samples on freezing is not the primary reason for concrete deterioration on freezing. Samples, which represented rock aggregates with good performance record in concrete contain freezable water and may increase their length on freezing (0 - 2.6 mm/m). Samples representing rock aggregates with very poor performance record in concrete did not contain freezable water and did not expand on freezing.

(8) The primary reason for rock deterioration on freezing is the presence of large amounts of water with low free energy (i.e. adsorbed water). The thermodynamic equilibrium between adsorbed water and bulk water is disturbed by changes in temperature and water vapour pressure (on freezing); this results in the osmotic migration of water from pores with

104

high free energy into pores with low free energy. This osmotic migration increases pressures in the pores which can result in the collapse of the pore walls.

6.2 Recommendations

(1) Since the second conclusion (2) is not fully supported, it requires some more research. It would be useful to perform the microwave test with wide range of porous media with known surfaces characteristics.

(2) Last part of conclusion six (6) and conclusion nine (9) should be also followed up. The research could be performed by freezing test of samples with high content of adsorbed water. However, this time, the test should be repeated by several freeze-thaw cycles on the same sample. To prevent desiccation, the sample should be sealed. If the conclusion are correct, as well as the hypothesis presented in Chapter 5.2.4 then no freezing and no length change can be expected in first cycles. However freezing and length change should be observed after several repeated freeze-thaw cycles.

References

Allaby, A., Allaby M. 1990. The Concise Oxford Dictionary of Earth Science. Oxford University Press. New York. pp. 410.

ASTM Standards, 1982. Concrete and Mineral Aggregates. Eston, USA.

Bager, D.H., Sellevold, E.J, 1986 a. Ice Formation in Hardened Cement Paste, Part I. - Room Temperature Cured Pastes With Variable Moisture Contents., Cement and Concrete Research, Vol. 16. pp. 709 - 720.

Bager, D.H., Sellevold, E.J, 1986 b. Ice Formation in Hardened Cement Paste, Part II. - Drying and Resaturation on Room Temperature Cured Pastes., Cement and Concrete Research, Vol. 16. pp. 835 - 844.

Bager, D.H., Sellevold, E.J, 1987. Ice Formation in Hardened Cement Paste, Part III. - Slow Resaturation of Room Temperature Cured Pastes., Cement and Concrete Research, Vol. 16. pp. 1 - 11.

Banthia, N., Pigeon, M., Lachance, L., 1989. calorimetric Study of Freezable Water in Cement Paste. Cement and Concrete Research. Col. 19. pp. 939 - 950.

Bates, R.L., Jackson, J.A., 1984. Dictionary of Geological Terms, Third Edition, The American Geological Institute, New York. pp. 571.

Beaudion, J.J., 1979. Porosity Measurement of Some Hydrated Cementitious Systems by High Pressure Mercury Intrusion - Microstructural Limitations. Cement and Concrete Research, Vol. 9. pp. 771-781.

Beaudoin, J.J., MacInnis, C., 1974. The Mechanism of Frost Damage in Hardened Cement Paste. Cement and Concrete Research. Vol. 4, pp. 139-147.

Beddoe, R.E., Seltzer, M.J. 1990. Phase Transformations of Water in Hardened Cement Paste a Low - Temperature DSC Investigation. Cement and Concrete Research Journal, Vol. 20., No. 2., pp. 236-242

Blachere, J.R., Young, J.E., 1972. The Freezing Point of Water in Porous Glass. Journal of American Ceramic Society, Vol 55. No. 12. pp.306-308.

Booth, D.M., (editor) 1989a. Limestone Industries of Ontario, Volume I - Geology , Properties and Economics., Ministry of Natural Resources, Ontario,

Booth, D.M., (editor) 1989b. Limestone Industries of Ontario, Volume II - Limestone Industries and Resources of Eastern and Northern Ontario., Ministery of Natural Resoures, Ontario,

Booth, D.M., (editor) 1989c. Limestone Industries of Ontario, Volume II - Limestone Industries and Resources of Central and Southwestern Ontario., Ministery of Natural Resoures, Ontario,

Carmichael, R.S. (editor), 1989. Practical Handbook of Physical Properties of Rocks and Minerals. CRC Press, Florida pp. 360-427.

Darr, G.M., Ludwig, U., 1973. Determination of Permeable Porosity. Materials and Structures. Vol 6. No. 33. pp. 185 - 190.

Douglas, R.J.W., 1970. Geology and Economic Minerals of Canada. Geological Survey of Canada, Ottawa. Vol. 1. pp.121- 130.

Drost, H.W., 1967. The Water-Ice Interface as Seen From the Liquid Side. Journal of Colloid and Interface Science, Vol. 25. pp. 131-160.

Dullien, F.A.L., 1979. Porous Media, Fluid Transport and Pore Structure, Academic Press, pp. 395.

Dunn, J.R., Hudec, P.P., 1972. Frost and Sorption Effects in Argillaceous Rocks: Highway Research Record No. 393, Nat. Res. Council, Washington, D.C., pp. 95-78.

Durekovic, A., Calgovic, V., Popovic, K., 1989. Frost Resistance of OPC-CSFZ Investigated by Means of Repeated Cycles and One Cycle Freezing Test. Cement and Concrete Research, Vol. 19. pp. 267 - 277.

Everett, D.H. 1961. Thermodynamics of Frost Damage in Porous Solids, Trans Faraday Society, N. 57, pp. 1541 - 1551.

Fagerlund, G., 1973a. Determination of Pore Size Distribution by Suction Porosimetry. Material and structures, Vol. 6. No. 33. pp. 199 - 202.

Fagerlund, G., 1973b. Determination of Pore Size Distribution From Freezing-point Depression. Material and Structures, Vol. 6. No. 33. pp. 115 - 225.

Fagerlund, G., 1973c. Determination of the Specific Surface by BET method. Material and Structures, Vol. 6. No. 33. pp. 115 - 225.

Fetter, C.W., 1994. Applied Hydrogeology, Second Edition, Macmillan Collage Publishing Company, pp 77-128

Frankovsky, L., 1973. Relationship Between Sorption Characteristics, Dielectric Heating Characteristics and Soundness in Carbonate Rocks, Bachelor Thesis, University of Windsor, Windsor, Ontario, Canada. pp. 46.

Freeze, R.A., Cherry J.A. 1979. Ground Water. Pentice-Hall Inc. A Simon & Schuster Company. pp 15-75.

Gažo, J. Kohout, J., Serator, M., Sramko, T., Zikmund, M., 1981. Všeobecná a Anorganická Chémia. (General and Anorganic Chemistry)., ALFA, Bratislava, Slovakia, pp. 804.

Grimshaw, R.W., 1971, The Chemistry and Physics of Clays and Other Ceramic Materials. Ernest Benn Limited, Great Britain, Fourth Edition, pp. 1024.

Gu, G., Xie, P., Fu, Y., Beaudoin, J.J., 1993. A.C. Impedance Phenomena in Hydrating Cement Systems: the Drying - Rewetting Process. Cement and Concrete Research, Vol. 24. pp. 89-91.

Haynes, J.M., 1973a. Determination of Pore Properties of Constructional and Other Materials. - General Introduction and Classification of Methods. Materials and Structures, Vol 6. No. 33. pp. 169 - 174.

Haynes, J.M., 1973b. Pore Size Distribution According to the Kelvin's Equation. Materials and Structures, Vol 6. No. 33. pp. 209 - 226.

Higgs, N.B., 1987. Chlorite: A Detelerious Constituent with Respect to Freeze - Thaw Durability of Concrete Aggregates. Cement and Concrete Research. Vol. 17. pp. 793-804.

Hillerborg, A., 1985. A Modified Absorption Theory. Cement and Concrete Research . Vol. 15. pp. 809-816.

Hoekstra, P., Miller, R.D. 1967. On the Mobility of Water Molecules in the Transition Layer Between Ice and a Solid Surface. Journal of Colloid and Interface Science, Vol. 25. pp. 199-173.

Hudec, P.P., 1983. Aggregate test - Their Relationship and Significance: Durability of Building Materials, No. 1, Elsevier Scientific Publishing Company, Amsterdam, pp. 275-300.

Hudec. P.P., 1984. Statistical Methods of Aggregate Durability Evaluation. Bulletin of the International Association of Engineering Geology., Paris, No 29. pp. 377-380.

Hudec, P.P., 1987. Deterioration of Aggregates - The Underlying Causes, Katharine and Bryant Mather International Conference on Concrete Durability. American Concrete Institution, Detroit, Michigan, pp 1325 -1342.

Hudec, P.P. 1989. Durability of Rocks as Function of Grain Size, Pore Size, and Rate of Capillary Absorption of Water. Journal of Material in Civil Engineering, 1(1), 3-9.

Hudec, P.P. 1991. Freezing of Osmosis as Deterioration Mechanism of Concrete and Aggregate? Low Temperature Effects on Concrete Proceedings, Second Canadian/Japan Workshop, August, 1-2, Ottawa, Ontario.

Hudec, P.P., 1993 Aggregate and Concrete Durability as Controlled by Water and Cation Adsorption and Osmosis. Proceeding of Del Seminario International Sobre Technologia del Concreto, Concrete Durability, Monterrey, Mexico, pp. 32 - 52.

Hudec, P.P., MacInnis, C. Moukwa, M., 1986. Microclimate of Concrete Walls: Temperature, Moisture and Salt Content. Cement and Concrete Research, Vol. 16, pp. 615-623.

Hudec, P.P., Sitar, N. 1975. Effect of Sorption on Carbonate Rock Expansion, Canadian Geotechnical Journal. Vol. 12. No. 2. pp. 179 - 186.

Instruction Manual, 1976. Litton 420 Microwave Oven, Litton System Inc. pp.19.

Instruction Manual, 1991. Endocal RTE-Series Refrigerated Bath / Circulator., NESTLAB Instruments, Incorporated. Newington, New Hampshire, pp. 24.

Instruction Manual, 1991. NESTLAB Instruments M-RS-232, Interface Accessory User Manual., NESTLAB Instruments, Icorporated. Newington, New Hampshire, pp. 24.

Instruction Manual 1973, Model 165 Autoranging Multimeter, Keithley Instruments Incorporated., pp. 51.

Jacques, B.J., 1978. The Feasibility of Using the Microwave Oven as Means of Rapid Water Content Determination. Bachelor Thesis, University of Windsor, Windsor, Ontario, Canada. pp. 49.

Jaeger, C. 1972. Rock Mechanics and Engineering., Cambridge University Press, pp 416.

Kaneuji, M., Winslow, D.N., Dolch, W.L., 1980. The relationship between an aggregate pore size distribution and its freeze-thaw durability in concrete. Cement and concrete Research. 10(3), pp. 433-441.

Kenji, A., Keisuke, H., Takehisa, Y., 1990. Storage of Refrigerated Liquefied Gases in Rock Caverns: Characteristics of Rock Under Very Low Temperatures. Tunnelling and Underground Space Technology. Vol 5, No. 4, pp. 319 - 325.

Kleen, W.J., 1958. Electronics of Microwave Tubes., Academic Press Inc. New York, 339p.

Laboratory testing manual, 1994. Ministry of Transportation, Ontario, Volume 1, 2.

Litvan, G.G., 1972a. Phase Transition of Absorbates: III, Heat Effects and Dimensional Changes in Nonequilibrium Temperature Cycles. Journal of Colloid and Interface Science, Vol. 38, No. 1. pp. 75-83.

Litvan, G.G., 1972b. Phase Transition of Absorbates: IV, Mechanism of Frost Action in Harden Cement Paste. Journal of The American Ceramic Society, Vol. 55, No. 1. pp. 38-42.

Litvan, G.G., 1973. Phase Transition of Absorbates: V. Agueoud Sodium Chloride Solutions Adsorbed of Porous Silica Glass. Journal of Colloid and Interface Science, Vol. 45, No. 1. pp. 154-169.

Litvan, G.G., 1975. Phase Transition of Absorbates: VI, Effect of Deicing Agents on the Freezing of Cement Paste. Journal of The American Ceramic Society, Vol. 58, No. 1-2. pp. 26-30.

Litvan, G.G. 1983. Freeze-Thaw Durability of Porous Building Materials, A.S.T.M., STP 691, p 455.

MacInnis, C., Lau, E.C., 1971. Maximum aggregate size effect on frost resistance of concrete. ACI Journal, 68 144-149.

Metaxas, A.C., Meredith, R.J., 1983. Industrial Microwave Heating. Peter Peregrinus Ltd., London, 357 p.

Morioka, Y., Kobayashi, J., Higuchi, L., 1973. Freezing of the Capillary Liquid Condensing in Fine Pores. Journal of Colloid and Interface Science. Vol 42. No. 1. pp. 156 - 164.

Morison, S.R., 1977. The Chemical Physics of Surface. Plenum Press, New York. pp. 403.

Moukwa, M., Aitcin, P.C., 1988. The effect of Drying on Cement Pastes Pore Structure as Determined by Mercury Porosimetry. Cement and Concrete Research, Vol, 18., pp. 745 - 752.

National Instruments, 1992a. Lab-PC+, User Manual., National Instruments Corporation.

National Instruments, 1992b. NI-DAQ Software Reference Manual for DOS/Windows/Lab Windows., National Instruments Corporation.

National Instruments, 1992c. NI-DAQ, Function Reference Manual for DOS/Windows/Lab Windows., National Instruments Corporation.

Niesel, K., 1973. Determination of the Specific Surface by measurement of permeability. Material and Structures, Vol. 6. No. 33. pp. 115 - 225.

North, F.K., 1985. Petroleum Geology. Allen & Unwin, Boston, USA, pp. 115-126.

Norusis, M.J. 1990: SPSS/PC+ Statistics 4.0 for the IBM PC/TX/AT and PS/2. SPSS Inc., USA

Olsen, M.P.J., 1984. Mathematical Modelling of the Freezing Process of Concrete and Aggregates. Cement and Concrete Research, Vol. 14., pp. 113 - 122.

Omega, 1993. Thermocouple Reference Tables Based on the ITS-90. Omega Engineering Inc.

Parrot, L.J., 1992. Water Absorption in Cover Concrete. Material and Structures. Vol. 25. pp. 284-292.

Pigeon, M., Pleau, R., 1995. Modern Concrete Technology 4, Durability of Concrete in cold Climates. E&FN SPON, 244p.

Powers, T.C. 1949. The air requirements of frost-resistant concrete. Proceedings of the Highway Research Board. 29, 184-211

Powers, T.C., 1955. Basic Considerations Pertaining to Freezing and Thawing Tests. Proceedings of the American Society for Testing and Materials, Vol. 55, 1132 -1155.

Powers, T.C., 1975. Freezing Effect in Concrete: Durability of Concrete, ACI SP47, American Concrete Institute, Detroit, Michigan, pp. 1-11.

Prout, W., Hoff, W.D., 1990. Fundamental Studies of Frost Damage in Clay Brick. Durability of building Materials and Components, Proceedings of the fifth International Conference held in Brighton, UK, 7-9 November, pp. 39-51.

Reed, M.A., Lovell, C.W., Altschaeffl, A.G., Wood. L.E., 1979. Frost-Heaving Rate Predicted From Pore-Size Distribution., Canadian Geotechnical Journal, Vol. 16., pp. 463-471.

Reynolds, W.C., 1968. Thermodynamics, Second Edition. McGraw-Hill Book Company, New York., pp. 496.

Rigbey, S.J. 1980. The Effect of Sorbed Water on Expansivity and Durability of Rock Aggregates. Master Thesis, University of Windsor, Windsor, Ontario, Canada, pp. 165.

Sellevold, E.J., Radjy, F., 1986. Low Temperature Mechanical Response of Porous Vycor glass as a Function of Moisture Content. Part. I: The Capillary Tension. Cement and concrete research Journal, Vol. 16.

Smith, J.M., Van Ness H.C., 1975. Introduction to Chemical Engineering Thermodynamics., McGraw-Hill Book Company, pp. 632.

Van Zante, H.J., 1973. The Microwave Oven. Houghton Mifflin Comp., USA, 184 p.

Verbeck, G., Landgren, R., 1960. Influence of physical characteristics of aggregates on frost resistance of concrete. Proceedings of the American Society for Testing and Materials, 60, pp. 1063 -1079.

Von Hippel, A.R. (editor), 1958. Dielectric Materials and Applications., The Technology PressM.I.T., John Wiley&Son Inc., New York, 438 p.

Weast, R.C., 1973. Hand Book of Chemistry and Physics, CRC, 54th edition.

Wells, L.K., 1994. The LabVIEW Student Edition, User's Guide, Prentice Hall, Englewood Cleffs, New Jersey, pp. 387.

Whitehead, S., 1951. Dielectric Breakdown of Solids., Oxford, Clarendon Press, 269 p.

Williams, F., 1986: Reasoning with Statistics, How to Read Quantitative Research. third edition, Holt, Rinehart and Winson, The Dryden Press, Saunders College Publishing, USA.

APPENDIX   A

Sample Location and Description

Table A.1 List of Precambrioan Samples

Sample Number	Quarry Numger	Rock Type
98_M	31	Marble
99_M	31	Marble
100_M	31	Marble
114_G	38	Granite
115_SY	39	Syenite
117_SY	39	Syenite
118_HD	40	Diorite

Table A.2 List of Paleozoic samples (Part 1)

Sample Number	Quarry Numger	Rock Type	Formation *
1_Lcf	1	Limestone	Lucas
3_Lcf	1	Limestone	Lucas
4_L	1	Limestone	Lucas
5_Df	2	Dolomite	Lockport
6_Df	2	Dolomite	Lockport
8_D	2	Dolomite	Lockport
10_L	3	Limestone	Gull River
15_D	5	Dolomite	Oxford
16_D	5	Dolomite	Oxford
17_Lf	6	Limestone	Bois Blanc
18_D	6	Dolomite	Bertie
19_Df	6	Dolomite	Bertie
20_Dcf	7	Dolomite	Lockport
21_Dcf	7	Dolomite	Guelph
22_Dcf	7	Dolomite	Guelph
23_Dcf	7	Dolomite	Lockport
24_Dcf	7	Dolomite	Lockport
26_Df	8	Dolomite	Bartie
28_L	9	Limestone	Gull River
32_Df	10	Dolomite	Lockport
34_Df	10	Dolomite	Lockport
37_D	11	Dolomite	Gull River
37.1_L	11	Limestone	Gull River
39_L	12	Limestone	Gull River
40_L	12	Limestone	Gull River
41_Df	14	Dolomite	Oxford
42_Dgf	14	Dolomite	Oxford
45_Df	15	Dolomite	Bertie
46_Df	15	Dolomite	Bertie
50_L	15	Limestone	Bois Blanc
51_Lgf	15	Limestone	Bois Blanc
52_Df	15	Dolomite	Bertie
53_Df	15	Dolomite	Bertie
54_Dcf	16	Dolomite	Lockport
55_Dcf	16	Dolomite	Lockport

* For the age of Formation see Table 3.1

114

Table A.2 List of Paleozoic samples (Part 2)

Sample Number	Quarry Numger	Rock Type	Formation *
56_Dcf	16	Dolomite	Guelph
57_D	16	Dolomite	Guelph
58_Dcf	17	Dolomite	Amable
60_Dcf	17	Dolomite	Amable
61_Dcf	17	Dolomite	Reynales
62_L	18	Limestone	Gull River
65_L	19	Limestone	Bobcaygeon
68_L	21	Limestone	Gull River
70_L	21	Limestone	Gull River
74_L	24	Limestone	Gull River
75_Lf	24	Limestone	Gull River
75.1_L	24	Limestone	Gull River
76_Dgf	25	Dolomite	Lockport
78_Df	25	Dolomite	Lockport
79_Dcf	25	Dolomite	Lockport
80_Lf	26	Limestone	Dundee
81_L	26	Limestone	Dundee
83_L	27	Limestone	Middle Black River
84_Df	27	Dolomite	March or Oxford
85_L	27	Limestone	Middle Black River
87_L	28	Limestone	Gull River
88_D	29	Dolomite	Bertie
90_D	29	Dolomite	Bertie
91_Df	29	Dolomite	Bertie
92_Df	29	Dolomite	Bertie
93_Df	30	Dolomite	Decew
94_Lf	30	Limestone	Lockport
95_Dcf	30	Dolomite	Lockport
96_Lf	30	Limestone	Lockport
97_Lgf	30	Limestone	Lockport
101_Sgf	32	Sandstone	Potsdam
102_Sgf	32	Sandstone	Potsdam
103_Sgf	33	Sandstone	Medina
108_SH	35	Shale	Billings
120_D	42	Dolomite	Decew
121_Df	42	Dolomite	Decew
122_Dgf	42	Dolomite	Lockport
123_SH	42	Shale	Rochester
124_Scf	43	Sandstone	Oriskany
125_D	43	Dolomite	Bertie
126_Lf	44	Limestone	Bois Blanc
127_D	44	Dolomite	Bertie
128_D	44	Dolomite	Bertie
129_Df	44	Dolomite	Bertie
130_Lf	45	Limestone	Dundee
131_Lgf	45	Limestone	Dundee

* For the age of Formation see Table 3.1

115

Table A.3 Sample Localization and Lithological Description

1 MacGregor Quarry

County Essex; Township Anderdon; Lot 10; 10 km northeast of Amherstburg.

1_Lcf Limestone; Formation Lucas; Member Anderdon; buff to brown; aphanitic; fossiliferous, vuggy with some calcite.

3_Lcf Limestone; Formation Lucas; Member Anderdon; light grey; fine crystalline; some dark grey shaly partings, slightly vuggy with calcite crystals.

4_L Limestone; Formation Lucas; Member Anderdon; buff and light grey colour bonding; aphanitic to microcrystalline.

2 Vinemount Quarry

County Wentworth; Township Saltfleet; Lot 5; 4 km south of Winona.

5_Df Dolomite; Formation Lockport; Member Decew; dark grey to brown; argillaceous, slightly calcareous, medium crystalline.

6_Df Dolomite; Formation Lockport; Member Gasport; light brown to buff; calcareous, medium crystalline.

8_D Dolomite; Formation Lockport; Member Eramosa; medium brown with dark grey streaks; argillaceous, silty, aphanitic.

3 Collins Bay Quarry

County Frontenac; Township Kingston; Lots 2,3; 2.5 km west of the highway 38 - highway 2 intersection.

10_L Limestone; Formation Gull River; Member A; dark grey; argillaceous, minor calcite crystals, microcrystalline; thick bedded.

5 Wings (Maitland) Quarry

County Grenville; Township Augusta; Lot 24; 6km north of Maitland.

15_D Dolomite; Formation Oxford; brown to dark grey; medium crystalline; shaly partings.

16_D Dolomite; Formation Oxford; brown to dark grey; calcareous, medium crystalline .

6 Ridgemount Quarry

116

County Welland; Township Bartie; Lot 8; 4km south of Stevensvill.

17_Lf   Limestone; Formation Bois Blanc; light grey to green; fine crystalline, silty; buff weathering, chert nodules, dendritic manganese, oxide along partings.

18_D   Dolomite; Formation Bertie; Member Arcon; medium brown to grey; fine crystalline to aphanitic; shaly partings.

19_Df   Dolomite; Formation Bertie; Member Arcon; mottled light and medium grey; aphanitic.

7 Dundas Quarry
         County Wentworth; Township West Flamborough; Lots 10, 11; north west of Hamilgton.

20_Dcf   Dolomite; Formation Lockport; Member Eramosa; medium brown; thin colour laminations, shaly partings, fine crystalline to aphanitic.

21_Dcf   Dolomite; Formation Guelph; light grey; vuggy, fine crystalline to aphanitic.

22_Dcf   Dolomite; Formation Guelph; light grey; buff weathering, slightly vuggy, fine crystalline to aphanitic.

23_Dcf   Dolomite; Formation Lockport; Member Eramosa; light brown; fine crystalline aphanitic; thick bedded, occasional shaly parting.

24_Dcf   Dolomite; Formation Lockport; Member Eramosa; grey to dark brown; fine crystalline to aphanitic; thick bedding.

8 Cayuga Quarry
         County Haldimand; Township North Cayuga; Lots 45,46; 5.5km west of the village Cayuga.

26_Df   Dolomite; Formation Bartie; Member Arcon; light brown and light grey; aphanitic; thin laminated clastic in part.

9 Waubaushene Quarry
         County Simcoe; Township Tay; Lot 9; 7km north of the village Coldwater.

28_L   Limestone; Formation Gull River; Member Lower; medium brown to greyish green; glauconitic, aphanitic.

10 Stoney Creek Quarry
         County Wentworth; Township Saltfleet; Lots 27, 28; west of Highway 20, southern edge of Stoney Creek.

32_Df   Dolomite; Formation Lockport; Member Eramosa; grey - brown; aphanitic, spots of calcite; shaly.

34_Df   Dolomite; Formation Lockport; Member Eramosa; medium brown; aphanitic; grey shale partings.

11 MacLeod Quarry
County Stormont; Township Cornwall; Lot 4; 5km north of Cornwall.

37_D   Dolomite; Formation Gull River; Member Lower; light grey; fine crystalline to aphanitic; thick bedded.

37.1_L   Limestone; Formation Gull River; Member Lower; light grey; fine crystalline to aphanitic; thick bedded.

12 J.Dennison (Napanee) Quarry
County Lennox and Addington; Township North Fredericksburgh; Lot 21; North side of Highway 2, eastern of Napanee.

39_L   Limestone; Formation Gull River; Member D; brownish grey; aphanitic; shale partings.

40_L   Limestone; Formation Gull River; Member D; brownish grey; aphanitic; medium bedded, similar to sample # 39.

14 Boyce (South Gloucester) Quarry
Township Gloucester; Lot 25; 3km north of the hamlet of South Gloucester.

41_Df   Dolomite; Formation Oxford; light grey; calcareous, aphanitic; shaly partings, thinly laminated in part.

42_Dgf   Dolomite; Formation Oxford; dark grey; calcite crystals, fine crystalline; massive bedding.

15 Northwest Quarry
County Haldimand; Township Walpole; Lots 12, 13.

45_Df   Dolomite; Formation Bertie; medium to dark grey; argillaceous, fine crystalline; irregular shaly partings.

46_Df   Dolomite; Formation Bertie; buff to light brown; aphanitic; minor shaly partings.

50_L   Limestone; Formation Bois Blanc; light to medium grey; fine crystalline; chert modules, fossiliferous.

51_Lgf   Limestone; Formation Bois Blanc ; light grey; arenaceous, fine grained; minor shaly partings, clastic.

52_Df   Dolomite; Formation Bertie; buff to light brown; aphanitic; light buff weathering, thick bedded.

53_Df   Dolomite; Formation Bertie; medium brown; aphanitic; shaly laminations, similar to sample 45.

16 Flamboro Quarry
Township West Flamboro; Lot 6; west side of Brock Road.

54_Dcf   Dolomite; Formation Lockport; Medium brown; aphanitic; sugary.

55_Dcf   Dolomite; Formation Lockport; Member Eramosa; light to medium brown; aphanitic; minor shale as thin laminations.

56_Dcf   Dolomite; Formation Guelph; light grey; aphanitic; vuggy with crystal development.

57_D   Dolomite; Formation Guelph; light grey to buff; aphanitic.

17 Halton Quarry
County Halton; Township Nassagaweya; Lot 8; 6 km west of Milton.

58_Dcf   Dolomite; Formation Amable; medium grey; reefy, fossiliferous, , fine crystalline.

60_Dcf   Dolomite; Formation Amable; Member middle silurian; light grey; fossiliferous, stylolitic megaporous, fine crystalline.

61_Dcf   Dolomite; Formation Reynales; Member lower silurian; medium grey; mottled, slightly fossiliferous, aphanitic.

18 Uhthoff Quarry
County Simcoe; Township Orillia; Lot 10.

62_L   Limestone; Formation Gull River; Member Middle Ordovician; dark brown; abundant shaly laminations, lithographic.

19 Gamebridge Quarry
County Ontario; Township Mara; Lot 11; 1 km northwest of Gamebridge.

65_L   Limestone; Formation Bobcaygeon; medium grey to buff; diliceousm clastic, medium grained.

21 Kinbgston Quarry

County Frontenac; Township Kingston; Lot 9; west of Highway 38 - Highway 401 interchange.

68_L   Limestone; Formation Gull River; light grey; Aphanitic, calcite crystals and stringers.

70_L   Limestone; Formation Gull River; medium brownish grey; fine crystalline to aphanitic; some calcite crystals and shaly partings.

24 Pittsburg Quarry

County Frontenac; Township Pittsburg; 3.5 km north of Barriefield.

74_L   Limestone; Formation Gull River; Member Middle Ordovician; light brownish grey; fine crystalline; buff weathering, silty.

75_Lf   Limestone; Formation Gull River; Member Middle Ordovician; medium brownish grey; aphanitic; occasional calcite crystals.

75.1_L   Limestone; Formation Gull River; Member Middle Ordovician; medium brownish grey; aphanitic; occasional calcite crystals.

25 MacLanchlan (Beamsville) Quarry

County Lincoln; Township Clinton; Lot 20; 6.4 km south of town.

76_Dgf   Dolomite; Formation Lockport; Member Erasoma; medium brown; sugary, fine crystalline; occasional shaly partings.

78_Df   Dolomite; Formation Lockport; Member Eramosa; brownish grey; aphanitic; shaly partings.

79_Dcf   Dolomite; Formation Lockport; Member Eramosa; brownish grey; aphanitic; mottled, vuggy with some calcite crystals.

26 Port Dover Quarry

County Norfolk; Township Woodhouse; Lot 13; 3.2 km northeast of town.

80_Lf   Limestone; Formation Dundee; light brown; aphanitic; thick bedded, slightly cherty.

81_L   Limestone; Formation Dundee; light brown grey; aphanitic; chert nodules.

27 Brockville Quarry

County Leeds; Township Elizabethtown; Lot 4; Eastern outskirts of the city Brockville.

83_L   Limestone; Formation Middle Black River; medium grey; fine crystalline.

84_Df   Dolomite; Formation March or Oxford; light grey; aphanitic; abundant shaly partings, reefal in part.

85_L   Limestone; Formation Middle Black River; medium brownish grey; fine crystalline; dolomitic, massive.

28 Cornwall Quarry
          County Stormont; Township Cornwall; Lot 25; 6 km northwest of Cornwall.

87_L   Limestone; Formation Gull River; dark grey; aphanitic; massive, minor calcite filled fractures.

29 Port Colborne Quarry
          County Welland; Township Humberstone; Lots 24, 24; 2 km northeast of Port Colborne.

88_D   Dolomite; Formation Bertie; Member Akron; medium brownish; aphanitic; very shaly, slightly mottled, thin bedded.

90_D   Dolomite; Formation Bertie; Member Arkon; dark grey; aphanitic; streaked, laminated layers with small dolomite rhombs, abundant shaly partings.

91_Df   Dolomite; Formation Bertie; Member Arkon; dark brown to grey, mottled; aphanitic; medium bedded, some shale partings.

92_Df   Dolomite; Formation Bertie; Member Arkon; medium grey; aphanitic; laminated, pyritiferous, shaly partings.

30 Queenston Quarry
          County Lincoln; Township Niagara; Lots 47,48,49; 3 km west of Queenston.

93_Df   Dolomite; Formation Decew; medium grey; aphanitic; massive.

94_Lf   Limestone; medium grey; calcitic, calcite crystals in vugs, massive, medium crystalline.

95_Dcf   Dolomite; Formation Lockport; Member Gasport; light grey; ; some large vugs with calcite crystals, massive, medium crystalline.

96_Lf   Limestone; Formation Irondequoit; light grey; aligned elongate crystals throughout, slightly fossiliferous, medium to fine crystalline.

97_Lgf   Limestone; Formation Irondequoit; light to medium grey; ; medium to fine crystalline.

31 Madam Area Quarry
      4.8 km southeast of town

98_M   Marble; light greenish grey; aphanitic; some dark grey argillaceous impurities.

99_M   Marble; white; aphanitic; massive, fine crystals.

100_M   Marble; dark grey; aphanitic; fine crystals, fine colour laminations.

32 Kingston Quarries
      County Frontenac; Township Storrington; Lot 11.

101_Sgf   Sandstone; Formation Potsdam; greyish - pink to red; coarse to medium grained; medium bedded.

102_Sgf   Sandstone; Formation Potsdam; grey pink, black; coarse to medium grained; colour banding, medium bedded, some argillaceous material.

33 Rice and McHarg Quarry
      County Halton; Township Esquesing; Lot 21; 1 km south of town.

103_Sgf   Sandstone; Formation Medina; Member Whirlpool; light grey, brown spotted; fine grained; thin bedded.

35 Cooksville Quarry
      County Peel; Township Toronto; Lots 19, 20.

108_SH   Shale; Formation Billings; medium grey; limy, hard, medium bedded.

38 road cut, flesh blast
      County Peterborough; Township Burleigh; Highway 36, 1km west of highway 28 near Burleigh Falls.

114_G   Granite; pink and black; coarse grained; 20% quartz, 65% orthoclase, 15% mafics.

39 Nephton Quarry
      County Peterborough; Township Methuel.

115_SY   Nepheline Syenite; white with black dots; phaneritic; random orientation of mafics, approximately 5%.

117_SY   Syenite; white with black dots; phaneritic; random orientation of mafics, approximately 5%.

40 road cut
County Hastings; Township Marmora; on Highway 7, 1.6 km west of Marmora.

118_HD   Hornblende Diorite; greenish black; phaneritic, medium crystalline; slightly weathered.

42 Thorold Quarry
Lots 30, 31; 4 km northwest of the town Stamford.

120_D   Dolomite; Formation Decew; medium to dark grey, weathers dark tan to rust; fine crystalline; very irregularly bedded, vuggy and porous, bituminous and clayey.

121_Df   Dolomite; Formation Decew; medium to dark grey, weathers dark tan to rust; fine crystalline; very irregularly bedded, vuggy and porous, bituminous.

122_Dgf   Dolomite; Formation Lockport; Member Gasport; pink grey, weathers tan - buff; fine to coarse crystalline; medium to thick bedded.

123_SH   Shale; Formation Rochester; ; black to dark grey, weathers black; sub to fine crystalline; thin and medium bedded.

43 Cayuga Quarry
Township North Cayuga; Lots 44-47; 5.5 km west of the village of Cayuga.

124_Scf   Sandstone; Formation Oriskany; light cream to white, weathers buff; medium to coarse grained; thick bedded, shaly, fossiliferous.

125_D   Dolomite; Formation Bertie; grey to brown, weathers blue-grey to brown; fine crystalline; shaly, thin to medium bedded.

44 Ridgemount Quarry
Township Bartie; Lots 5-8; 4 km southeast of Stevensville.

126_Lf   Limestone; Formation Bois Blanc; light grey, weathers mottled buff to grey; fine crystalline; thin to medium bedded, chert nodules, fossiliferous.

127_D   Dolomite; Formation Bertie; Member Williamsville; light to medium brown, weathers buff; sub to fine crystalline; thin bedded, bituminous and shaly partings.

128_D   Dolomite; Formation Bertie; Member Scajaquanda; dark brown to dark grey, weathers blue grey; sub to fine crystalline and fine grained; Thin to medium bedded, shaly.

129_Df   Dolomite; Formation Bertie; Member Falkirk; light to dark brown, weathers medium to dark brown; very fine to fine crystalline; thin to medium bedded, bituminous partings.

45_Pelee Island Quarry
County Essex; Township Pelee Island; Lots 1, 2; 150 m north of the north shore.

130_Lf   Limestone; Formation Dundee; brown, weathers buffs; fine to medium crystalline; thin bedded, fossiliferous.

131_Lgf   Limestone; Formation Dundee; light brown, weathers buff; medium crystalline; thick bedded, chert nodules, fossiliferous, petroliferous odour.

APPENDIX   B

Statistical Tables and Figures

TABLE B.1 Cluster Group Mean Comparison

	Cluster group mean		Gr N vs Gr F	Cluster group mean			Cl1 vs Cl2	Cl1 vs Cl3	Cl2 vs Cl3	Cluster group mean		Cl4 vs Cl5	Standard deviation						
	Group N	Group F		Cluster 1	Cluster 2	Cluster 3				Cluster 4	Cluster 5		Group N	Group F	Cluster 1	Cluster 2	Cluster 3	Cluster 4	Cluster 5
RDEN	2.81	2.84	*	2.68	2.60	2.60	*			2.72	2.66		0.20	0.12	0.05	0.09	0.05	0.06	0.34
RMGSO4	3.63	8.46	**	6.61	4.37	10.96				3.39	7.41		16.17	23.96	8.56	27.47	26.79	3.84	30.10
RFRTH	7.24	7.08		7.94	4.68	9.12				5.37	24.55	*	11.57	8.63	7.75	7.33	11.86	7.12	10.80
CRDL		17.34		8.01	26.49	14.70	*							16.07	8.56	13.47	20.15		
CTF		-3.50		-3.60	-4.00	-2.90	**							1.17	0.95	0.70	1.62		
RBUS	0.14	1.02	*	0.72	1.15	2.09	*	*	*	0.11	0.30	*	0.28	1.14	0.41	0.38	0.60	0.07	0.19
RDRYLOSS	0.05	0.12	*	5.62	0.06	0.11	*			0.04	0.08	*	0.24	0.84	0.92	0.02	1.41	0.07	0.04
RADS	0.09	0.12	*	0.22	0.03	0.11	*	**	*	0.05	0.26	**	0.30	0.16	0.21	0.03	0.06	0.04	0.13
RVABGNS	0.05	0.23	*	0.26	0.12	0.44	**	**		0.04	0.07		0.14	0.21	0.16	0.10	0.20	0.10	0.02
RCAP32S	0.01	0.18	*	0.11	0.28	0.42	**	*		0.01	0.02		0.08	0.82	0.17	0.58	0.26	0.02	0.01
RPORO	0.37	1.91	*	1.45	2.45	2.62	*	*	*	0.30	0.74	*	0.57	1.54	0.60	0.75	0.73	0.13	0.27
CFWS		1.01		0.37	0.72	1.48	*							1.08	0.29	0.26	0.48		
CUFBUS		0.75		0.49	0.79	0.91	*		**					0.39	0.23	0.25	0.37		
CUFWS		0.88		0.74	0.83	1.02		**						0.39	0.32	0.25	0.36		
MQABS	0.72	1.32	*	1.48	0.91	1.48	*	*	**	0.52	1.29	*	0.77	1.05	0.65	0.55	0.50	0.16	0.57
MQADS	0.12	0.11	*	0.22	0.03	0.08	*	*		0.09	0.32	*	0.26	0.18	0.23	0.03	0.10	0.09	0.18
MQBUS	0.51	1.12	*	1.20	0.87	1.35		**		0.38	0.85	*	0.58	0.99	0.68	0.53	0.57	0.17	0.49
RBUB	59.30	84.30	*	73.70	97.50	95.10	**	*		62.40	52.10	*	22.37	11.91	10.56	2.45	2.99	28.60	17.85
RADSB	39.60	15.90	*	25.40	4.20	6.00	*	*		35.30	46.00		20.95	10.34	9.11	3.43	2.61	20.63	19.32
RBUGNB	21.90	27.90		34.20	16.70	25.10	*			24.10	13.80	**	113.66	44.50	16.93	11.81	74.04	55.39	67.43
RCAP32B	15.40	20.00		13.90	31.10	22.00	**		**	11.70	7.00		22.87	20.46	9.12	22.66	7.83	10.75	2.21
RSATBIF	63.70	77.50		88.30	48.80	84.90	*			84.80	93.40	*	15.78	18.60	11.29	10.13	8.68	8.39	3.91
RABGNV	15.60	20.50		25.90	9.20	20.40	*	*	*	32.50	11.50		36.17	13.81	13.19	7.86	7.23	47.87	5.51
RBUV	43.90	55.60	*	52.20	47.20	74.40	*	*	*	41.30	43.60	*	17.00	14.34	12.63	8.64	5.72	17.59	15.30
CFWB		45.90		34.30	46.70	58.80	*							18.35	10.89	8.56	8.61		
CFWV		36.05		28.00	29.50	52.90								16.68	9.66	5.70	7.49		
CUFBUB		44.88		46.20	51.40	36.80	*							17.84	16.19	7.84	8.98		
CUFBUV		34.16		37.10	33.10	33.30								13.62	9.69	7.97	8.56		
CUFWB		54.10		65.70	53.30	41.20	*							18.35	10.89	8.58	8.61		
CUFWV		41.84		53.00	34.30	37.20		*						15.19	12.90	8.24	8.44		
RSATAFT		77.69	*	81.10	63.80	90.10	*	*	*					13.06	10.35	9.00	4.22		
MQABAB	512.86	239.88	*	281.84	218.78	173.78				618.60	467.74		1394.45	172.40	137.70	112.54	84.99	429.47	412.64
MQADAD	134.90	102.33		97.72	126.82	91.20				162.18	501.19		193.79	169.99	91.58	87.60	87.55	305.43	60.23
MQBUBU	302.00	112.20	*	165.96	75.86	64.57				346.74	288.40		450.23	0.30	0.25	0.22	0.25	0.39	0.46

* = mean are different with two tailed signifacance 0.01
** = mean are different with two tailed signifacance 0.05

126

TABLE B.2 List of the sample distribution in the clusters.

Count	Group F	Group N	Cluster 1	Cluster 2	Cluster 3	Cluster 4	Cluster 5
1	1_Lcf	4_L	6_Df	20_Dcf	5_Df	16_D	4_L
2	3_Lcf	8_D	17_Lf	23_Dcf	26_Df	39_L	8_D
3	5_Df	10_L	19_Df	54_Dcf	41_Df	57_D	18_D
4	6_Df	15_D	21_Dcf	55_Dcf	45_Df	62_L	28_L
5	17_Lf	16_D	32_Df	58_Dcf	51_Lgf	65_L	37_D
6	19_Df	18_D	34_Df	60_Dcf	53_Df	68_L	37.1_L
7	20_Dcf	28_L	42_Dgf	76_Dgf	91_Df	74_L	40_L
8	21_Dcf	37_D	50_L	79_Dcf	129_Df	81_L	88_D
9	22_Dcf	37.1_L	61_Dcf	95_Dcf	130_Lf	83_L	128_D
10	23_Dcf	39_L	75_Lf	102_Sgf		99_M	
11	24_Dcf	40_L	78_Df	124_Scf		100_M	
12	26_Df	57_D	84_Df			114_G	
13	32_Df	62_L	85_L				
14	34_Df	65_L	92_Df				
15	41_Df	68_L	93_Df				
16	42_Dgf	70_L	94_Lf				
17	45_Df	74_L	96_Lf				
18	46_Df	75.1_L	121_Df				
19	50_L	81_L	122_Dgf				
20	51_Lgf	83_L	126_Lf				
21	52_Df	87_L					
22	53_Df	88_D					
23	54_Dcf	90_D					
24	55_Dcf	98_M					
25	56_Dcf	99_M					
26	58_Dcf	100_M					
27	60_Dcf	108_SH					
28	61_Dcf	114_G					
29	75_Lf	115_SY					
30	76_Dgf	117_HD					
31	78_Df	118_DI					
32	79_Dcf	120_D					
33	80_Lf	123_SH					
34	84_Df	125_D					
35	85_L	128_D					
36	91_Df						
37	92_Df						
38	93_Df						
39	94_Lf						
40	95_Dcf						
41	96_Lf						
42	97_Lgf						
43	101_Sgf						
44	102_Sgf						
45	103_Sgf						
46	121_Df						
47	122_Dgf						
48	124_Scf						
49	126_Lf						
50	127_D						
51	129_Df						
52	130_Lf						
53	131_Lgf						

g - visible grain size
c - cavities
f - freezable water
D - Dolomite
DI - Diorite
G - Granite
HD - Hornblade Diorite
M - Marble
S - Sandstone
SH - Shale
SY - Syenite

Table B.3   Number of cases included into the correlation test,. (part 1)

	CFWB	CFWS	CFWV	CRDL	CTF	CUFBUB	CUFBUS	CUFBUV	CUFWB	CUFWS	CUFWV	RDRYLOSS
CFWS	50											
CFWV	50	50										
CRDL	17	17	17									
CUFBUB	49	49	49	17	47		48	49	49	48		71
CUFBUV	50	50	50	17	48	49	48	50	49	48	50	84
CUFWB	49	49	49	17	47	49	48	49		48	50	84
CUFWS	48	48	48	17	46	48	48	48			50	84
CUFWV	50	50	50	17	48	49	48	49		47	49	79
RFRTH	43	43	43	17	41	42	41	42	42	41	42	80
RABS	50	50	50	17	48	49	48	49	49	48	49	81
RBUB	50	50	50	17	48	49	48	49	49	48	49	81
RBUS	50	50	50	17	48	49	48	49	49	48	49	76
RBUV	50	50	50	17	48	49	48	49	49	48	49	76
MQABAB	49	49	49	17	47	48	47	48	48	47	48	84
MQABS	50	50	50	17	48	49	48	49	49	48	49	81
MQADAD	48	48	48	17	46	47	46	47	47	46	48	81
MQADS	48	48	48	17	46	47	46	47	47	46	48	76
MQBUBU	46	46	46	17	44	45	44	45	45	44	46	76
MQBUS	46	46	46	17	44	45	44	45	45	44	48	84
RABGNV	50	50	50	17	48	49	48	49	49	48	50	84
RADS	50	50	50	17	48	49	48	49	49	48	50	84
RADSB	50	50	50	17	48	49	48	49	49	48	50	84
RBUGNB	47	47	47	17	45	46	45	46	46	45	47	79
RCAP32B	50	50	50	17	48	49	48	49	49	48	50	84
RCAP32S	50	50	50	17	48	49	48	49	49	48	50	84
RDEN	50	50	50	17	48	49	48	49	49	48	50	84
RSATAFT	50	50	50	17	48	49	48	49	49	48	50	49
RSATBIF	50	50	50	17	48	49	48	49	49	48	50	84
RVABGNS	50	50	50	17	48	49	48	49	49	48	50	79
RPORO	50	50	50	17	48	49	48	49	49	48	50	84
CUFBUS				17								

Table B.3   Number of cases included into the correlation test. (part 2)

	RFRTH	RABS	RBUB	RBUS	RBUV	RMGSO4	MQABAB	MQABS	MQADA	MQADS	MQBUBU	MQBUS
RBUB	73	87	87									
RBUS	73	87	87	87								
RBUV	73	87	87	87	87							
MQABAB	69	82	82	82	82	69	82					
MQABS	70	83	83	83	83	70	82	83				
MQADAD	70	84	84	84	84	70	80	80	84	84		
MQADS	70	84	84	84	84	70	80	80	84	77		
MQBUBU	66	79	79	79	79	66	79	79	77	77	79	
MQBUS	66	79	79	79	79	66	79	79	77	77	79	79
RADS	73	87	87	87	87	73	82	83	84	84	79	79
RADSB	73	87	87	87	87	73	82	83	84	84	79	79
RCAP32B	73	87	87	87	87	73	82	83	84	84	79	79
RCAP32S	73	87	87	87	87	73	82	83	84	84	79	79
RDEN	73	87	87	87	87	73	82	83	84	84	79	79
RSATAFT	43	50	50	50	50	43	49	50	48	48	46	46
RSATBIF	73	87	87	87	87	73	82	83	84	84	79	79
RVABGNS	68	81	81	81	81	68	78	79	78	78	75	75
RPORO	73	87	87	87	87	73	82	83	84	84	79	79

	RABGNV	RADS	RADSB	RBUGNB	RCAP32B	RCAP32S	RDEN	RSATAFT	RSATBI	RVABGNS	RPORO
RADSB	88	88	88								
RBUGNB	81	81	81	81							
RCAP32B	88	88	88	81	88						
RCAP32S	88	88	88	81	88	88					
RDEN	88	88	88	81	88	88	88				
RSATAFT	50	50	50	47	50	50	50	50			
RSATBIF	88	88	88	81	88	88	88	50	88		
RVABGNS	81	81	81	76	81	81	81	50	81	81	
RPORO	88	88	88	81	88	88	88	50	88	81	88

Rescaled Distance Cluster Combine

```
          C A S E      0        5        10       15       20       25
        Label    Num   +---------+---------+---------+---------+---------+

        93_Df     26    ┐┐
        94_Lf     27    ┘│
        6_Df       2    ┐├───┐
        17_Lf      3    ┤   │
        84_Df     23    ┘   ├─────────────┐
        121_Df    31    ┐   │             │
        34_Df     10    ┴──────┐          │
        96_Lf     29          ├───┐      │
        21_Dcf     6          ┘   │      ├──────────────────┐
        19_Df      4    ┐         │      │                  │
        78_Df     21    ┴┐        │      │                  │
        75_Lf     19    │├──┐     │      │                  │
        92_Df     25    ┤  │     │      │                  │
        122_Dgf   32    ┘  ├─────┘      │                  │
        32_Df      9    ┐  │            │                  │
        61_Dcf    18    ┴──┘            │                  ├─────1
        42_Dgf    11    ┐               │                  │
        126_Lf    34    ┴───────────────┘                  │
        76_Dgf    20    ┐                                  │
        124_Scf   33    ┴───┐                              │
        102_Sgf   30       ├──────┐                        │
        58_Dcf    16    ┐  │      │                        │
        60_Dcf    17    ┴─┐│      │                        │
        23_Dcf     7    ┐ ├┘      ├──────┐                 │
        55_Dcf    15    ┴─┘       │      │                 │
        54_Dcf    14    ┐         │      ├────2────┐
        20_Dcf     5    ┴─────────┘      │         │
        79_Dcf    22    ──────────────────┘         │
        95_Dcf    28    ──────────────────           │
        5_Df       1    ┐                            │
        53_Df     13    ┴────┐                       │
        26_Df      8    ─────┤                       │
        91_Df     24    ┐    ├────────┐              │
        130_Lf    36    ┴──┐ │        ├────3─────────┘
        129_Df    35    ───┘ │
        51_Lgf    12    ─────┘
```

Figure B1 Dendogram of clustering of Group F

130

Rescaled Distance Cluster Combine

```
          C A S E              0         5        10        15        20        25
       Label        Num        +---------+---------+---------+---------+---------+

       4_L            1         ┐
       28_L           5         ┤
       37_D           6         ┐
       127_D         21         ┘
       8_D            2         ┐
       88_D          17         ┤
       18_D           4         ┤
       40_L           9         ┘
       128_D         22                                    4
       37.1_L         7
       16_D           3         ┐
       114_G         19         ┤
       65_L          12         ┤
       81_L          15         ┘
       39_L           8
       57_D          10
       62_L          11         ┐
       68_L          13         ┤
       74_L          14                                    5
       83_L          16
       99_M          18
       125_D         20
```

Figure B2 Dendogram of clustering of Group N

131

APPENDIX   C

Discussion - Figures
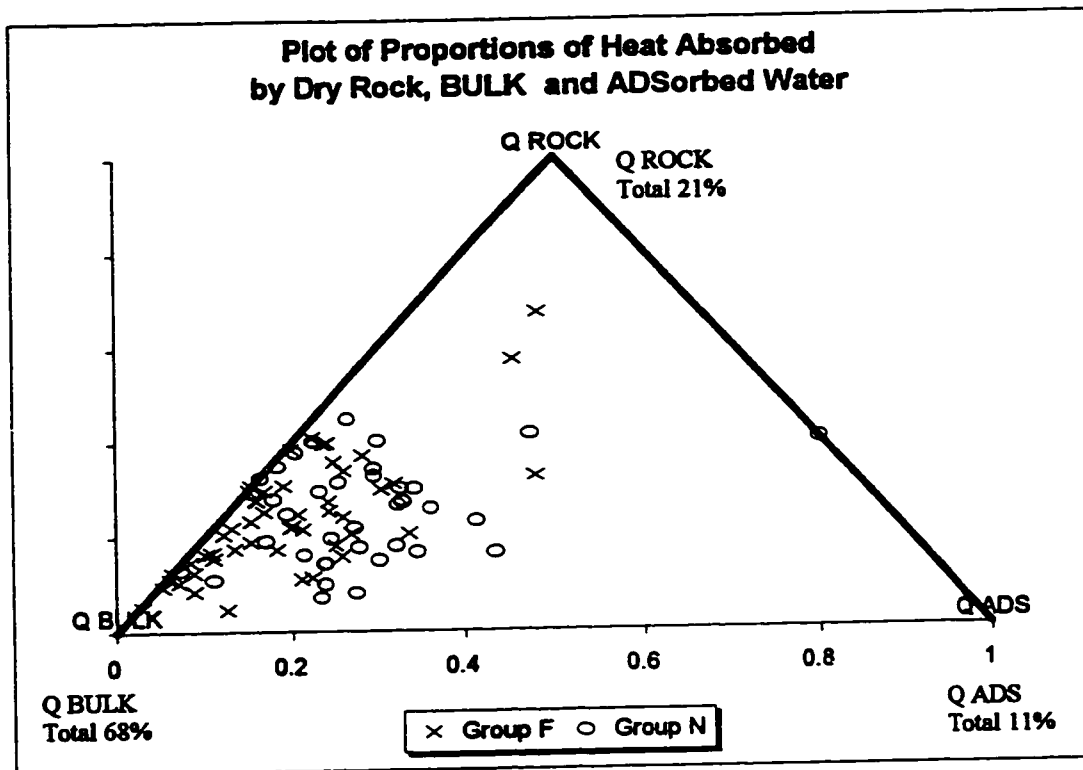
Figure C.1 Triangular plot of the proportions of the total microwave heat adsorbed by dry rock, adsorbed water and bulk water.
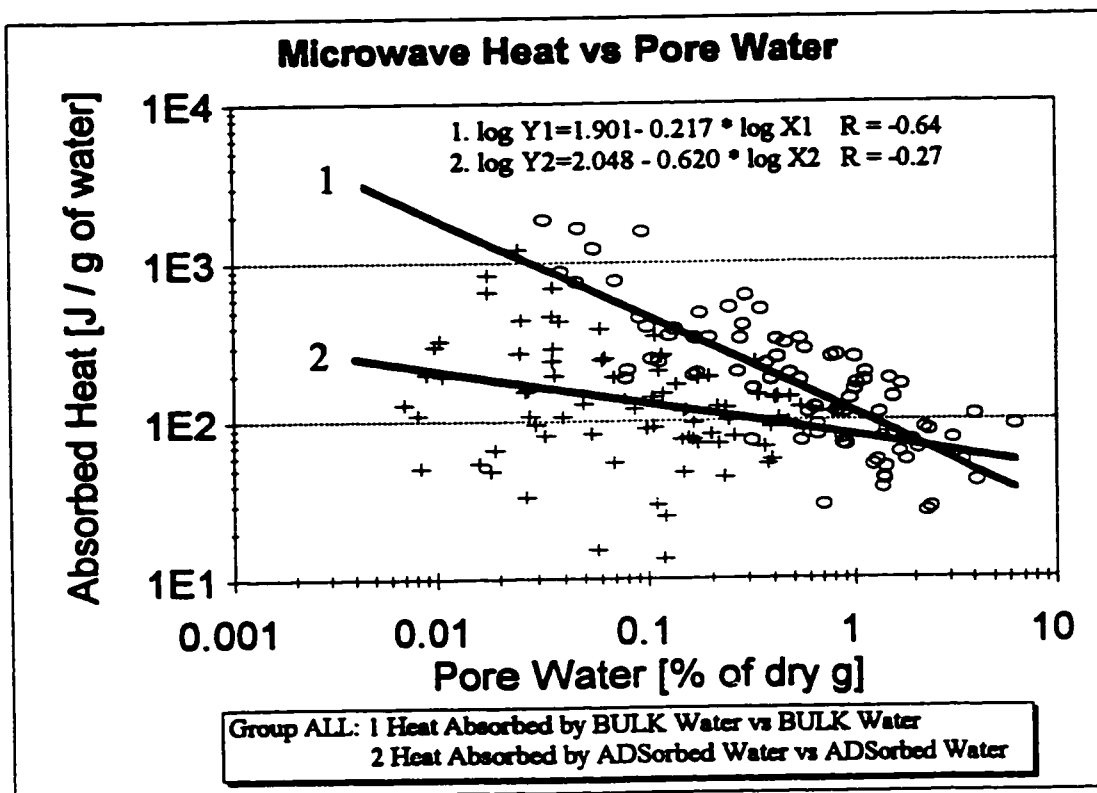
Figure C.2 Comparison of the total microwave heat absorption by bulk woter and by adsorbed water
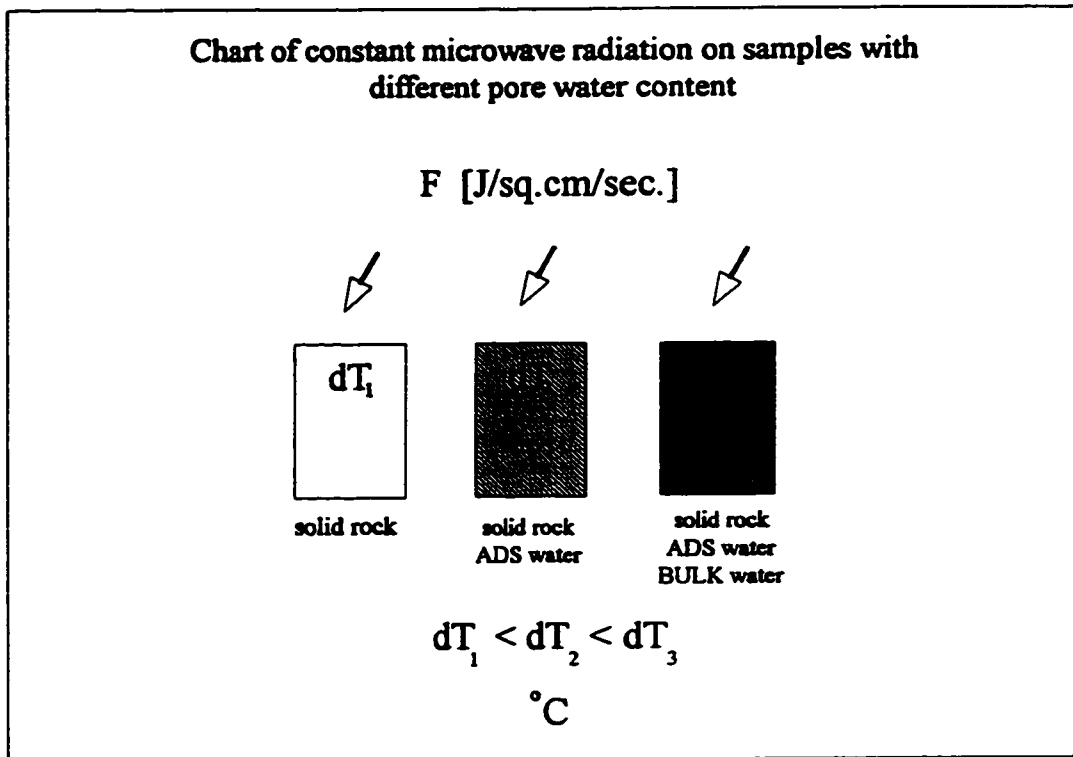
Figure C.3 Illustration of samples with different water content exposed to constant microwave flux.
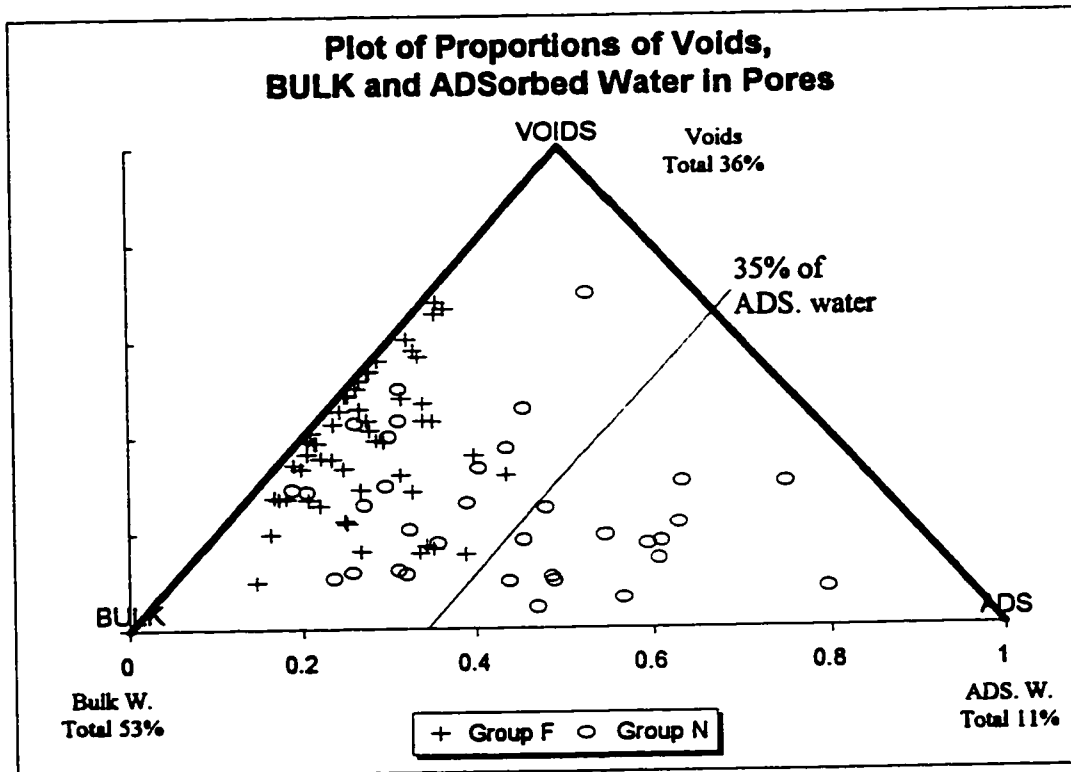
Figure C.4 Triangular plot of proportions of voids, bulk water and adsorbed water in rock pores.
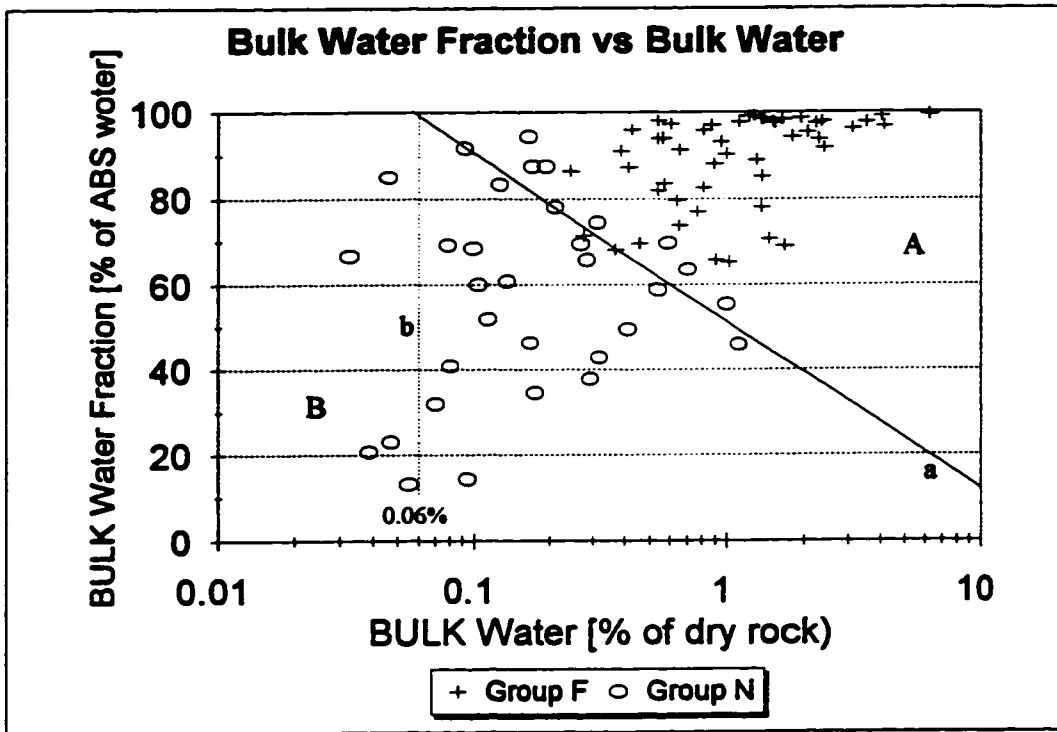
Figure C.5 Graph of bulk water fraction versus bulk water. A - domain of the samples which showed freezing, B - Domain of the samples which did not show freezing, a - border between A and B, b - threshold limit of sensitivity of the calorimetric syste
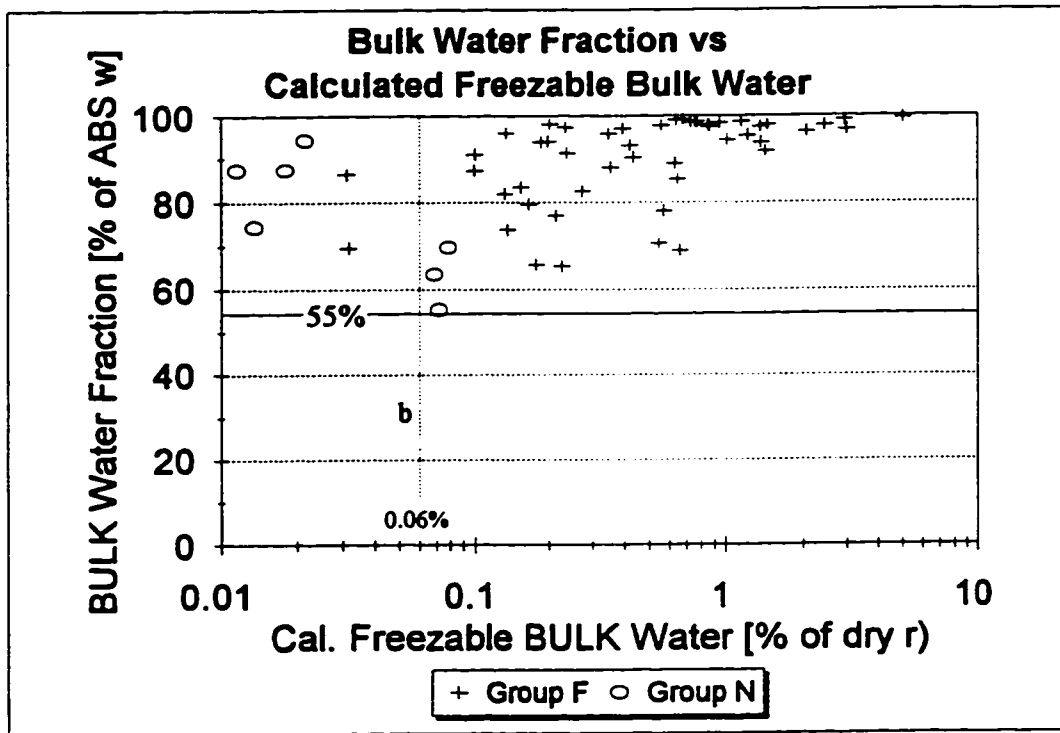
Figure C.6 Graph of bulk water fraction versus calculated freezable bulk water b - threshold limit of the calorimetric system, 55% - minimal content of bulk water (weight percent of total absorbed water) below which the bulk water does not freeze.

Bulk Water Fraction vs Observed Frozen Water

BULK Water Fraction [% of ABS w]

100
80
60
55%
40
b
20

0.06%

0.01   0.1   1   10

Observed Frozen Water [% of dry rock)

+ Group F
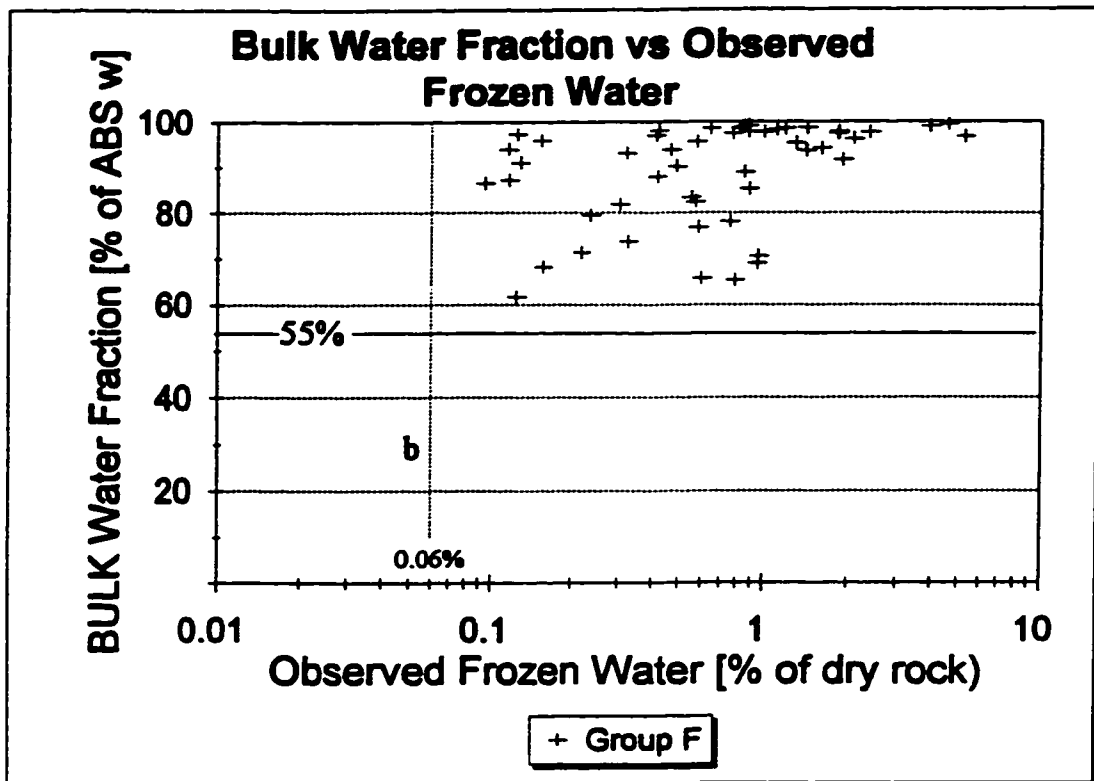
Figure C.7 Graph of bulk water fraction versus observed frozen water. b - threshold limit of the calorimetric system, 55% - minimal content of bulk water (weight percent of total absorbed water) below which the bulk water does not freeze.

Expansion on freezing of samples with different pore size distribution, degree of saturation and amount of frozen water

dL   <   dL   =<   dL   >   dL

A   B   C   D

D.Sat.: 81%   90%   64%   64%

Porosity : A < B = C = D

Amount of Frozen Water: A < B < C = D

■ water saturated rock sample

○ empty large pore

⊜ large pore filled with water

dL - length change on freezing

D.Sat. - degree of saturation

A   - Cluster 1
B   - Cluster 2
C, D - Cluster 3
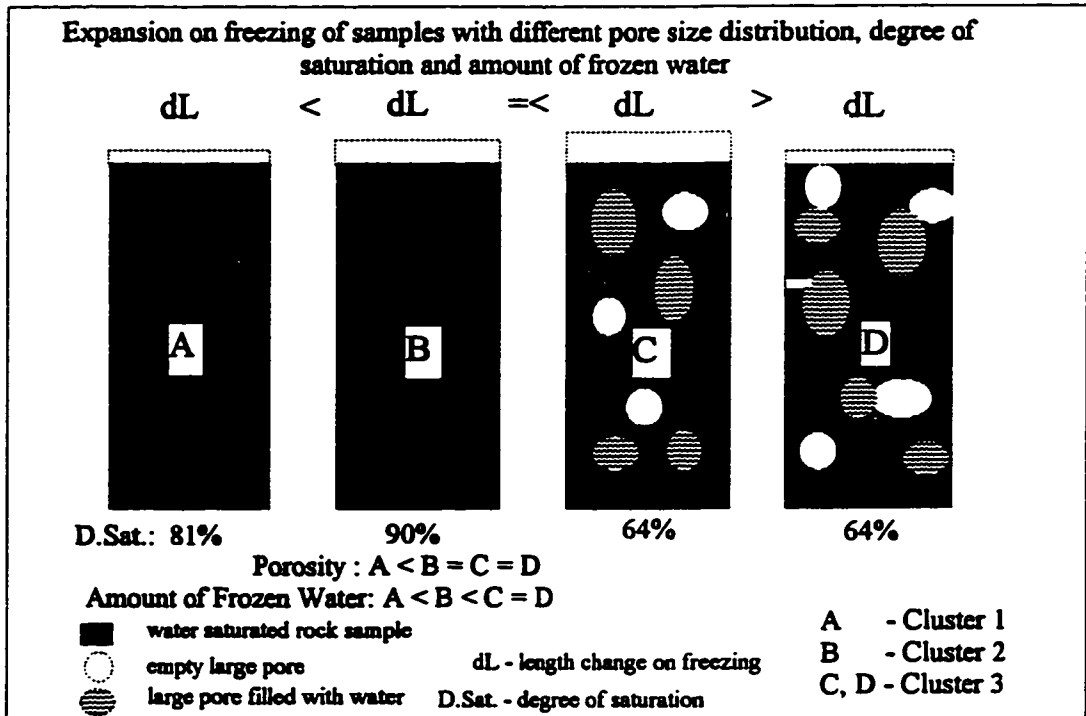
Figure C.8 Illustration of an expansion on freezing of samples with different pore size distribution, degree of saturation and amount of frozen water.

136

- curved liquid water - water vapour interface in
capillary pore filled with water

rock with low porosity   pore water   empty void
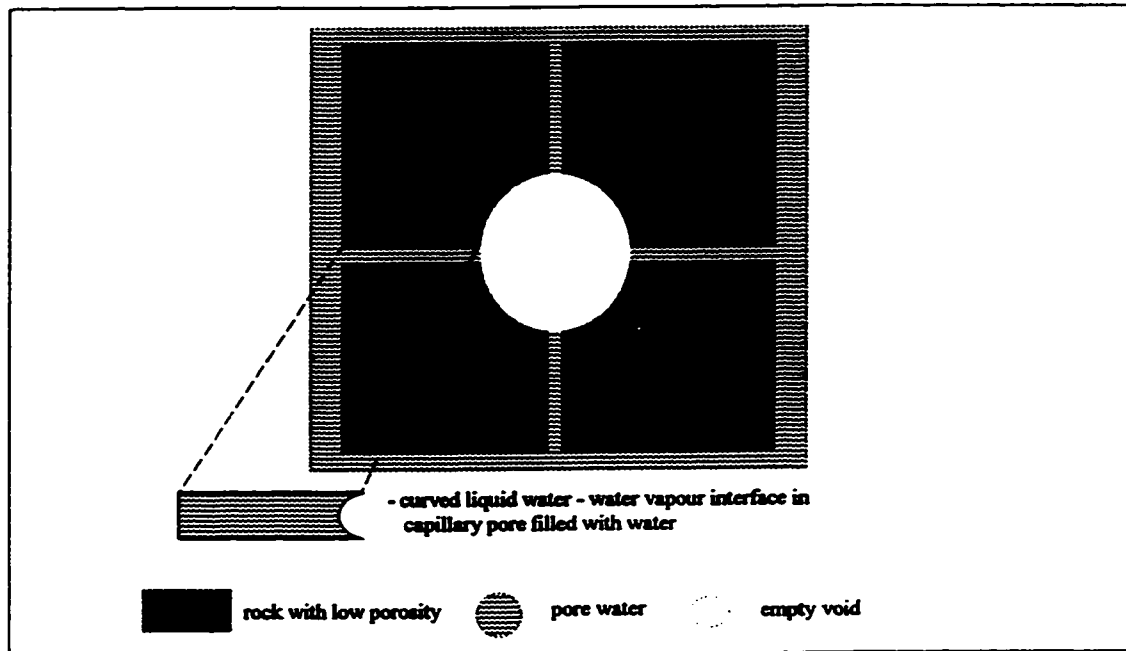
Figure C.9 Illustration of a ink bottle like pore.

Vp2
P
Vp1
T > 0C
1

Vp1
P
Vp2
T < 0C
2.

3.

Vp2
P
Vp1

4.
Vp1
P
Vp2

porous rock saturated mostly
with adsorbed water   bulk (freezable) water   ice   Vp1 < Vp2
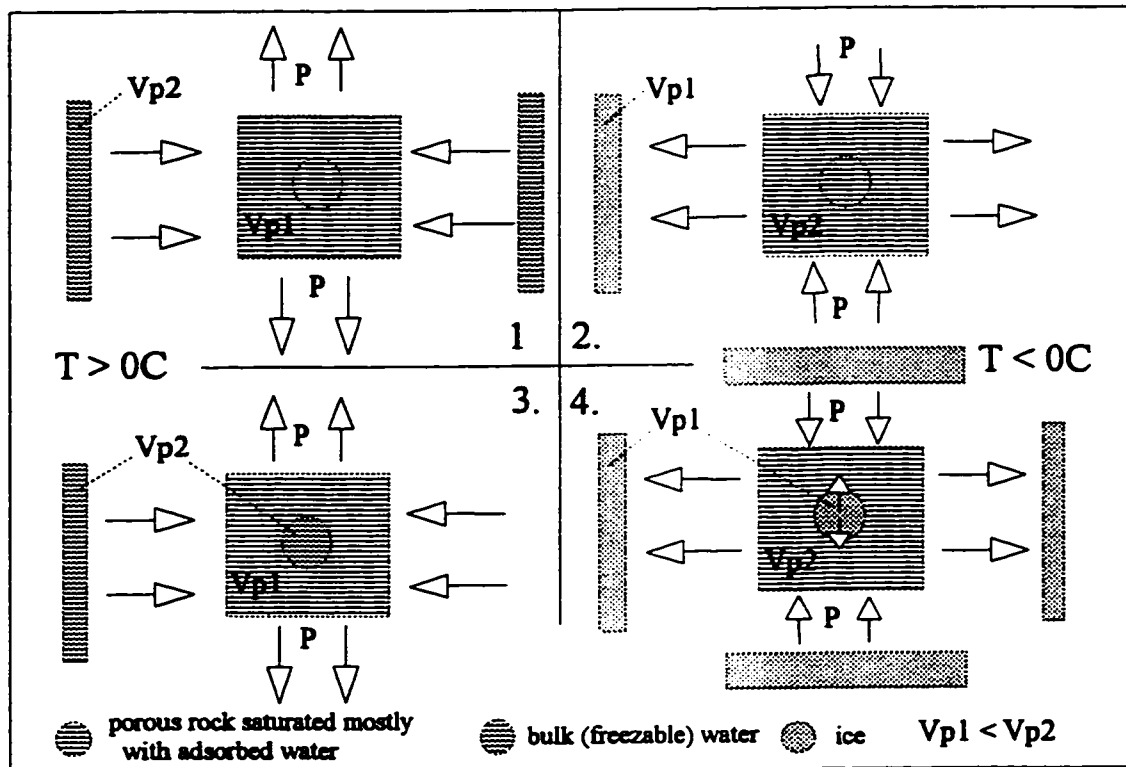
Figure C.10 Illustration of a damage of micro pores and small capillary pores
on a thermodynamic unbalance and frost action. Vp1, Vp2 - water vapor pressure,
P - pressure, T - temperature

T < 0C

| porous rock saturated mostly by adsorbed water | ice | direction of pressure generated by 9 % volume increase of water on freezing |
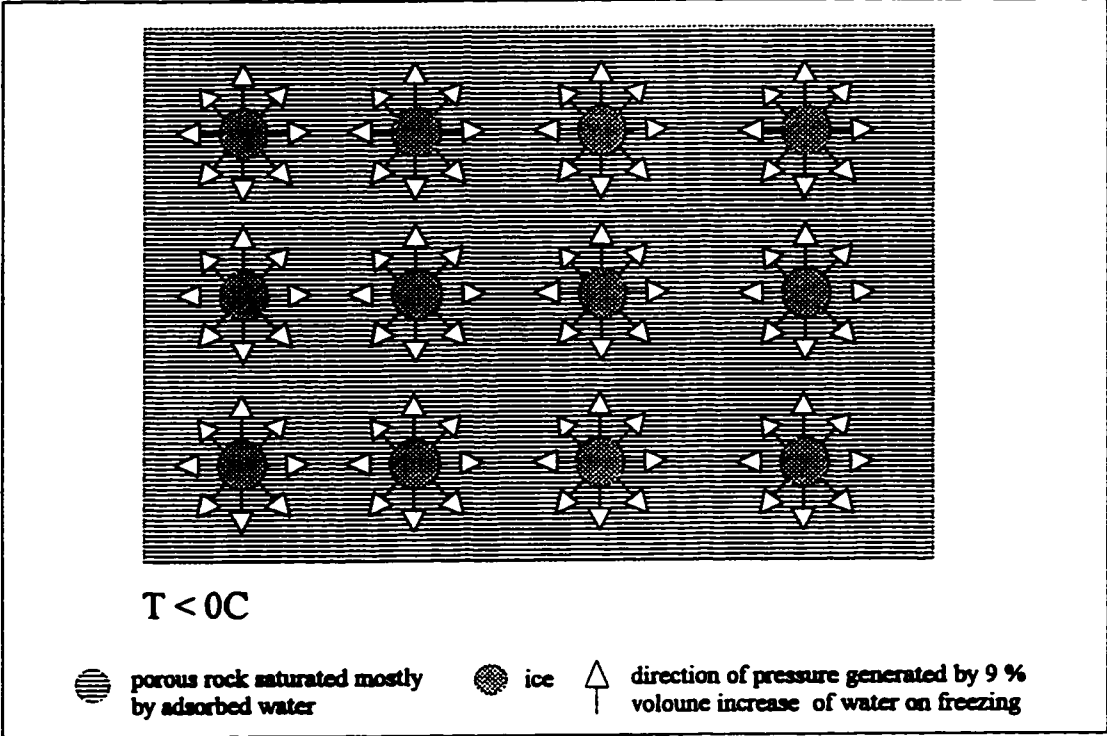
Figure C.11 Illustration of a matrix of ice causing frost damage in a rock with micro and small capillary pores.

APPENDIX   D

Formulas Used for Calculations of the Variables.

D.1 Variables Describing the Water Adsorption Test:

RADS -*Adsorbed water* is weight of adsorbed water expressed as weight percent of total weight of dry rock:

$$RADS = \frac{ADS_w}{m_t} * 100 \%$$

Where
ADS_w -observed weight of adsorbed water [g]
m_t -observed weight of dry rock [g]

RADB -*Adsorbed water fraction* is weight of adsorbed water expressed as weight percent of weight of absorbed water:

$$RADB = \frac{ADS_w}{ABS_w} * 100 \%$$

Where
ABS_w -observed weight of absorbed water [g]

D.2 Variables Describing the Water Absorption Test

RABS - *Absorbed water* is a observed weight absorbed water expressed as weight percent of weight of dry rock:

$$RABS = \frac{ABS_w}{m_t} * 100 \%$$

RSATBIF - *Degree of saturation before testing* is a observed weight of absorbed water expressed as weight percent of vacuum saturated water. This variable refer to the results from water absorption test done prior to microwave and freezing tests.

$$RSATBIF = \frac{ABS_w}{VABS_w} * 100 \%$$

Where
$VABS_w$ - observed weight of vaccum saturated water [g]

RSATAFT -*Degree of saturation after testing* is a observed weight of absorbed water expressed as weight percent of vacuum saturated water (VABSw). This variable refer to the results from water absorption test done after microwave and freezing tests.

140

$$RSATAFT = \frac{2ABS_w}{VABS_w} * 100 \%$$

Where

2ABS$_w$ — observed weight of absorbed water (after microwave and freezing tests) [g]

RBUS -*Bulk water* is a weight of bulk water present in the pores of tested samples. It is expressed as weight percent of dry weight of the samples:

$$RBUS = \frac{ABS_w - ADS_w}{m_s} * 100 \%$$

Where

m$_s$ —observed weight of dry rock [g]

RBUB -*Bulk water fraction* is a weight of bulk water expressed as weight percent of absorbed water:

$$RBUB = \frac{ABS_w - ADS_w}{ABS_w} * 100 \%$$

Where

ABS$_w$ - observed weight of absorbed water [g]
ADS$_w$ - observed weight of aDsorbed water [g]

RBUV -*Bulk water pore fraction* is a weight of bulk water expressed as weight percent of vacuum saturated water (VABSW):

$$RBUV = \frac{ABS_w - ADS_w}{VABS_w} * 100 \%$$

RBUGNB -*Gain of bulk water fraction* is a gain of bulk water detected by absorption test performed after microwave and freezing tests. It is expressed as weight percent of absorbed water (weight of absorbed water prior to the microwave and freezing test):

$$RBUGNB = \frac{(2ABS_w - 2ADS_w) - (ABS_w - ADS_w)}{ABS_w} * 100 \%$$

141

Where

2ABS$_w$ -observed weight of absorbed water (after microwave and freezing tests) [g]

2ADS$_w$ -observed weight of adsorbed water (after microwave and freezing tests) [g]

D.3 Variables Describing the Vacuum Saturation Test

RPORO -*Porosity* is weight of vacuum saturated water (VABSW) expressed as weight percent of dry rock:

$$RPORO = \frac{VABS_w}{m_t} * 100 \%$$

Where

m$_t$ -observed weight of dry rock [g]

VABS$_w$ - observed weight of vaccum saturated water [g]

RVABGNS -*Gain of vacuum absorbed water* is a gain of vacuum saturated water after the microwave and freezing tests. It is expressed as weight percent of dry sample:

$$RVABGNS = \frac{2VABS_w - VABS_w}{m_t} * 100 \%$$

Where

2VABS$_w$ -weight of vacuum absorbed water after the microwave and freezing tests.

RVABGNV -*Gain of absorbed water pore fraction* is a gain of vacuum absorbed water after the microwave and freezing tests. It is expressed as weight percent of vacuum absorbed water prior to the microwave and freezing tests:

$$RVABGNB = \frac{2VABS_w - VABS_w}{VABS_w} * 100 \%$$

D.4 Variables Describing the Rate of Water Adsorption Test

RCAP32S -*Rate of water absorption* is calculated weight of absorbed water after 32 minutes of absorption. It si calculated from equation of linear line derived from bivariate regression between observed rate of water absorption and time. The calculated absorbed water after 32 minutes is expressed as weight percent of dry rock.

$$RCAP32S = \frac{a + b * 32 \text{ min}}{m_s} * 100 \%$$

Where

a   - constant of equation of regression line between rate of absorption (weight of abs. water) and the time

b   -slope of regression line between rate of absorption (weight of abs. water) and the time

m_s -observed weight of dry rock in grams

RCAP32B -*Rate of water fraction absorption* is calculated weight of absorbed water after 32 minutes of absorption. It si calculated from equation of linear line derived from bivariate regression between observed rate of water absorption and time. The calculated absorbed water after 32 minutes is expressed as weight percent of absorbed water.

$$RCAP32B = \frac{a + b * 32 \text{ min}}{ABS_w} * 100 \%$$

Where
ABS_w - observed weight of absorbed water [g]

D.5 Variables Describing the Macrowave Heat Absorption Test

MQABS   *Heat absorbed by absorbed water* is the total microwave heat absorbed by absorbed water present in the sample prior to the test. It is calculated from the portion of the total observed temperature increase of the sample caused by heat absorbed by absorbed water. It is expressed as a total absorbed energy (Joules) per gram of the dry rock and per 9 seconds. [J/(g*9 sec.)]. However, for a simplicity, in the text it is refered as energy absorbed per gram of dry rock [J/g of dry rock].

$$MQABS = \frac{C_w * ABS_w + C_s * m_s + C_{Cu} * m_{Cu}}{m_s} * dT_{ab}$$

Where
C_w, C_v, C_{Cu} - heat capacity of water, dry rock, copper respectively [J/(g*°C)]
ABS_w, m_v, m_{Cu} - observed weigth of absorbed water, dry rock, copper cylinder respectively [g]
dT_{ab} - temperature increases due to wacrowave heat adsorbed by absorbed water [°C]

MQBUS   *Heat absorbed by bulk water* is the total microwave heat absorbed by bulk water present in the sample prior to the test. It is calculated from the portion of the total observed

143

temperature increase of the sample caused by heat absorbed by bulk water. It is expressed as a total absorbed energy (Joules) per gram of the dry rock and per 9 seconds. [J/(g*9 sec.)]. However, for a simplicity, in the text it is refered as energy absorbed per gram of dry rock [J/g of dry rock].

$$MQBUS = \frac{C_w * (ABS_w - ADS_w) + C_r * m_r + C_{Cu} * m_{Cu}}{m_r} * dT_b$$

Where

C_w, C_v, C_{Cu} - heat capacity of water, dry rock, copper respectively [J/(g*°C)]

m_v, m_{Cu} - observed weigth of water, dry rock, copper cylinder respectively [g]

$(ABS_w - ADS_w)$ - weight of bulk water [g]

dT_b - temperature increases due to wacrowave heat adsorbed by bulk water [°C]

MQADS   *Heat absorbed by adsorbed water* is the total microwave heat absorbed by adsorbed water present in the sample prior to the test. It is calculated from the portion of the total observed temperature increase of the sample caused by heat absorbed by adsorbed water. It is expressed as a total absorbed energy (Joules) per gram of the dry rock and per 9 seconds. [J/(g*9 sec.)]. However, for a simplicity, in the text it is refered as energy absorbed per gram of dry rock [J/g of dry rock].

$$MQADS = \frac{C_w * ADS_w + C_r * m_r + C_{Cu} * m_{Cu}}{m_r} * dT_{ad}$$

Where

C_w, C_v, C_{Cu} - heat capacity of water, dry rock, copper respectively [J/(g*°C)]

ADS_w, m_v, m_{Cu} - observed weigth of adsorbed water, dry rock, copper cylinderrespectively [g]

dT_{ad} - temperature increases due to wacrowave heat adsorbed by absorbed water [°C]

MQABAB   *Heat absorbed by absorbed water fraction* is the total microwave heat absorbed by gram of absorbed water. It is calculated from the portion of the total observed temperature increase of the sample caused by heat absorbed by absorbed water. It is expressed as a total absorbed energy (Joules) per gram of the dry rock and per gram of adsorbed water and per 9 seconds. [J/(g*g*9 sec.)]. However, for a simplicity in the text, it is refered as energy absorbed per gram of absorbed water [J/g of absorbed water].

$$MQABAB = \frac{C_w * ABS_w + C_r * m_r + C_{Cu} * m_{Cu}}{m_r * ABS_w} * dT_{ab}$$

Where

C_w, C_D, C_{Cu} — heat capacity of water, dry rock, copper respectively [J/(g*°C)]

ABS_w, m_D, m_{Cu} — observed weigth of absorbed water, dry rock, copper cylinder respectively [g]

dT_{ab} — temperature increases due to wacrowave heat adsorbed by absorbed water [°C]

AQBUBU *Heat absorbed by bulk water fraction* is the total microwave heat absorbed by gram of bulk water. It is calculated from the portion of the total observed temperature increase of the sample caused by heat absorbed by bulk water. It is expressed as a total absorbed energy (Joules) per gram of a dry rock and per gram of bulk water and per 9 seconds. [J/(g*g*9 sec.)]. However, for a simplicity in the text, it is refered as energy absorbed per gram of bulk water [J/g of bulk water].

$$MQBUBU = \frac{C_w*(ABS_w-ADS_w) + C_s*m_s + C_{Cu}*m_{Cu}}{m_s * (ABS_w-ADS_w)} * dT_b$$

Where

C_w, C_D, C_{Cu} — heat capacity of water, dry rock, copper respectively [J/(g*°C)]

m_D, m_{Cu} — observed weigth of water, dry rock, copper cylinder respectively [g]

$(ABS_w - ADS_w)$ — calculated weight of bulk water [g]

dT_b — temperature increases due to wacrowave heat adsorbed by bulk water [°C]

MQADAD *Heat absorbed by adsorbed water fraction* is the total microwave heat absorbed by gram of adsorbed water. It is calculated from the portion of the total observed temperature increase of the sample caused by heat absorbed by adsorbed water. It is expressed as a total absorbed energy (Joules) per gram of a dry rock and per gram of adsorbed water and per 9 seconds. [J/(g*g*9 sec.)]. However, for a simplicity in the text, it is refered as energy absorbed per gram of adsorbed water [J/g of adsorbed water].

$$MQADAD = \frac{C_w*ADS_w + C_s*m_s + C_{Cu}*m_{Cu}}{m_s * ADS_w} * dT_{ad}$$

Where

C_w, C_D, C_{Cu} — heat capacity of water, dry rock, copper respectively [J/(g*°C)]

ADS_w, m_D, m_{Cu} — observed weigth of absorbed water, dry rock, copper cylinder respectively [g]

dT_{ad} — temperature increases due to wacrowave heat adsorbed by absorbed water [°C]

D.6 Variables Describing the Freezing Test:

CFWS *Observed frozen water* is an amount of frozen water calculated from calorimetric output (area A outlined by curve of differential temperature and by X axis). It is expressed as weight

145

percent of weight of dry rock.

$$CFWS = \frac{A * C * L}{m_r} * 100\%$$

Where

A - area enclosed by curve of differential temperature and by X axis.
C - system constant in gram per degree Celsius and second and millimetre [g/(C*s*mm]
L - length of sample in [mm]
m_r - weight of dry rock [g]

CFWB - *Observed frozen water fraction* is a total amount of frozen water calculated from calorimetric output expressed as weight percent of absorbed water present in the sample prior to the test.

$$CFWB = \frac{A * C * L}{ABS_w} * 100\%$$

Where

ABS_w is weight of absorbed water [g]

CFWV *Observed frozen water pore fraction* is a total amount of frozen water calculated from calorimetric output expressed as weight percent of vacuum absorbed water.

$$CFWV = \frac{A * C * L}{ABS_{wv}} * 100\%$$

Where
ABS_{wv} — weight of vacuum saturated water [g]

CUFWS *Observed total unfrozen water* is a total amount of unfrozen water calculated by subtracting of weight of frozen water from weight of absorbed water present in the sample prior to the testing. It is expressed as weight percent of weight of dry rock.

$$CUFWS = \frac{ABS_w - (A * C * L)}{m_r} * 100\%$$

Where
(A * C * L)   — weight of frozen water calculated from calorimetric measurement [g]

CUFWB *Observed total unfrozen water fraction* is a total amount of unfrozen water calculated

146

by subtracting of weight of frozen water from weight of absorbed water present in the sample prior to the testing. It is expressed as weight percent of weight of absorbed water present in the sample prior to the test.

$$CUFWB = \frac{ABS_w - (A * C * L)}{ABS_w} * 100\ \%$$

CUFWV *Observed total unfrozen water pore fraction* is a total amount of unfrozen water calculated by subtracting of weight of frozen water from weight of absorbed water present in the sample prior to the testing. It is expressed as weight percent of weight of vacuum absorbed water.

$$CUFWV = \frac{ABS_w - (A * C * L)}{ABS_{wv}} * 100\ \%$$

Where
ADS_w -weight of adsorbed water [g]
ABS_{wv} - weight of vacuum saturated water [g]
$(A * C * L)$ - weight of frozen water calculated from calorimetric measurement [g]

CUFBUS *Observed unfrozen BULK water* is an amount of bulk unfrozen water calculated by subtracting of weight of frozen water and weight of adsorbed water from the weight of absorbed water present in the sample prior to the testing. It is expressed as weight percent of weight of the dry rock.

$$CUFBUS = \frac{(ABS_w - ADS_w) - (A * C * L)}{m_s} * 100\ \%$$

Where
$(ABS_w - ADS_w)$ - weight of bulk water [g]
m_s - observed weight of dry rock

CUFBUB *Observed unfrozen bulk water fraction* is an amount of bulk unfrozen water calculated by subtracting of weight of frozen water and weight of adsorbed water from the weight of absorbed water present in the sample prior to the test. It is expressed as weight percent of weight of absorbed water present in the sample prior to the test.

$$CUFBUS = \frac{(ABS_w - ADS_w) - (A * C * L)}{ABS_w} * 100\ \%$$

CUFBUV *Observed unfrozen bulk water pore fraction* is an amount of bulk unfrozen water calculated by subtracting of weight of frozen water and weight of adsorbed water from the weight of absorbed water present in the sample prior to the test. It is expressed as weight percent of weight of vacuum absorbed water.

147

$$CUFBUV = \frac{(ABS_{wv} - ADS_{v}) - (A * C * L)}{ABS_{wv}} * 100\ \%$$

CRDL *Expansion on freezing* is observed expansion of the sample on freezing. It is expressed as length change in millimetres per 10 meters.

$$CRDL = \frac{dL}{L} * 10000$$

Where

  dL -observed length change in millimetres

CTF *Freezing temperature* is observed temperature when freezing of pore water took place. It is calculated by subtracting of temperature difference between water satureted sample and dry sample. It is expressed in degree of Celsius.

$$CTF = T_{obs} - dT$$

Where

  T_{obs} - observed temperatura of dry sample on freezing of water saturated sample [C]
  dT   - differencial temperature between dry sample and water saturated sample.

APPENDIX E

Tables of Test Results.

Table E.1 Results of the tests for adsorption, and absorption (Part 1)

Sample #	RDEN [g/cm3]	RADS [%]	RADB [%]	RABS [%]	RSATBIF [%]	RSATAFT [%]	RBUS [%]	RBUB [%]	RBUV [%]
1_Lcf	2.207	0.06	1.12	6.32	61.91	75.71	6.29	99.53	70.44
3_Lcf	2.504	0.03	1.99	1.61	81.62	62.93	1.57	97.56	54.42
4_L	2.772	0.40	43.33	0.83	98.36		0.41	49.54	40.60
5_Df	2.622	0.16	9.09	1.92	82.16	86.27	1.81	94.37	65.69
6_Df	2.629	0.86	36.82	2.47	99.61	88.85	1.70	69.00	61.31
8_D	2.809	0.13	32.61	0.38	93.88		0.27	69.57	57.14
10_L	2.678	0.20	63.41	0.42	75.93		0.06	13.21	14.00
15_D	2.786	0.06	20.59	0.27	89.47		0.21	78.12	65.79
16_D	2.791	0.03	21.05	0.15	86.36		0.13	83.33	55.56
17_Lf	2.570	0.36	25.83	1.39	94.97	77.25	0.91	65.77	46.45
18_D	2.767	0.26	29.70	0.85	97.12		0.59	69.70	60.53
19_Df	2.720	0.14	17.78	0.81	90.91	89.66	0.64	79.57	63.79
20_Dcf	2.691	0.03	3.12	0.91	71.11	73.30	0.88	97.09	56.82
21_Dcf	2.748	0.10	21.67	0.39	70.59	68.87	0.28	71.43	33.02
22_Dcf	2.682	0.05	9.23	0.58	51.59	61.29	0.54	93.94	40.00
23_Dcf	2.657	0.02	1.56	1.25	58.18	71.08	1.24	99.14	55.74
24_Dcf	2.786	0.03	10.26	0.28	70.91	73.91	0.24	86.49	46.38
26_Df	2.611	0.14	6.30	2.46	89.75	91.69	2.31	93.75	73.07
28_L	2.653	0.40	49.00	0.77	96.15		0.29	37.89	32.43
32_Df	2.749	0.05	12.20	0.43	80.39	82.86	0.39	91.11	58.57
34_Df	2.709	0.11	12.28	0.99	87.69	81.87	0.82	82.54	60.82
37_D	2.744	0.56	82.28	0.65	97.53		0.09	14.47	12.79
37.1_L	3.818	0.24	69.23	0.36	86.67		0.17	46.34	33.93
39_L	2.698	0.11	60.00	0.20	86.96		0.08	40.91	13.64
40_L	2.673	0.32	66.67	0.51	91.68		0.18	34.48	28.99
41_Df	2.616	0.09	4.81	2.17	84.21	90.71	2.08	95.45	74.04
42_Dgf	2.759	0.19	34.25	0.56	98.65	74.56	0.34	61.64	39.47
45_Df	2.523	0.14	4.26	3.60	86.58	96.47	3.53	97.83	79.47
46_Df	2.572	0.15	5.23	3.23	86.66	96.42	3.12	96.32	81.15
50_L	2.638	0.06	10.00	0.72	84.51		0.66	91.30	76.83
51_Lgf	2.505	0.27	10.82	2.63	95.04	95.62	2.41	91.76	86.20
52_Df	2.640	0.05	3.82	1.43	78.11	84.77	1.41	98.75	61.72
53_Df	2.585	0.06	3.86	2.41	82.48	83.78	2.36	97.95	70.52
54_Dcf	2.717	0.03	5.08	0.55	44.36	64.43	0.54	98.13	42.15
55_Dcf	2.643	0.02	1.52	1.30	52.17	70.07	1.29	99.32	52.92
56_Dcf	2.652	0.04	7.84	0.44	41.46	52.70	0.43	96.00	32.43
57_D	2.786	0.05	16.67	0.22	73.17		0.19	87.50	39.62
58_Dcf	2.633	0.12	11.93	1.11	47.81	61.51	1.00	90.32	44.44
60_Dcf	2.631	0.08	9.89	0.85	35.55	51.65	0.81	95.79	33.33
61_Dcf	2.716	0.07	14.29	0.48	60.22	64.81	0.42	87.27	44.44
62_L	2.684	0.09	47.62	0.22	77.78		0.11	52.00	46.43
65_L	2.695	0.08	42.11	0.22	79.17		0.13	60.87	40.00
68_L	2.693	0.12	56.00	0.22	92.59		0.07	32.00	25.81
70_L	2.689	0.05	35.29	0.17	73.91		0.10	60.00	52.17
74_L	2.746	0.12	62.50	0.18	88.89		0.04	20.83	17.86

150

Table E.1 Results of the tests for adsorption, and absorption (Part 2)

Sample #	RDEN [g/cm3]	RADS [%]	RADB [%]	RABS [%]	RSATBIF [%]	RSATAFT [%]	RBUS [%]	RBUB [%]	RBUV [%]
75_Lf	2.698	0.11	23.73	0.54	73.75	80.77	0.37	68.12	45.19
75.1_L	2.602	1.40	57.20	2.45	98.47		1.12	45.91	43.07
76_Dgf	2.576	0.03	1.82	1.45	44.35	56.68	1.43	98.73	41.71
78_Df	2.731	0.20	22.55	0.89	89.47	84.67	0.66	73.79	50.67
79_Dcf	2.601	0.04	2.41	1.70	54.61	72.67	1.67	98.40	55.26
80_Lf	2.675	0.07	12.50	0.60	87.67	89.53	0.57	94.12	74.42
81_L	2.688	0.11	22.64	0.42	100.00		0.31	74.47	58.33
83_L	2.706	0.13	61.54	0.20	92.86		0.05	23.08	19.05
84_Df	2.676	0.38	22.28	1.77	94.15	95.65	1.38	78.11	68.26
85_L	2.701	0.36	40.74	0.87	98.18		0.48	55.00	36.97
87_L	2.683	0.04	40.00	0.11	12.66		0.08	69.23	58.25
88_D	2.800	0.11	27.78	0.43	88.52		0.28	65.79	55.15
90_D	2.755	0.41	44.71	0.92	96.59		0.54	58.82	48.08
91_Df	2.687	0.12	8.02	1.49	91.67	92.27	1.32	89.01	72.96
92_Df	2.723	0.07	6.90	1.02	84.67	87.78	0.95	93.22	61.11
93_Df	2.644	0.62	30.47	2.10	97.64	88.82	1.48	70.61	60.86
94_Lf	2.682	0.50	32.31	1.57	97.01	90.17	1.02	65.33	55.56
95_Dcf	2.563	0.06	5.07	1.15	32.02	45.14	1.13	97.84	31.48
96_Lf	2.665	0.18	19.83	1.00	75.82	62.56	0.77	76.98	44.29
97_Lgf	2.646	0.11	17.28	0.68	86.17	80.70	0.57	83.53	62.28
98_M	3.082	0.04	35.71	0.14	70.00		0.10	68.42	61.90
99_M	2.814	0.01	8.33	0.10	70.59		0.09	91.67	52.38
100_M	2.690	0.01	6.25	0.18	80.00		0.17	94.38	67.11
101_Sgf	2.554	0.02	4.00	0.62	80.65	68.70	0.61	97.33	55.73
102_Sgf	2.379	0.04	2.07	1.98	47.89	62.50	1.96	98.65	52.88
103_Sgf	2.249	0.24	6.85	4.29	54.81	81.77	4.15	96.82	63.87
108_SH	2.654	0.36	47.13	0.74	95.60		0.32	42.86	39.56
114_G	2.603	0.04	19.23	0.20	89.66		0.17	87.50	60.00
115_SY	2.618	0.01	12.50	0.05	88.89		0.03	66.67	25.00
117_HD	2.619	0.01	16.67	0.05	75.00		0.05	85.00	51.00
118_DI	3.048	0.01	85.71	0.01	52.50		0.01	50.00	33.33
120_D	2.700	0.89	48.79	1.81	97.64		1.00	55.34	49.14
121_Df	2.648	0.30	18.28	1.63	93.94	92.44	1.39	85.25	65.55
122_Dgf	2.716	0.13	14.71	1.02	69.39	86.90	0.90	88.03	61.31
123_SH	2.686	1.10	64.02		95.91				
124_Scf	2.461	0.02	1.56	1.40	49.23	72.56	1.38	98.63	51.99
125_D	3.936	0.08	8.97	0.93	81.25		0.88	94.19	74.31
126_Lf	2.558	0.21	16.31	0.66	95.92	61.04	0.54	81.94	25.54
127_D	2.791	0.20	31.17	0.66	88.51		0.46	69.62	59.14
128_D	2.736	0.32	28.46	1.11	95.59		0.71	63.57	55.41
129_Df	2.578	0.07	3.33	2.31	70.80	84.95	2.25	97.51	69.90
130_Lf	2.607	0.04	3.13	1.58	81.22	89.30	1.55	97.94	78.19
131_Lgf	2.412	0.06	1.78	4.08	66.05	83.90	4.05	99.13	70.74

Table E.2 Results of the tests for vacuum saturation and rate of absorption (Part 1)

Sample #	RBUGNB [%]	RPORO [%]	RVABGNS [%]	RVABGNV [%]	DRYLOSS [%]	RCAP32S [%]	RCAP32B [%]
1_Lcf	7.62	8.96	0.40	4.72	0.49	4.69	84.99
3_Lcf	72.19	2.89	1.07	58.92	0.12	0.38	26.02
4_L	10.83	1.02	0.06	9.02	0.17	0.02	2.44
5_Df	34.34	2.76	0.59	26.97	0.13	0.16	9.50
6_Df	17.44	2.87	0.42	17.76	4.15	0.42	17.63
8_D	228.26	0.47	0.06	14.29	0.03	0.03	6.25
10_L	34.15	0.39	-0.03	-7.41	0.03	0.00	0.26
15_D	5.88	0.32		0.00	0.03	0.04	14.38
16_D	21.05	0.23	0.04	22.73	0.04	0.03	16.67
17_Lf	45.03	1.96	0.48	32.70	0.06	0.03	2.08
18_D	10.89	0.97	0.09	9.62	0.09	0.01	1.06
19_Df	23.33	1.00	0.15	17.17	0.06	0.16	17.19
20_Dcf	42.71	1.55	0.36	30.37	0.07	0.05	6.90
21_Dcf	24.71	0.83	0.17	24.71	0.07	0.04	8.84
22_Dcf	43.06	1.36	0.25	23.02	0.05	0.10	16.27
23_Dcf	20.47	2.22	0.26	13.18	0.07	0.11	9.47
24_Dcf	197.44	0.53	0.11	25.45	0.08	0.13	34.31
26_Df	27.17	3.16	0.60	23.32	0.13	0.57	24.65
28_L	15.00	0.90	0.06	6.73	0.06	0.04	5.09
32_Df	43.90	0.66	0.18	37.25	0.12	0.03	7.69
34_Df	45.61	1.34	0.32	31.54	0.15	0.02	2.63
37_D	8.86	0.74	0.04	6.17	0.07	0.03	3.70
37.1_L	10.26	0.49	0.10	24.44	0.09	0.03	7.14
39_L	220.00	0.59	0.38	186.96	0.04	0.03	12.50
40_L	18.70	0.61	0.09	17.15	0.10	0.00	0.26
41_Df	-208.17	2.94	0.58	26.32	4.57	0.40	21.38
42_Dgf	71.23	0.87	0.31	54.05	0.27	0.06	11.12
45_Df	-38.60	4.44	0.71	19.21	0.04	0.86	26.98
46_Df	22.19	3.84	0.60	18.66	0.05	0.42	15.75
50_L	18.33	0.86	0.11	15.49	0.05	0.11	20.03
51_Lgf	5.97	2.80	0.14	5.32	0.13	0.96	39.27
52_Df	34.39	2.28	0.49	27.36	0.02	0.17	12.79
53_Df	36.29	3.36	0.77	29.62	0.11	0.34	15.74
54_Dcf	29.15	1.29	0.14	12.03	0.05	0.18	43.94
55_Dcf	15.91	2.45	0.19	8.30	0.04	0.23	19.08
56_Dcf	49.02	1.32	0.22	20.33	0.04	0.14	24.96
57_D	40.00	0.49	0.11	29.27	0.04	0.00	0.40
58_Dcf	23.85	2.25	0.21	10.53	0.08	0.22	24.06
60_Dcf	14.29	2.44	0.15	6.64	0.07	0.18	22.45
61_Dcf	28.57	0.94	0.13	16.13	0.19	0.13	33.65
62_L	9.52	0.24	0.01	3.70	0.03	0.00	0.55
65_L	47.37	0.34	0.11	45.83	0.09	0.03	14.29
68_L	24.00	0.27	0.04	14.81	0.03	0.00	0.54
70_L	17.65	0.20		0.00	0.01	0.03	16.67
74_L	20.83	0.22	0.01	3.70	0.03	0.02	12.50

Table E.2 Results of the tests for vacuum saturation and rate of absorption (Part 2)

Sample #	RBUGNB [%]	RPORO [%]	RVABGNS [%]	RVABGNV [%]	DRYLOSS [%]	RCAP32S [%]	RCAP32B [%]
75_Lf	45.76	0.82	0.19	30.00	0.12	0.02	4.76
75.1_L	19.46	2.61	0.12	4.96	0.15	0.44	18.86
76_Dgf	1.21	3.42	0.02	0.54	0.05	0.54	37.77
78_Df	43.14	1.30	0.31	31.58	0.18	0.10	10.32
79_Dcf	16.27	3.03	0.28	9.54	0.09	2.22	94.25
80_Lf	17.19	0.76	0.11	17.81	0.04	0.19	33.27
81_L	11.32	0.54	0.06	13.21	0.05	0.03	5.00
83_L	38.46	0.25	0.03	12.50	0.27	0.00	0.53
84_Df	20.73	2.03	0.22	12.20	0.11	0.41	23.52
85_L	67.28	1.31	0.40	44.24	1.32	0.19	22.89
87_L	-610.00	0.14	-0.55	-79.75	-0.01	0.00	1.26
88_D	19.44	0.51	0.05	11.48	0.05	0.02	5.56
90_D	15.29	1.12	0.17	18.18	0.20	0.03	3.57
91_Df	19.25	1.82	0.23	14.22	0.05	0.29	18.85
92_Df	37.93	1.56	0.37	31.39	0.10	0.06	6.00
93_Df	22.58	2.44	0.33	15.94	0.33	0.22	11.11
94_Lf	25.64	1.85	0.28	16.42	0.10	0.17	10.85
95_Dcf	-0.00	3.59	0.01	0.23	0.04	0.29	24.22
96_Lf	68.97	1.75	0.52	43.14	0.56	0.17	17.85
97_Lgf	27.16	0.92	0.16	21.28	0.08	0.12	18.68
98_M	21.43	0.16	0.01	5.00	0.02	0.00	1.09
99_M	25.00	0.18	0.03	23.53	0.04	0.03	25.00
100_M	11.88	0.25	0.03	12.50	-0.28	0.03	16.67
101_Sgf	48.00	1.09	0.31	40.86	0.52	0.27	45.77
102_Sgf	6.74	3.70	0.12	3.23	0.10	0.42	23.83
103_Sgf	0.60	6.50	0.07	1.14	0.09	3.20	99.74
108_SH	13.79	0.81		0.00	0.04	0.03	3.57
114_G	15.38	0.28	0.05	20.69	0.02	0.09	36.34
115_SY	87.50	0.13	0.06	77.78	0.06	0.02	50.00
117_HD	48.33	0.09	0.02	25.00	0.04	0.03	100.00
118_DI	-0.00	0.02	-0.01	-25.00	0.01	0.02	100.00
120_D	9.66	2.04	0.18	9.43	0.19	0.16	8.71
121_Df	20.97	2.13	0.36	20.20	0.15	0.22	13.40
122_Dgf	22.55	1.46	0.18	14.29	0.11	0.07	10.86
123_SH	0.00	1.79				0.06	3.90
124_Scf	13.28	2.65	0.16	6.54	0.03	0.47	36.26
125_D	16.67	1.18	0.14	13.54	0.73	0.05	6.54
126_Lf	47.52	2.11	0.77	57.14	-0.34	0.70	36.39
127_D	11.69	0.77	0.05	6.90	0.09	0.21	33.76
128_D	18.46	1.27	0.10	8.82	0.15	0.05	4.55
129_Df	22.92	3.22	0.44	15.63	0.05	0.37	18.37
130_Lf	30.00	1.98	0.37	23.35	0.03	0.31	23.58
131_Lgf	4.33	5.74	0.45	8.57	0.34	2.20	62.57

Table E.3 Results of the tests for the microwave heat absorption and rock durability (Part 1)

Sample #	MQABS [J/(g*9s)]	MQBUS [J/(g*9s)]	MQADS [J/(g*9s)]	MQABAB [J/(g*g*9s)]	MQBUBU [J/(g*g*9s)]	MQADAD [J/(g*g*9s)]	RFRTH [%]	RMGSO4 [%]
1_Lcf	5.84	5.81	0.03	187.94	92.36	95.58	12.48	16.20
3_Lcf	1.33	1.29	0.04	189.18	82.10	107.07	24.35	7.15
4_L	1.94	1.35	0.59	467.90	326.94	140.97	15.65	0.65
5_Df	1.39	1.01	0.37	401.39	55.77	345.62	24.93	16.60
6_Df	3.72	2.85	0.87	280.63	167.24	113.39	19.06	2.15
8_D	0.85	0.54	0.31	465.75	203.47	262.29	25.97	92.00
10_L	0.92	0.67	0.25	1288.15	1219.77	68.39	29.24	1.20
15_D			0.23			384.12	2.68	2.50
16_D	0.55	0.44	0.11	784.49	346.42	438.07	1.84	0.85
17_Lf	1.10	0.64	0.46	167.37	70.24	97.13	28.78	10.60
18_D	0.86	0.66	0.20	191.15	111.75	79.41	26.10	4.20
19_Df	0.93	0.77	0.16	217.28	119.76	97.52	9.14	8.30
20_Dcf	0.72	0.68	0.04	230.63	77.27	153.36	1.57	1.30
21_Dcf	0.94	0.91	0.03	359.74	330.10	29.65	1.46	0.70
22_Dcf	0.25		0.16	479.73		463.44	1.54	1.65
23_Dcf	0.67	0.65	0.02	245.84	52.24	193.60	7.71	1.50
24_Dcf	1.27	1.26		518.10	517.63		10.14	2.65
26_Df	0.80	0.61	0.18	144.24	26.63	117.61	18.47	12.75
28_L	2.46	1.79	0.67	750.88	610.91	139.97	50.96	10.65
32_Df	0.87	0.71	0.16	610.34	182.24	428.10	17.47	2.95
34_Df	2.43	2.11	0.32	444.65	258.29	186.36	13.88	2.70
37_D	1.95	1.47	0.48	1644.94	1559.11	85.83	21.98	10.00
37.1_L	0.93	0.56	0.37	524.46	334.30	190.16		
39_L	0.47	0.17	0.30	466.42	211.76	254.66	10.12	5.35
40_L	1.33	0.84	0.49	623.92	477.61	146.31	22.99	7.80
41_Df	1.46	1.37	0.09	155.59	66.06	89.53	1.31	8.50
42_Dgf	2.00	1.73	0.26	625.19	502.42	122.77	9.14	7.05
45_Df	2.04	1.93	0.11	192.58	54.71	137.87	1.89	1.27
46_Df	2.39	2.37	0.02	89.71	76.18	13.53	18.40	27.15
50_L	0.70	0.54	0.16	333.25	81.81	251.44	19.13	5.65
51_Lgf	0.83	0.68	0.15	99.26	28.00	71.26	36.97	85.30
52_Df	0.71	0.59	0.12	694.10	42.11	651.99	1.13	2.70
53_Df	2.10	2.03	0.06	215.16	85.92	129.24	9.62	5.15
54_Dcf	0.44	0.40	0.03	397.47	73.74	323.73	22.67	2.35
55_Dcf	0.73	0.72	0.02	253.81	55.23	198.58	12.82	2.65
56_Dcf	0.19		0.15	843.09		834.18	14.71	1.40
57_D	0.68	0.65	0.03	444.14	335.92	108.22	11.02	1.35
58_Dcf	1.66	1.56	0.10	247.50	156.04	91.45	17.95	12.80
60_Dcf	0.99	0.92	0.07	308.21	112.53	195.68	2.32	4.50
61_Dcf	1.19	1.05	0.15	495.00	251.72	243.27	1.66	8.65
62_L	0.42	0.27	0.15	379.11	238.30	140.80	27.05	7.30
65_L	0.62	0.51	0.10	500.32	380.53	119.78	10.80	12.90
68_L	0.71	0.53	0.17	877.46	762.04	115.41	4.46	9.20
70_L	0.39	0.26	0.13	437.70	246.94	190.76	6.03	3.00
74_L	0.45	0.34	0.11	950.84	874.36	76.48	11.55	1.90

Unit [J/(g*g*9)] is total heat in Joules absorbed per gram
of dry rock and gram of water and per 9 seconds.

154

Table E.3 Results of the tests for the microwave heat absorption and rock durability (Part 2)

Sample #	MQABS [J/(g*9s)]	MQBUS [J/(g*9s)]	MQADS [J/(g*9s)]	MQABAB [J/(g*g*9s)]	MQBUBU [J/(g*g*9s)]	MQADAD [J/(g*g*9s)]	RFRTH [%]	RMGSO4 [%]
75_Lf	0.98	0.85	0.13	302.01	229.76	72.24	4.34	4.35
75.1_L	3.05	1.99	1.05	256.98	177.35	79.63		
76_Dgf	0.73	0.72	0.01	98.50	50.16	48.33	1.37	2.00
78_Df	0.89	0.61	0.28	214.11	93.32	120.79	2.70	4.15
79_Dcf	1.09	1.04	0.04	220.64	62.38	158.26	2.36	7.85
80_Lf	0.28		0.24	698.15		692.25	3.87	3.05
81_L	0.38	0.23	0.14	207.94	74.45	133.49	12.36	5.45
83_L	0.89	0.77	0.12	1714.53	1636.31	78.22	3.67	0.55
84_Df	1.43	1.08	0.35	168.77	77.88	90.89	6.85	16.95
85_L	1.17	0.95	0.22	253.96	197.39	56.57	8.82	7.15
87_L	0.23	0.15	0.08	427.52	186.42	241.09	6.20	3.60
88_D	1.20	1.13	0.07	446.68	399.52	47.16	18.17	5.50
90_D	1.96	1.76	0.20	379.81	326.48	53.33	24.54	20.30
91_Df	1.59	1.46	0.12	186.70	110.55	76.15	13.30	18.35
92_Df	1.34	1.30	0.04	191.69	136.74	54.95	2.75	4.55
93_Df	3.43	2.70	0.73	300.42	181.93	118.49	15.90	31.90
94_Lf	2.41	1.75	0.66	292.01	170.60	121.41	17.32	28.50
95_Dcf	2.33	2.26	0.07	470.31	200.28	270.03	1.05	2.25
96_Lf	2.05	1.95	0.10	296.18	252.18	44.01	2.38	8.95
97_Lgf	1.85	1.62	0.23	492.08	283.80	208.29	2.14	11.35
98_M	0.39	0.39		397.41	395.45		0.64	1.35
99_M	0.41	0.41	0.00	497.91	447.10	50.81	1.55	3.45
100_M	0.35	0.32	0.03	493.65	194.89	298.76	1.25	9.70
101_Sgf	0.31						16.17	73.30
102_Sgf	1.46	1.45	0.01	107.24	73.99	33.25	9.54	95.00
103_Sgf	1.94	1.70	0.23	211.55	41.04	170.51	11.61	97.10
108_SH	0.95	0.51	0.44	263.60	159.98	103.62	20.54	3.60
114_G	0.64	0.35	0.29	1401.63	202.03	1199.60	1.99	2.40
115_SY			0.01	1918.88	1864.52	54.35	1.63	2.20
117_HD			0.01	857.35	748.46	108.89	1.04	1.10
118_DI			0.01	8666.70		127.13		
120_D	3.40	2.49	0.91	361.44	248.51	112.93		
121_Df	0.85	0.60	0.24	144.90	43.39	101.50		
122_Dgf	1.03	1.00	0.03	136.85	111.95	24.90		
123_SH			0.77			236.22		
124_Scf	0.53	0.51	0.01	103.61	37.33	66.28		
125_D	0.67	0.62	0.04	153.58	70.99	82.59		
126_Lf	1.15	0.97	0.18	329.66	179.37	150.29		
127_D	1.57	1.41	0.16	390.30	308.18	82.11		
128_D	0.77	0.21	0.56	167.71	29.18	138.53		
129_Df	2.03	2.02	0.01	104.83	89.51	15.32		
130_Lf	2.18	2.16	0.03	220.33	139.21	81.12		
131_Lgf	4.48	4.38	0.10	396.32	108.18	288.14		

Unit [J/(g*g*9)] is total heat in Joules absorbed per gram
of dry rock and gram of water and per 9 seconds.

Table E.4 Results of the freezing test (Part 1)

Sample #	CFWS [%]	CFWB [%]	CFWV [%]	CUFWS [%]	CUFWB [%]	CUFWV [%]	CUFBUS [%]	CUFBUB [%]	CUFBUV [%]	CRDL [mm/10m]	CTF [C]
1_Lcf	4.60	68.03	51.51	2.16	31.97	24.21	2.13	31.54	23.88	11.89	-5.6
3_Lcf	0.77	42.56	26.78	1.04	57.44	36.15	1.00	55.28	34.79	67.24	-2.8
4_L											
5_Df	1.61	67.71	58.42	0.77	32.29	27.86	0.66	27.75	23.94	4.66	-2.7
6_Df	0.95	38.32	34.05	1.52	61.68	54.80	0.76	30.68	27.26	8.00	-1.9
8_D											
10_L											
15_D											
16_D											
17_Lf	0.60	39.38	30.42	0.92	60.62	46.83	0.44	29.33	22.66	1.35	-2.7
18_D											
19_Df	0.24	26.37	23.64	0.66	73.63	66.01	0.50	55.36	49.63	9.97	-3.2
20_Dcf	0.41	36.34	28.63	0.72	63.66	46.66	0.70	61.34	44.96	19.32	-4.3
21_Dcf	0.22	38.06	26.21	0.36	61.94	42.66	0.25	42.76	29.45	7.92	-5.6
22_Dcf	0.47	55.97	34.31	0.37	44.03	26.98	0.33	39.82	24.40	18.55	-3.8
23_Dcf	0.85	53.97	38.36	0.73	46.03	32.72	0.71	45.36	32.24	21.97	-4.2
24_Dcf	0.10	24.41	18.04	0.29	75.59	55.87	0.26	65.78	48.62	10.79	-4.6
26_Df	1.42	49.07	44.99	1.47	50.93	46.70	1.32	45.62	41.83	7.99	-2.1
28_L											
32_Df	0.13	23.39	19.38	0.42	76.61	63.48	0.38	69.72	57.77	4.40	-2.9
34_Df	0.57	51.74	42.36	0.53	48.26	39.51	0.36	32.55	26.65	2.99	-3.9
37_D											
37.1_L											
39_L											
40_L											
41_Df	1.30	51.13	46.38	1.24	48.87	44.33	1.14	44.98	40.80	0.00	-1.5
42_Dgf	0.12	19.10	14.24	0.53	80.90	60.32	0.31	47.96	35.76	8.35	-3.1
45_Df	2.40	55.96	53.98	1.89	44.04	42.49	1.81	42.21	40.72	6.28	-1.2
46_Df	2.10	56.84	54.81	1.60	43.16	41.61	1.48	39.94	38.51	37.81	
50_L											
51_Lgf	1.91	71.45	68.32	0.76	28.55	27.30	0.55	20.45	19.56	58.05	-2.4
52_Df	1.43	74.18	62.88	0.50	25.82	21.89	0.48	24.90	21.11	2.65	
53_Df	1.86	66.05	55.34	0.95	33.95	28.45	0.90	32.19	26.97	0.00	-1.3
54_Dcf	0.42	50.53	32.56	0.41	49.47	31.87	0.40	48.22	31.07	28.61	-3.9
55_Dcf	0.88	51.34	35.97	0.83	48.66	34.10	0.83	48.14	33.73	45.87	-4.2
56_Dcf	0.15	22.16	11.68	0.54	77.84	41.02	0.52	75.27	39.67	19.32	-4.1
57_D											
58_Dcf	0.49	35.26	21.69	0.90	64.74	39.82	0.79	56.99	35.06	37.82	-3.8
60_Dcf	0.58	45.69	23.60	0.69	54.31	28.05	0.65	51.47	26.58	37.18	-4.5
61_Dcf	0.12	19.24	12.47	0.49	80.76	52.34	0.43	70.76	45.86	18.62	-3.2
62_L											
65_L											
68_L											
70_L											
74_L											

Table E.4 Results of the freezing test (Part 2)

Sample #	CFWS [%]	CFWB [%]	CFWV [%]	CUFWS [%]	CUFWB [%]	CUFWV [%]	CUFBUS [%]	CUFBUB [%]	CUFBUV [%]	CRDL [mm/10m]	CTF [C]
75_Lf	0.16	23.74	19.17	0.50	76.26	61.59	0.33	50.07	40.44	1.20	-3.0
75.1_L											
76_Dgf	0.82	42.33	23.99	1.12	57.67	32.69	1.10	56.73	32.16	13.33	-3.9
78_Df	0.33	29.73	25.18	0.77	70.27	59.49	0.54	49.01	41.49	23.27	-4.0
79_Dcf	1.12	50.82	36.94	1.08	49.18	35.74	1.05	47.94	34.84	45.31	-5.2
80_Lf	0.12	17.01	15.23	0.56	82.99	74.31	0.53	77.80	69.66	3.34	-3.8
81_L											
83_L											
84_Df	0.76	39.02	37.32	1.18	60.96	58.33	0.79	40.96	39.20	0.00	-2.1
85_L											
87_L											
88_D											
90_D											
91_Df	0.85	50.93	47.00	0.82	49.07	45.28	0.66	39.30	36.27	41.64	-5.1
92_Df	0.32	23.49	20.62	1.05	76.51	67.16	0.98	71.45	62.71	11.98	-3.6
93_Df	0.96	44.17	39.23	1.21	55.83	49.59	0.59	27.31	24.26	0.00	-4.2
94_Lf	0.79	47.34	42.69	0.88	52.66	47.48	0.33	19.95	17.99	5.99	-2.9
95_Dcf	1.01	62.22	28.08	0.61	37.78	17.05	0.59	36.24	16.36	4.80	-2.9
96_Lf	0.58	53.27	33.32	0.51	46.73	29.23	0.28	25.57	15.99	21.53	-4.3
97_Lgf	0.55	74.63	60.23		25.37	20.48		10.16	8.20	0.00	-2.3
98_M											
99_M											
100_M											
101_Sgf	0.13	16.72	11.49	0.62	83.28	57.21	0.61	81.05	55.69	0.00	-5.5
102_Sgf	1.19	51.70	32.31	1.12	48.30	30.19	1.09	47.15	29.47	29.91	-4.8
103_Sgf	5.31	100.00	81.77		0.00	0.00		-2.56	-2.10	5.99	-2.5
108_SH											
114_G											
115_SY											
117_HD											
118_DI											
120_D											
121_Df	0.89	45.11	41.70	1.08	54.89	50.74	0.84	42.62	39.39	3.33	-3.2
122_Dgf	0.41	32.60	28.33	0.86	67.40	58.58	0.73	57.81	50.24	7.33	-3.2
123_SH											
124_Scf	0.64	33.42	24.25	1.28	66.58	48.32	1.26	65.59	47.59	9.30	-2.8
125_D											
126_Lf	0.30	23.44	14.31	0.99	76.56	46.73	0.87	67.34	41.11	7.97	-1.5
127_D											
128_D											
129_Df	1.84	67.18	57.07	0.90	32.82	27.88	0.84	30.72	26.09	10.17	-4.6
130_Lf	0.88	49.75	44.43	0.89	50.25	44.87	0.86	48.41	43.23	3.58	-5.7
131_Lgf	3.95	82.30	69.05	0.85	17.70	14.85	0.81	16.96	14.23	0.00	-3.5

157

VITA AUCTORIS

NAME: Martin Ondrášik

PLACE OF BIRTH: Bratislava, Slovakia
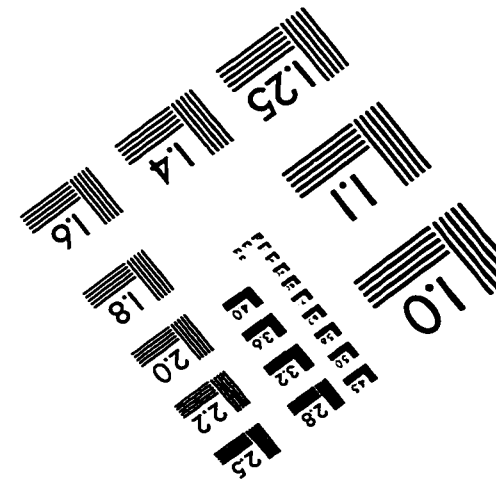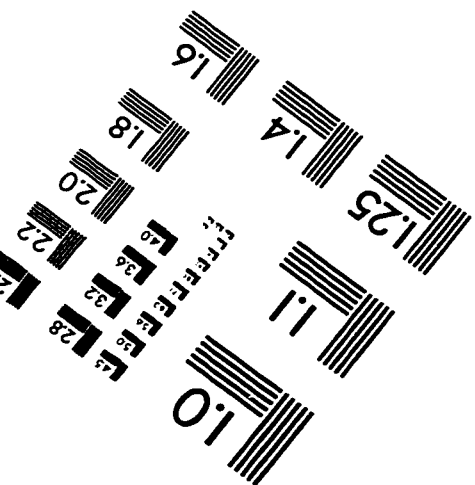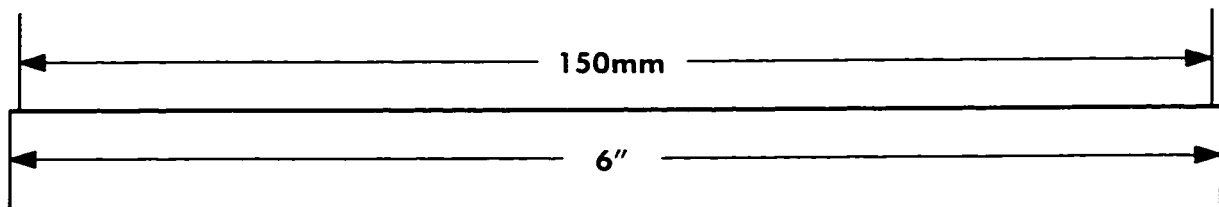
YEAR OF BIRTH: 1966
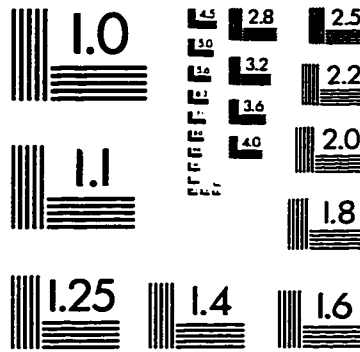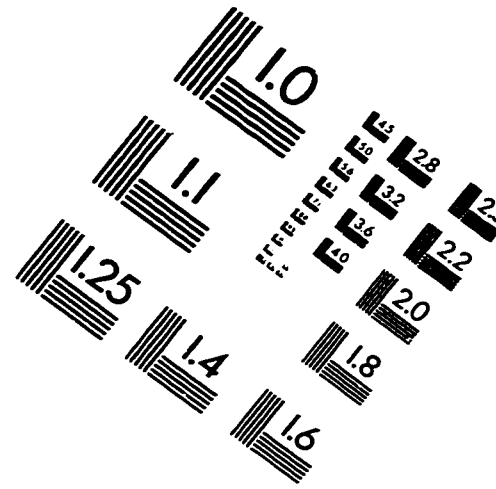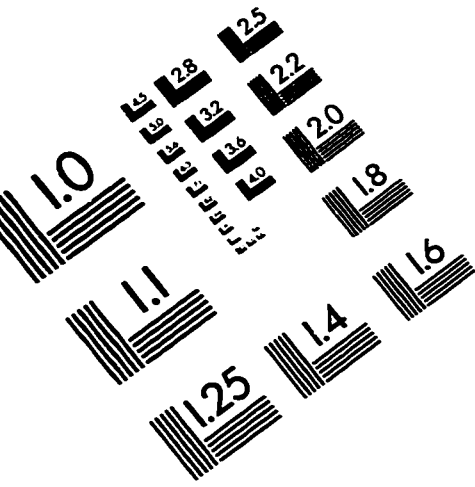
EDUCATION:

Comenius University, Bratislava, Slovakia
1984 - 1989   B.Sc.   Hydrogeology and Engineering
Geology

University of Windsor, Windsor, Canada
1995 - 1996   M.Sc.   Geological Engineering

WORKING EXPERIENCES:

Dionyz Štúr Institute of Geology
1989 - 1994   Engineering Geologist

IMAGE EVALUATION
TEST TARGET (QA-3)

150mm

6"